A 3% Solution: Determination of the Hubble Constant with the Hubble Space Telescope and Wide Field Camera 3 [1]

Adam G. Riess[2,3], Lucas Macri[4], Stefano Casertano[3], Hubert Lampeitl[5], Henry C. Ferguson[3], Alexei V. Filippenko[6], Saurabh W. Jha[7], Weidong Li[6], and Ryan Chornock[8]

ABSTRACT

We use the Wide Field Camera 3 (WFC3) on the *Hubble Space Telescope (HST)* to determine the Hubble constant from optical and infrared observations of over 600 Cepheid variables in the host galaxies of 8 recent Type Ia supernovae (SNe Ia), which provide the calibration for a magnitude-redshift relation based on 240 SNe Ia. Increased precision over past measurements of the Hubble constant comes from five improvements: (1) more than doubling the number of infrared observations of Cepheids in the nearby SN hosts; (2) increasing the sample size of ideal SN Ia calibrators from six to eight with the addition of SN 2007af and SN 2007sr; (3) increasing by 20% the number of Cepheids with infrared observations in the megamaser host NGC 4258; (4) reducing the difference in the mean metallicity of the Cepheid comparison samples between NGC 4258 and the SN hosts from $\Delta\log[\mathrm{O/H}] = 0.08$ to 0.05; and (5) calibrating all optical Cepheid colors with a single camera, WFC3, to remove cross-instrument zeropoint errors. The result is a reduction in the uncertainty in H_0 due to steps beyond the first rung of the distance ladder from 3.5% to 2.3%. The measurement of H_0 via the geometric distance to NGC 4258 is 74.8 ± 3.1 km s^{-1} Mpc^{-1}, a 4.1% measurement including systematic uncertainties. Better precision independent of the distance to NGC 4258 comes from the use of two alternative Cepheid absolute calibrations: (1) 13 Milky Way Cepheids with trigonometric parallaxes measured with *HST*/FGS and *Hipparcos*, and (2) 92 Cepheids in the Large Magellanic Cloud, for which multiple accurate and

---

[1]Based on observations with the NASA/ESA *Hubble Space Telescope*, obtained at the Space Telescope Science Institute, which is operated by AURA, Inc., under NASA contract NAS 5-26555.

[2]Department of Physics and Astronomy, Johns Hopkins University, Baltimore, MD 21218.

[3]Space Telescope Science Institute, 3700 San Martin Drive, Baltimore, MD 21218; ariess@stsci.edu.

[4]George P. and Cynthia Woods Mitchell Institute for Fundamental Physics and Astronomy, Department of Physics & Astronomy, Texas A&M University, 4242 TAMU, College Station, TX 77843-4242.

[5] Institute of Cosmology and Gravitation, University of Portsmouth, Portsmouth, PO1 3FX, UK

[6]Department of Astronomy, University of California, Berkeley, CA 94720-3411.

[7]Department of Physics and Astronomy, Rutgers University, 136 Frelinghuysen Road, Piscataway, NJ 08854.

[8]Harvard/Smithsonian Center for Astrophysics, 60 Garden St. Cambridge, MA 02138.

precise eclipsing binary distances are available yielding 74.4 ± 2.5 km s^{-1} Mpc^{-1}, a 3.4% uncertainty including systematics. Our best estimate uses all three calibrations but a larger uncertainty afforded from any two: $H_0 = 73.8 \pm 2.4$ km s^{-1} Mpc^{-1} including systematic errors, corresponding to a 3.3% uncertainty. The improved measurement of H_0, when combined with the Wilkinson Microwave Anisotropy Probe (WMAP) 7-year data, results in an improved constraint on the equation-of-state parameter of dark energy of $w = -1.08 \pm 0.10$. It also rules out the best fitting gigaparsec-scale void models, posited as an alternative to dark energy. The combined H_0 + WMAP results also have implications for the number of relativistic particle species in the early Universe, yielding $N_{\rm eff} = 4.2 \pm 0.7$, an excess for the value expected from the three known neutrino flavors, though not with high significance. The distance ladder used here for the determination of H_0 does not yet appear to be limited by systematic errors, suggesting that further improvements in precision approaching 1% may be feasible.

Subject headings: galaxies: distances and redshifts — cosmology: observations — cosmology: distance scale — supernovae: general

1. Introduction

Measurements of the expansion history, $H(z)$, from Type Ia supernovae (SNe Ia) provide crucial, empirical constraints to help guide the emerging cosmological model. While high-redshift SNe Ia reveal that the Universe is now accelerating (Riess et al. 1998; Perlmutter et al. 1999), nearby ones provide the most precise measurements of the present expansion rate, H_0.

Recently, high-redshift measurements from the cosmic microwave background radiation (CMB), baryon acoustic oscillations (BAO), and SNe Ia have been used in concert with an assumed cosmological model to *predict* the value of H_0 (e.g., Komatsu et al. 2011). They are not, however, a substitute for its *measurement* in the local Universe. Such forecasts of H_0 from the high-redshift Universe also make specific assumptions about unsettled questions: the nature of dark energy, the global geometry of space, and the basic properties of neutrinos (number and mass). Instead, we can gain insights into these unknowns from a precise, local measurement of H_0. The most precise measurements of H_0 have come from distance ladders which calibrate the luminosities of nearby SNe Ia through *Hubble Space Telescope (HST)* observations of Cepheids in their host galaxies (see Freedman & Madore 2010 for a review).

In the early Cycles of *HST*, the SN Ia *HST* Calibration Program (Sandage et al. 2006, hereafter SST) and the *HST* Key Project (Freedman et al. 2001, hereafter KP) each calibrated H_0 via Cepheids and SNe Ia using the Wide Field/Planetary Camera 2 (WFPC2) and the Large Magellanic Cloud (LMC) as the first rung on their distance ladder. Unfortunately, the LMC was not an ideal anchor for the cosmic ladder because its distance was constrained to only 5–10% (Gibson 2000), its Cepheids (observed from the ground) are of shorter mean period ($\Delta < P > \approx 25$ d), and lower

metallicity (Δ[O/H] = 0.4) than those of the spiral galaxies hosting nearby SNe Ia. These differences and uncertainties between ground-based and space-based photometric zeropoints introduced a 7% systematic error in the determinations of H_0 obtained by those teams (see §4). Additional uncertainty arose from the unreliability of the measurements from several of the SNe Ia selected by SST, which were *photographically* observed, highly reddened, atypical, or discovered after peak brightness. Only three SNe Ia (SNe 1990N, 1981B, and 1998aq) from the SST sample lacked these shortcomings, defining only a small set of nearby SNe suitable to calibrate H_0. Despite careful work, the teams' estimates of H_0, each with an uncertainty of $\sim 10\%$, differed from each other's by 20%, due to the aforementioned systematic errors. Additional progress required rebuilding the distance ladder to address these systematic errors.

The installation of the Advanced Camera for Surveys (ACS) extended the range of *HST* for observing Cepheids, reduced their crowding with finer pixel sampling, and increased their rate of discovery by doubling the field of view. In Cycle 11, members of our team began using ACS to measure Cepheids at optical wavelengths in the hosts of more modern SNe Ia (SN 1994ae by Riess et al. 2005; SN 1995al and SN 2002fk by Riess et al. 2009b) and in a more ideal anchor galaxy (NGC 4258 by Macri et al. 2006).

In *HST* Cycle 15, we began the "Supernovae and H_0 for the Equation of State" (SH0ES) project to measure H_0 to better than 5% precision by addressing the largest remaining sources of systematic error. The SH0ES program constructed a refurbished distance ladder from high-quality light curves of SNe Ia, a geometric distance to NGC 4258 determined through radio (very long baseline interferometry; VLBI) observations of megamasers, and Cepheid variables observed with *HST* in NGC 4258 and in the hosts of recent SNe Ia. The reduction in systematic errors came from additional observations of NGC 4258 and from our use of purely *differential* measurements of the fluxes of Cepheids with similar metallicities and periods throughout all galaxies in our sample. The latter rendered our distance scale insensitive to possible changes in Cepheid luminosities as a function of metallicity or to putative changes in the slope of the period-luminosity relations from galaxy to galaxy. We measured H_0 to 4.7% precision (Riess et al. 2009a, hereafter R09), a factor of two better than previous measurements with *HST* and WFPC2. An alternate analysis using the Benedict et al. (2007) parallax measurements of Milky Way Cepheids in lieu of the megamaser distance to NGC 4258 showed good agreement, with comparable 5.5% precision.

This result formed a triumvirate of constraints in the Wilkinson Microwave Anisotropy Probe (WMAP) 7-year analysis (i.e., BAO + H_0 + WMAP-7yr) which were selected as the combination most insensitive to systematic errors with which to constrain the cosmological parameters (Komatsu et al. 2011). Together with the WMAP constraint on $\Omega_M h^2$, this measurement of H_0 provides a constraint on the nature of dark energy, $w = -1.12 \pm 0.12$ (R09 and Komatsu et al. 2011), which is comparable to but independent of the use of high-redshift SNe Ia. It also improves constraints on the properties of the elusive neutrinos, such as the sum of their masses and the number of species (Komatsu et al. 2011).

In *HST* Cycle 17 we used the newly installed Wide Field Camera 3 (WFC3) to increase the sample sizes of both the Cepheids and the SN Ia calibrators along the ladder used by SH0ES to determine H_0. The near-infrared (IR) channel of WFC3 provides an order of magnitude improvement in efficiency for follow-up observations of Cepheids over the Near-Infrared Camera and Multi-Object Spectrograph (NICMOS), while the finer pixel scale of the visible channel (relative to ACS) is valuable for reducing the effects of crowding when searching for Cepheids. We present these new observations in §2, the redetermination of H_0 in §3, and an analysis of the error budget including systematics in §4. In §5, we address the use of this new measurement along with external datasets to constrain properties of dark energy and neutrinos.

2. WFC3 Observations of Cepheids in the SH0ES Program

The SH0ES program was developed to improve upon the calibration of the luminosity of SNe Ia in order to better measure the Hubble constant. To ensure a reliable calibration sample we selected SNe Ia having the following qualities: (1) modern photometric data (i.e., photoelectric or CCD), (2) observed before maximum brightness, (3) low reddening (implying $A_V < 0.5$ mag), (4) spectroscopically normal, and (5) optical *HST*-based observations of Cepheids in its host galaxy. In addition to providing robust distance measures, these qualities are crucial for producing a calibration sample which is a good facsimile of the SN Ia sample they are used to calibrate — i.e., those defining the modern SN Ia magnitude-redshift relation at $0.01 < z < 0.1$ (e.g., Hicken et al. 2009a).

In *HST* Cycles 16 and 17, we used WFC3, ACS, and WFPC2 to discover Cepheids in two new SN Ia hosts: NGC 5584 (host of SN 2007af; Macri et al. 2011b) and NGC 4038/9 ("the Antennae," host of SN 2007sr; Macri et al. 2011c) whose light curves were presented in Hicken et al. (2009a)[1]. We also employed the optical channel of WFC3 to *reobserve all previous SN Ia hosts in the calibration sample and NGC 4258*. This provided for the first time a calibration of all Cepheid optical and infrared photometry using the same zeropoints. In the case of some hosts, the additional epoch (obtained well after the prior ones) allowed us to discover previously unidentified, longer period ($P > 60$ d) variables. We also used these observations to search for additional Cepheids in the hosts which previously had the smallest numbers of Cepheids: NGC 3021, NGC 3982, NGC 4536, and NGC 4639 (Macri et al. 2011a). The new observations, together with those from Riess et al. (2009b), Saha et al. (1996, 1997, 2001), Gibson et al. (2000), Stetson & Gibson (2001), and Macri et al. (2006), provide the position, period, and phase of 730 Cepheids in 8 hosts with reliable SN Ia data as well as NGC 4258. The Cepheids in each host were typically imaged on 14 epochs in $F555W$ and 2–5 epochs with $F814W$ (except for NGC 4258, which has 12 epochs of $F814W$ data). An illustration of the entire dataset used to observe the Cepheids is shown in Figure

[1] We augmented the Hicken et al light curve of SN 2007sr with 3 pre-discovery V-band observations from the All-Sky Automated Survey (ASAS) extending to pre-maximum; MJD,mag,error triplets are (4441.85,13.44,0.12), (4448.86,12.65,0.05),(4452.85,12.73,0.08)

1. Having previously determined the positions, periods, and optical magnitudes of these Cepheids, it is highly advantageous to observe their near-IR magnitudes with a single photometric system in order to (1) reduce the differential extinction by a factor of five over visual bands, (2) reduce the possible dependence of Cepheid luminosities on chemical composition (Marconi et al. 2005), and (3) negate zeropoint errors. This was previously done with NICMOS on *HST* in Cycle 15 by R09 for a subset of these Cepheids.

The near-IR channel on WFC3 provides a tremendous gain over NICMOS for the study of extragalactic Cepheids. Photometry of comparable signal-to-noise ratio can be obtained in a quarter of the exposure time. More significant for Cepheid follow-up observations is the factor of 40 increase in area of WFC3-IR over NICMOS/Camera 2 (NIC2), the channel which offered the best compromise between area and uniform pixel sampling. The one advantage of NIC2 over WFC3-IR is better sampling of the point-spread function (PSF); the $0\farcs13$ pixels of WFC3-IR undersample the *HST* PSF by a factor of 1.6 at 1.6 μm. However, the finer sampling of NIC2 is largely offset by the numerous photometric anomalies unique to that camera, whose subsequent correction leads to correlated noise among neighboring pixels which reduces the independence of the NICMOS pixel sampling. In contrast, the detector of WFC3-IR is much better behaved and pixel sampling noise can be mitigated with dithering.

2.1. WFC3 Data Reduction

Each host galaxy was observed for 2–7 ks with individual exposures 400–700 s in length, using integer and half-pixel dithering between exposures to improve sampling of the PSF (see Table 1). The WFC3 images of the two new hosts, NGC 5584 and NGC 4038, are shown in Figures 2 and 3. Figure 4 shows an example of a host previously observed with NIC2 by R09 and with WFC3-IR in this study.

We developed an automated pipeline to calibrate the raw WFC3 $F160W$ frames. The first step was to pass the data through the STScI-supported *calwf3* pipeline in the *STSDAS* suite of routines in *PyRAF* to remove the bias and dark current, reject cosmic rays through up-the-ramp sampling, and flat-field the data. A small correction to the standard flat-field frame was used to correct the WFC3 "blobs," which are 10% depressions in flux covering $\sim 1\%$ of the area due to spotting on the WFC3 Channel Select Mechanism (CSM). Next, we used *multidrizzle* to combine the exposures from each visit into a master image, resampling onto a finer pixel scale while correcting for the known geometric distortions in the camera. We utilized a final pixel scale of $0\farcs08$ per pixel and an input-to-output fraction of 0.6.

We identified the positions of Cepheids in the WFC3-IR images by deriving geometric transformations from the $F814W$ images to those in $F160W$, successively matching fainter sources to improve the registration. This procedure empirically determined the difference in plate scale between ACS-WFC, WFPC2, WFC3-UVIS, and WFC3-IR. We typically identified more than 100

sources in common, resulting in an uncertainty in the mean position of each Cepheid below 0.03 pixels (< 2.4 milliarcsec).

We carried out the photometry of Cepheids using the algorithms developed by R09; they employ PSF fitting to model the crowded regions around Cepheids, fixing their positions to those derived from optical data and using artificial-star tests to determine photometric errors and crowding biases. As an example, we show in Figure 5 the *HST* optical image, near-IR image, model, and residuals for 8 typical Cepheids spanning a wide range of periods in the SN host NGC 5584. We used the same approach to determine zeropoints as in R09 from the Persson et al. (1998) standard star P330E.

Table 1: Hosts Observed with WFC3-IR $F160W$ by GO-11570

Host	SN Ia	Exp. time (s)
NGC 4536	SN 1981B	2564
NGC 4639	SN 1990N	5377
NGC 3982	SN 1998aq	4016
NGC 3370	SN 1994ae	4374
NGC 3021	SN 1995al	4424
NGC 1309	SN 2002fk	6988
NGC 4038/9	SN 2007sr	6794[a]
NGC 5584	SN 2007af	4926
NGC 4258	———	2011[b]

[a]Data in GO-11577

[b]Depth per pointing; galaxy covered in 16 pointing mosaic

Due to the low amplitudes of their near-IR light curves (< 0.3 mag), Cepheid magnitudes determined at random phases provide nearly the same precision as mean fluxes for determining the intercept of their P–L relations (Madore & Freedman 1991).[2]

Since we had previously observed with NIC2 many of the Cepheids now observed with WFC3-IR, we can directly compare their $F160W$ photometry on these two systems. Figure 6 shows the magnitude differences for the Cepheids utilized in the P–L relations in both R09 and in §2.2. The mean difference is 0.036 ± 0.027 mag (in the sense that photometry with WFC3 is brighter), with no apparent dependence on Cepheid brightness. While the difference in photometry between instruments may include differences in system zeropoints, the subsequent determination of H_0 via

[2]In R09 we corrected the measured NICMOS $F160W$ magnitude to the mean-phase magnitude using the Cepheid phase, period, and amplitude from the optical data, the dates of the NICMOS observations, and the Fourier components of Soszyński et al. (2005) which quantify the relations between Cepheid light curves in the optical and near-IR. However, these phase corrections of $\sigma \sim 0.1$ mag were found to be insignificant in the subsequent analysis, since the dispersion of the observed P–L relations is $\sigma \sim 0.3$ mag. Here we have not attempted such corrections because the Cepheid phases at the time of the WFC3 $F160W$ observations were too poorly constrained to allow for a significant correction.

Cepheids observed with a single instrument in the SN Ia hosts and in NGC 4258 will be independent of instrument zeropoints. Thus, for the determination of H_0 it is more relevant to calculate the change in magnitudes between Cepheids in NGC 4258 and the SN hosts between WFC3 and NIC2; the measurement of this change is 0.019 ± 0.054 mag.

Table 2 contains relevant parameters for each Cepheid observed with WFC3 $F160W$. The first 8 columns give the Cepheid's host, position, identification number (from Macri et al. 2006, Riess et al. 2009b, Macri et al. 2011b,c,a), period, mean $V - I$ color, WFC3 $F160W$ magnitude, and the magnitude uncertainty. Column 9 contains the displacement of the flux centroid in the near-IR data relative to the optical Cepheid position, expressed in units of pixels (1 pixel = 0.″08), a quantity used to refine the determination of the crowding bias. Column 10 gives the photometric crowding bias determined using the artificial-star tests for each Cepheid's environment (see §2.3 of R09) and the displacement tabulated in the previous column; this correction has already been applied to the magnitudes listed in Column 7. Column 11 contains the root-mean square of the residual image, weighted by the inverse distance from the Cepheid position, useful for determining the quality of the crowded-scene fit. Column 12 contains the metallicity parameter, $12 + \log[\mathrm{O/H}]$ (Zaritsky et al. 1994) derived from the deprojected galactocentric radii of each Cepheid and the abundance gradient of its host.[3] Column 13 contains a rejection flag used for the P–L relations.

2.2. Near-Infrared Cepheid Relations

The nine individual P–L relations measured with WFC3 $F160W$ and fit with a common slope are shown in Figure 7. Intercepts relative to NGC 4258 are given in Table 3 and compared in Figure 8 to the SN distances. While 636 Cepheids previously identified at optical wavelengths were measurable[4] in the WFC3-IR $F160W$ images, $\sim 20\%$ appeared as outliers in the IR P–L relations. This is not surprising, as we expect outliers to occur from (1) a complete blend with a bright, red source such as a red giant, (2) a poor model reconstruction of a crowded group when the Cepheid is a small component of the group's flux, (3) objects misidentified as classical Cepheids in the optical (e.g., blended Type II Cepheids), and (4) Cepheids with the wrong period (aliasing or incomplete sampling of a single cycle). As expected, the outlier fraction is greater in WFC3 images than in NIC2 ones because the former contain a larger fraction of Cepheids from crowded regions (such as the nucleus) which yield more outliers and were intentionally avoided in the small, selective NIC2 pointings (see Figure 4).

---

[3]These gradients were published in R09 for NGC 4258 and the previously observed six SN hosts; the values for the new hosts, following the same convention as Table 12 of that paper, are $12 + \log[\mathrm{O/H}] = 8.981 - 0.064(x - 30'')/10''$ for NGC 5584 and $12 + \log[\mathrm{O/H}] = 9.129 - 0.043(x - 30'')/10''$ for NGC 4038/9.

[4]Cepheids were considered to be measured if our software reported a possible magnitude for the source with an uncertainty less than 0.7 mag, a model residual with rms better than 3σ from the distribution of all model residuals, and a crowding correction less than 1.5 magnitudes. While these thresholds are somewhat arbitrary, they are sufficient to remove catastrophic failures in convergence on the measurement of the photometry for a source.

As in R09, we eliminated outliers > 0.75 mag or $> 2.5\sigma$ (following Chauvenet's criterion) from an initial fit of the P–L relations, refitted the relations and repeated these tests for outliers until convergence. This resulted in a reduction of the sample to 484 objects; the next section considers the effect of this rejection on the determination of H_0 and an alternative method for contending with outliers.

3. Measuring the Hubble Constant

The determination of the Hubble constant follows from the relations given in §3 of R09. To summarize, we perform a single, simultaneous fit to all Cepheid and SN Ia data to minimize the χ^2 statistic and measure the parameters of the distance ladder. We express the jth Cepheid magnitude in the ith host as

$$m_{W,i,j} = (\mu_{0,i} - \mu_{0,4258}) + zp_{W,4258} + b_W \log P_{i,j} + Z_W \Delta\log [\mathrm{O/H}]_{i,j}, \quad (1)$$

where the "Wesenheit reddening-free" mean magnitude (Madore 1982) is given as

$$m_{W,i,j} = m_{H,i,j} - R(m_{V,i,j} - m_{I,i,j}), \quad (2)$$

and $R \equiv A_H/(A_V - A_I)$. The Cepheid parameters with i, j subscripts are given in Table 2. For a Cardelli et al. (1989) reddening law, a Galactic-like value of $R_V = 3.1$, and the H band corresponding to the WFC3 $F160W$ band, we have $R = 0.410$. In the next section we consider the sensitivity of H_0 to the value of R_V.

We determine the values of the nuisance parameters b_W and Z_W — which define the relation between Cepheid period, metallicity, and luminosity — by minimizing the χ^2 for the global fit to all Cepheid data. The reddening-free distances, $\mu_{0,i}$, for the hosts relative to NGC 4258 are given by the fit parameters $\mu_{0,i} - \mu_{0,4258}$, while zp_{4258} is the intercept of the P–L relation simultaneously fit to the Cepheids of NGC 4258.

The SN Ia magnitudes in the SH0ES hosts are simultaneously expressed as

$$m^0_{v,i} = (\mu_{0,i} - \mu_{0,4258}) + m^0_{v,4258}. \quad (3)$$

where the value $m^0_{v,i}$ is the maximum-light apparent V-band brightness of a SN Ia in the ith host at the time of B-band peak corrected to the fiducial color and luminosity. This quantity is determined for each SN Ia from its multi-band light curves and a light-curve fitting algorithm, either from the MLCS2k2 (Jha et al. 2007) or the SALT-II (Guy et al. 2005) prescription (see §4.2 for further discussion).

A minor change from R09 is the inclusion of a recently identified, modest relationship between host-galaxy mass and the calibrated SN Ia magnitude. Several studies (Hicken et al. 2009b; Kelly et al. 2010; Lampeitl et al. 2010; Sullivan et al. 2010) have shown the existence of a correlation between the corrected SN magnitude and the mass of its host, with a value of 0.03 mag per dex in $M_{\rm stellar}$, in the sense that more massive (and metal rich) hosts produce more luminous SNe. This correlation has been independently detected using both low- and high-redshift samples of SNe Ia, as well as with multiple fitting algorithms. The effect on H_0 is quite small, a decrease of 0.75%, due to the modest difference in mean masses for the nearby hosts (Neill et al. 2009, mean log $M_{\rm stellar} = 10.0$) and for those that define the magnitude-redshift relation (Sullivan et al. 2010, mean log $M_{\rm stellar} = 10.5$). We include these corrections based on host-galaxy mass in our present determination of $m^0_{v,i}$, given in Table 3, normalizing to a fiducial host mass of log $M_{\rm stellar} = 10.5$ as appropriate for the objects used to measure the Hubble flow.

Table 3: Distance Parameters

Host	SN Ia	Filters	$m^0_{v,i} + 5a_v$	σ^a	$\mu_{0,i} - \mu_{0,4258}$	μ_0 best
n4536	SN 1981B	$UBVR$	15.147	0.145	1.567 (0.0404)	30.91 (0.07)
n4639	SN 1990N	$UBVRI$	16.040	0.111	2.383 (0.0630)	31.67 (0.08)
n3370	SN 1994ae	$UBVRI$	16.545	0.101	2.835 (0.0284)	32.13 (0.07)
n3982	SN 1998aq	$UBVRI$	15.953	0.091	2.475 (0.0460)	31.70 (0.08)
n3021	SN 1995al	$UBVRI$	16.699	0.113	3.138 (0.0870)	32.27 (0.08)
n1309	SN 2002fk	$BVRI$	16.768	0.103	3.276 (0.0491)	32.59 (0.09)
n5584	SN 2007af	$BVRI$	16.274	0.122	2.461 (0.0401)	31.72 (0.07)
n4038	SN 2007sr	$BVRI$	15.901	0.137	2.396 (0.0567)	31.66 (0.08)
Weighted Mean	——	——	——	0.0417	—— (0.0133)	——

[a]For MLCS2k2, 0.08 mag added in quadrature to fitting error.

The simultaneous fit to all Cepheid and SN Ia data via Equations (1) and (3) results in the determination of $m^0_{v,4258}$, which is the expected reddening-free, fiducial, peak magnitude of a SN Ia appearing in NGC 4258. Lastly, the Hubble constant is determined from

$$\log\, H_0 = \frac{(m^0_{v,4258} - \mu_{0,4258}) + 5a_v + 25}{5}. \tag{4}$$

where $\mu_{4258,0}$ is the independent, geometric distance estimate to NGC 4258 obtained through VLBI observations of water megamasers orbiting its central supermassive black hole (Herrnstein et al. 1999; Humphreys et al. 2005; Argon et al. 2007; Humphreys et al. 2008; Greenhill 2009). The term a_v is the intercept of the SN Ia magnitude-redshift relation, approximately $\log cz - 0.2m^0_v$ but given for an arbitrary expansion history as

$$a_v = \log\, cz \left\{ 1 + \frac{1}{2}\left[1 - q_0\right] z - \frac{1}{6}\left[1 - q_0 - 3q_0^2 + j_0\right] z^2 + O(z^3) \right\} - 0.2m^0_v, \tag{5}$$

measured from the set of SN Ia (z, m_v^0) independent of any absolute (i.e., luminosity or distance) scale. As in R09, we determine a_v from a Hubble diagram for 240 SNe Ia from Hicken et al. (2009a) using MLCS2k2 (Jha et al. 2007) or the SALT-II (Guy et al. 2005) prescription to determine m_v^0. Limiting the sample to $0.023 < z < 0.1$ (to avoid the possibility of a local, coherent flow; z is the redshift in the rest frame of the CMB) leaves 140 SNe Ia. (In the next section we consider a lower cut of $z > 0.01$.) Together with the present acceleration $q_0 = -0.55$ and prior deceleration $j_0 = 1$ (Riess et al. 2007), we find $a_v = 0.698 \pm 0.00225$. Note that Ganeshalingam et al. (2010) recently published light curves of large sample of SNe Ia from the Lick Observatory Supernova Search, but there is a large overlap with those given by Hicken et al. (2009a). There are only 13 SNe Ia at $z > 0.023$ not already included in our sample, and their inclusion would have a negligible impact on the uncertainty in a_v, itself one of the smallest contributors to the error in H_0.

The full statistical error in H_0 is the quadrature sum of the uncertainty in the three *independent* terms in Equation (4): $\mu_{4258,0}$, $m^0_{v,4258}$, and $5a_V$, where $\mu_{4258,0}$ is the geometric distance estimate to NGC 4258 by Herrnstein et al. (1999), claimed by Greenhill (2009) to currently have a 3% uncertainty.

Hui & Greene (2006) point out that the peculiar velocities of SN Ia hosts and their correlations can produce an additional systematic error in the determination of the SN Ia m–z relation used for cosmography. However, by making use of a map of the matter density field, it is possible to correct individual SN Ia redshifts for these peculiar flows (Riess et al. 1997). Neill et al. (2007) made use of the IRAS PSCz density field (Branchini et al. 1999) to determine the effect of the density field on the low-redshift SN Ia m–z relation and its impact on the equation-of-state parameter of dark energy, $w = P/(\rho c^2)$ (where P is pressure and ρc^2 is energy density). Using their results for a light-to-matter bias parameter $\beta = 0.5$ and the dipole from Pike & Hudson (2005) results in an increase of the mean velocity of the low-redshift sample and in the Hubble constant by 0.4% over the case of uncorrelated velocities at rest with respect to the CMB. We use a new estimate of this mean peculiar velocity for the Hicken et al. (2009a) SN sample which is a slightly larger value of 0.5%. We account for this and assume an uncertainty of 0.1% resulting from a ± 0.2 error in the value of β.

The result is $H_0 = 74.8 \pm 3.0$ km s^{-1} Mpc^{-1}, a 4.0% measurement (top line, Table 4). It is instructive to deconstruct the individual sources of uncertainty to improve our insight into the measurement. In principle, the covariance between the data and parameters does not allow for an exact and independent allocation of propagated error for each term toward the determination of H_0. However, in our case, the diagonal elements of the covariance matrices provide a very good approximation to the individual components of error. These are given in Table 5 and shown in Figure 9 for past and present determinations of H_0.

A number of improvements since R09 are evident by comparing Columns 2 and 3 in Table 5 and as shown in Figure 9. The uncertainty in H_0 from all of the terms independent of the megamaser distance to NGC 4258 is 2.3%, 50% smaller than these same terms in R09, a result of

the increased sample of Cepheids and SN calibrators. This term includes uncertainties due to the form of the P–L relation, Cepheid metallicity dependences, photometry bias, and zeropoints — all of which were important systematic uncertainties in past determinations of the Hubble constant (see Column 1, which contains the values from Freedman et al. 2001). In this analysis, as in R09, these uncertainties have been reduced by the collection of samples of Cepheids whose measures (i.e., metallicity, periods, and photometric systems) are a good match between NGC 4258 and the SN hosts. Here the contribution from an unknown dependence of Cepheid luminosity on metallicity has been furthered reduced by 40% owing to a better match between the metallicity of the Cepheid samples in NGC 4258 and the expanded SN host sample. In R09, the mean metallicity of the NGC 4258 Cepheid sample on the ZHK abundance scale was 12 + log [O/H] =8.91, nearly the same as the present mean of 8.90. However, the mean metallicity of the Cepheid sample in the SN hosts has risen from 8.81 to 8.85. Some of this change can be attributed to the inclusion of Cepheids closer to the nuclei of the hosts and some to the inclusion of two new hosts, NGC 5584 and NGC 4038/9, with higher-than-average metallicities. The reduction in the mean abundance difference between NGC 4258 and the SN Ia hosts from 0.077 to 0.045 dex results in a decrease of the error propagated into H_0 from 1.1% to 0.6%. A similar reduction is seen with the use of Milky Way Cepheids whose mean metallicity of 8.9 is closer to the mean of the new Cepheid sample in the SN hosts. We consider an alternative calibration of abundances from Bresolin (2011) in §4.1.

3.1. Buttressing the First Rung

In our present determination of H_0, the 3% uncertainty in the distance to NGC 4258 claimed by Greenhill (2009) is now greater than all other sources combined (in quadrature). The next largest term, the uncertainty in mean magnitude of the eight nearby SNe Ia, is 1.9%. To significantly improve upon our determination of H_0, we would need an *independent* calibration of the first rung of the distance ladder as good as or better than the megamaser-based measurement to NGC 4258 in terms of precision and reliability. Independent calibration of the first rung is also valuable as an alternative to NGC 4258, should future analyses reveal previously unidentified systematic errors affecting its distance measurement.

A powerful alternative has recently become available through high signal-to-noise ratio measurements of the trigonometric parallaxes of Milky Way Cepheids using the Fine Guidance Sensor (FGS) on *HST*. Benedict et al. (2007) reported parallax measurements for 10 Cepheids, with mean individual precision of 8% and an error in the mean of the sample of 2.5%. These were used in R09 as a test of the distance scale provided by NGC 4258, but the improvement in precision beyond the first rung in the previous section suggests greater value in their use to enhance the calibration of the first rung.

van Leeuwen et al. (2007) reanalyzed *Hipparcos* observations and determined independent parallax measurements for the same 10 Cepheids (albeit with half the precision of *HST*/FGS) and for 3 additional Cepheids (excluding Polaris which is an overtone pulsator and whose estimated funda-

mental period is an outlier among the Cepheids pulsing in the fundamental mode). The resulting sample can be considered an independent anchor with a mean, nominal uncertainty of just 1.7%. We use the combined parallaxes tabulated by van Leeuwen et al. (2007) and their H-band photometry as an alternative to the Cepheid sample of NGC 4258 by replacing Equation (1) for the Cepheids in the hosts of SNe Ia with

$$m_{W,i,j} = \mu_{0,i} + M_{W,1} + b_W \log P_{i,j} + Z_W \Delta\log [\mathrm{O/H}]_{i,j}, \tag{6}$$

where $M_{W,1}$ is the absolute Wesenheit magnitude for a Cepheid with $P = 1$ d, and simultaneously fitting the Milky Way Cepheids with the relation

$$M_{W,i,j} = M_{W,1} + b_W \log P_{i,j} + Z_W \Delta\log [\mathrm{O/H}]_{i,j}. \tag{7}$$

Equation (3) for the SNe Ia is replaced with

$$m^0_{v,i} = \mu_{0,i} - M^0_V. \tag{8}$$

The determination of M^0_V for SNe Ia together with the previous term a_v then determines the Hubble constant,

$$\log H_0 = \frac{M^0_V + 5a_v + 25}{5}. \tag{9}$$

Since the near-IR magnitudes of these Milky Way Cepheids have not been directly measured with WFC3, the use of these variables requires an additional allowance for possible differences in their photometry. These may arise from differences in instrumental zeropoints, crowding, filter transmission functions, and detector well depth at which the sources are measured together with an uncertainty in detector linearity. Analysis of the absolute photometry from WFC3-IR (Kalirai et al. 2009) and the ground system (e.g., 2MASS; Skrutskie et al. 2006) claim absolute precision of 2%–3%. We therefore assume a *systematic* uncertainty in the relative magnitudes between *HST* WFC3 $F160W$ Cepheid photometry and the ground-based measurements of Milky Way Cepheids on the H-band system of Persson et al. (1998) of 4%. This reduces the effective precision of the parallax distance scale from 1.7% to 2.6%. The ground-based photometry of these Milky Way Cepheids is tabulated by Groenewegen (1999) and R09. This systematic error is included in the global fit as an additional calibration equation with uncertainty given in the error correlation matrix.

When using the Milky Way Cepheids, we now include an external constraint on the slope of the near-IR P–L relation. No such constraint was necessary or even of significant value in the previous section because the Cepheid periods in NGC 4258 (mean $\log P = 1.51$) are so similar to those in the SN Ia host (mean $\log P = 1.63$). In contrast, the mean period of the Milky Way sample (mean

$\log P = 1.0$) is substantially lower, giving an unconstrained slope of the P–L relation a greater and unrealistically large lever arm. Following analyses of optical and near-IR Cepheid data in the Milky Way (Fouqué et al. 2007) and the LMC (Persson et al. 2004; Udalski et al. 1999), we adopt a conservative constraint on the slope of the Wesenheit relation of -3.3 ± 0.1 mag per dex in $\log P$.

Using the Milky Way Cepheids instead of NGC 4258 as the first rung of the distance ladder gives 75.7 ± 2.6 km s^{-1} Mpc^{-1}, in good agreement with (and even greater precision than) the NGC 4258-based value. However, an overall improvement in precision is realized by the *simultaneous* use of both the Milky Way parallaxes and the megamaser-based distance to NGC 4258, yielding 74.5 ± 2.3 km s^{-1} Mpc^{-1}, a remarkably small uncertainty of 3.0% .

Another opportunity to improve upon the first rung on the distance ladder comes from the sample of H-band observations of Cepheids in the LMC by Persson et al. (2004). Recent studies of detached eclipsing binaries (DEBs) by different groups provide claims of a reliable and precise distance to the LMC. Guinan et al. (1998), Fitzpatrick et al. (2002), and Ribas et al. (2002) studied three B-type systems (HV2274, HV982, EROS1044) which lie close to the bar of the LMC and therefore provide a good match to the Cepheid sample of Persson et al. (2004). The error-weighted mean of these is 49.2 ± 1.6 kpc[5]. Pietrzyński et al. (2009) analyzed OGLE-051019.64-685812.3, an eclipsing binary system comprised of two giant G-type stars also located near the barycenter of the LMC, and found a distance of 50.2 ± 1.3 kpc. The average result, 49.8 kpc, provides a good estimate of the distance to the LMC[6]. Here we retain the larger of the two previous uncertainties to estimate the distance modulus as 18.486 ± 0.065 mag, or an effective error of ± 0.076 mag when including the aforementioned 0.04 mag uncertainty between the ground-based and *HST*-based near-IR photometric systems. Using this distance to the LMC and the Cepheid sample of Persson et al. (2004) yields 71.3 ± 3.8 km s^{-1} Mpc^{-1}, as seen in Table 4.

Combining all three first rungs (Milky Way, Large Magellanic Cloud, and NGC 4258) provides the most precise measurement of H_0: 73.8 ± 2.1 km s^{-1} Mpc^{-1}, a slightly smaller uncertainty of 2.9% . As expected, the use of all three anchors for the distance ladder instead of just one has the largest impact on the overall uncertainty, reducing the total contribution of the first rung to the error from 3.3% to 1.5%. However, a substantial penalty is paid for the mixing of ground-based and space-based photometric systems and the resultant uncertainties in Wesenheit or dereddened magnitudes, adding a 1.4% error to H_0 where for NGC 4258 alone none pertained. Modest increases in error also result from the larger difference in mean Cepheid metallicity (LMC) and period (LMC and Milky Way).

Past determinations of the absolute distance scale have had a checkered history, with revisions

[5]A fourth system (Fitzpatrick et al. 2003, HV5936,) is located several degrees away from the bar and yields a distance that is closer by 3σ. Additional lines of evidence presented in that paper suggest this system lies above the disk of the LMC, i.e., closer to the Galaxy.

[6]However, we note the analysis by Schaefer (2008), who suggests a level of agreement in recent distance estimates to the LMC which is too good to be consistent with statistics.

common. Thus, it may be prudent to rely on no more than any two of the three possible anchors of the distance scale in the determination of H_0. The omission of NGC 4258, Milky Way parallaxes, or the LMC yields a precision in H_0 of 3.3%, 3.2%, and 3.0%, respectively. We thus adopt as our best determination 73.8 ± 2.3 km s^{-1} Mpc^{-1}, the measurement from all three sources of the distance scale, but with the larger error associated from only two independent origins of the distance scale.

Should future work revise the distance to any one of the absolute distance scale determinations, we provide the following recalibration: H_0 decreases by 0.25, 0.30, and 0.14 km s^{-1} Mpc^{-1} for each increase of 1% in the distance to either NGC 4258, the Milky Way parallax scale, or the distance to the LMC.

In the last column of Table 3 we also give the best estimate of the distance to each host from the global fit to all first rungs, Cepheid and SN data. These are useful to compare to alternative methods of measuring distances to these hosts or to place a sample of relative measures of SNe Ia distances onto an absolute scale. For example, there has been recent dissagreement on the distance modulus of the Antennae (NGC 4038/9); Saviane et al. (2008) claim a value of μ_0=30.62 $\pm$0.17 mag based on the apparent tip of the red giant branch (TRGB), while Schweizer et al. (2008) obtain $\mu_0 = 31.74 \pm 0.27$ mag from SN 2007sr and $\mu_0 = 31.51 \pm 0.16$ mag from a different determination of the TRGB, in agreement with previous estimates by Whitmore et al. (1999) and Tonry et al. (2000) based on flow-field models. Our result of $\mu_0 = 31.66 \pm 0.08$ mag (with the uncertainty based on the global fit) strongly favors the "long" distance to the Antennae.

Although we have been careful to propagate our statistical errors, as well as past sources of systematic error such as metallicity dependence, system zeropoint, and instrumental uncertainties, we now consider a broader range of systematic uncertainties relating to alternative approaches to the analysis of the data.

4. Analysis Systematics

In the preceding section we presented our preferred approach to analyzing the Cepheid and SN Ia data, incorporating uncertainties within the framework used to model the data. Here we follow the same approach used by R09 to quantify the systematic uncertainty in the determination of H_0, by measuring the impact of a number of variants in the modeling of the Cepheid and SN Ia data.

In Table 4 we show 15 variants of the previously described analysis for every combination of choices of distance anchors (NGC 4258, Milky Way, or LMC), any two of the preceding or all three; these amount to a total of 105 combinations. Our primary analysis for any anchor choice is given in the first row (shown in bold) for which that choice initially appears. Column (1) gives the value of χ^2_ν, Column (2) the number of Cepheids in the fit, Column (3) the value and total uncertainty in H_0, and Column (4) whether the near-IR data for Cepheids with periods shorter than the completeness limit from the optical selection were included. Column (5) gives the SN Ia magnitude-redshift

intercept parameter, Column (6) gives the determination of M_V^0 which is specific to the light-curve fitter employed, Column (7) the calibration system for the metal abundances Column (8) the value and uncertainty in the metallicity dependence, and Column (9) the value and uncertainty of the slope of the Cepheid P–L or P–W relation. Column (10) gives the minimum SN Ia redshift used to define the m–z relation, Column (11) encodes aspects of the SN fitting routine and assumptions therein addressed below, and Column (12) is the choice of anchors to set the distance scale. Column (13) gives the type of P–L relation employed, either Wesenheit (H, V, I) or H-band only. Column (14) is the reddening law value used for the Cepheids. Column (15) lists the filters allowed for fitting the SN Ia light curves and column (16) gives the value of R_V used to fit the SN light curves.

4.1. Cepheid Systematics

In the preceding analysis of the Cepheid data, differences in the determination of H_0 may result from the following variants in the primary analysis: (1) retention of Cepheids with periods below the optical incompleteness limit; (2) not allowing for a metallicity dependence; (3) changing the Cepheid reddening law from $R_V = 3.1$ to $R_V = 2.5$; (4) using only near-IR magnitudes without reddening corrections; (5) no rejection of outliers in the P–L relations; and (6) a change in the calibration of chemical abundances. Each of these changes was implemented as a variant of the primary analysis with results given in Table 4. The rationale for the primary analysis over each variant was discussed in detail in §4 of R09, with the exception of (6) which is discussed below.

Taken individually, these variants result in H_0 rising or declining by $\lesssim 1.0$ km s^{-1} Mpc^{-1}, which is less than half of the statistical uncertainty. A variant resulting in a larger change occurs when we do not reject Cepheids which are outliers on the P–L relation, raising H_0 by 1.3 km s^{-1} Mpc^{-1}. However, the value of χ^2_ν also triples, with a total increase in χ^2 of 6 per rejected outlier. As we expect outliers *a priori* to arise from blending or misidentification of Cepheids (type or period), resulting in residuals in excess of the typical uncertainty, we believe it is most sensible to reject them to minimize their impact on the global solution. The use of higher or lower thresholds for outlier rejection has even less impact than including all outliers. Lowering the outlier threshold to 2.25σ (and its accompanying residual magnitude) reduces H_0 by 0.1 km s^{-1} Mpc^{-1}. Raising the threshold to 3.0 or 4.0σ reduces H_0 by 1.0 or 0.8 km s^{-1} Mpc^{-1}, respectively. Neglecting a reddening correction for the Cepheids also raises H_0 by 1.3 km s^{-1} Mpc^{-1} but we believe this correction is warranted.

As an alternative to rejecting outliers we also considered the approach of simultaneously modeling the distribution of Cepheids and the outliers. Following Kunz et al. (2007) we allowed for a nuisance population of sources along the P–L relation characterized by a broader distribution ($\sigma = 1$ mag) and an intercept independent from that of classical Cepheids. The *a posteri* likelihood function for the intercepts of the Cepheid hosts was then compared to that derived from outlier rejection. The mean zeropoint of the SN hosts is greater by 0.013 ± 0.012 mag. The mean uncertainty of the intercepts are a factor of 1.38 greater than those from outlier rejection but still small

compared to the distance precision of each SN. The only difference of note (i.e., > 0.03 mag) was for the intercept of NGC 4536 which was greater by 0.08 ± 0.05 mag in the outlier modeling over the use of rejection.

The chemical abundance values for the Cepheids used in R09 and here were estimated from nebular lines in H II regions of the Cepheid hosts using the R_{23} parameter and the transformation to an oxygen abundance following Zaritsky et al. (1994, hereafter ZKH). There are several alternative calibrations of the transformation from R_{23} to $\log[O/H]$ (e.g. McGaugh 1991; Pilyugin & Thuan 2005), but these primarily affect the absolute normalization of the metallicity scale and do not alter the relative host-to-host differences in abundance or the determination of H_0. Recently, Bresolin (2011) has redetermined the abundance gradient of NGC 4258 by adopting the Pilyugin & Thuan (2005) calibration of R_{23}. This calibration yields abundances that are consistent with those determined directly by Bresolin (2011) in 4 H II regions in the outer disk of NGC 4258, measuring the electron temperature (T_e) via the auroral line [O III] λ 4363. Given this agreement, Bresolin (2011) suggests the adoption of a so-called "T_e scale" for the determination of absolute chemical abundances of extragalactic Cepheids.

The T_e recalibration of nebular oxygen abundances not only reduces the values of $\log[O/H]$ by ~ 0.4 dex at the metal-rich end but also compresses the abundance scale by a factor of 0.69. Based on this scale and consistent atomic data, Bresolin (2011) finds a nebular oxygen abundance for the LMC of $12 + \log[O/H] = 8.36$, moderately lower than the "canonical" value of 8.5 in the ZKH scale. On the T_e scale, the mean apparent metallicity of the SN Ia and maser hosts would be $12 + log[O/H] = 8.42$; this is closer to the LMC Cepheids than to the Milky Way Cepheids and a departure from the ZKH scale. While the abundances of Milky Way Cepheids are not measured the same way (i.e., they are based on stellar absorption lines rather than on nearby ionized gas), they have been directly measured to be ~ 0.3 dex higher than those of LMC Cepheids (Andrievsky et al. 2002; Romaniello et al. 2008). The resulting estimate of 8.66 for the MW Cepheids on the T_e scale would agree well with recent estimates of the solar oxygen abundance of 8.69 (Asplund et al. 2009) together with a small gradient in metallicity away from the solar neighborhood. This LMC to MW Cepheid abundance difference of 0.3 dex also agrees well with the T_e scale compression of the 0.4 dex difference on the ZKH scale for which the value for MW Cepheids was taken (here and in R09) to be 8.9.

We determined the effect on H_0 of a change from the ZKH scale to the T_e scale by transforming the values of $12+\log[O/H]$ using equation (3) of Bresolin (2011) and assigning values of 8.36 and 8.66 to LMC and MW Cepheids, respectively. As seen in Table 4, the value of H_0 increases by 0.4 km s^{-1} Mpc^{-1} when using all 3 calibrators and increases by less than 1.0 km s^{-1} Mpc^{-1} for any combination of 2 calibrators. The biggest change, an increase of 2.0 km s^{-1} Mpc^{-1}, occurs when only the MW is used to calibrate the first rung, a direct consequence of the increase of the metallicity difference between the SN Ia host and MW Cepheids on the T_e scale. In the presence of uncertainties concerning the appropriate values of Cepheid abundances, the determination of H_0 based on *infrared* observations of Cepheids should be significantly less sensitive to metallicity

differences than optical Cepheid data (Marconi et al. 2005). Indeed, the metallicity correction empirically determined here, -0.10 ± 0.09 mag/dex (using all 3 calibrations) is less than half the value of ~ -0.25 mag/dex measured at optical wavelengths (Kennicutt et al. 1998; Sakai et al. 2004) and its absolute value is not significant. A better determination of the difference in metallicity between MW and extragalactic Cepheids may not occur until the launch of JWST.

4.2. SN Systematics

Here we consider the following variants in the analysis of the SN Ia data: (1) minimum range of SN Ia m–z relation lowered from $z = 0.023$ to $z = 0.01$, (2) discarding U-band SN Ia light-curve data (fit 61), (3) SN Ia reddening parameter $R_V = 1.5, 2.0, 3.1$ (fits 29, 28, and 20), (4) use of a SN Ia luminosity-color correction with no prior (i.e., as in the β parameter of SALT II instead of an extinction parameter, R_V, in MLCS2k2) (fit 26), (5) a host-galaxy extinction likelihood prior from galaxy simulations (fit 27), and (6) use of the SALT-II light-curve fitter (fit 42). The motivation for these variants is described in greater detail in R09.

As seen in Table 4, none of these variants taken individually alters the value of H_0 by more than ~ 1.5 km s^{-1} Mpc^{-1} from the preferred solution, less than half the statistical uncertainty. One of the more noteworthy variants is the use of the SALT-II light-curve fitter (Guy et al. 2005) *in lieu* of MLCS2k2, since the result of this change can be substantial for high-redshift data (Kessler et al. 2009). Observations of high-redshift SNe Ia typically have lower signal-to-noise ratios, and thus place greater reliance on fitters and on the assumptions they include (e.g., the relation between SN Ia color and distance). In contrast, the determination of H_0 is quite *insensitive* to the fitter; the use of SALT-II results in an increase in H_0 of 1 km s^{-1} Mpc^{-1}.

The dispersion of the 15 different determinations of H_0 is 0.7 or 0.8 km s^{-1} Mpc^{-1} for any selected pair of sources of the absolute distance scale. Adding this measure of analysis systematics to the previous yields 73.8 ± 2.4 km s^{-1} Mpc^{-1}, a 3.3% uncertainty, our best determination.

5. Dark Energy and Neutrinos

An independent and precise measurement of H_0 is an important complement to the determination of cosmological model parameters. Alternatively, it serves as a powerful test of model-constrained measurements at higher redshifts. It is beyond the scope of this paper to provide a complete analysis of the impact of the measurement of H_0 on the cosmological model from all extant data. We encourage others to do so. However, one such example using the present measurement of H_0 can be illustrative.

Making use of the simplest present hypothesis for the cosmological model (namely Λ-cold-dark-matter without curvature, exotic neutrino physics, or specific early-Universe physics), and using the

Table 5: H_0 Error Budget for Cepheid and SN Ia Distance Ladders*

Term	Description	Previous LMC	R09 N4258	Here N4258	Here All 3
$\sigma_{\rm anchor}$	Anchor distance	5%	3%	3%	1.3%
$\sigma_{{\rm anchor}-PL}$	Mean of P–L in anchor	2.5%	1.5%	1.4%	0.7%[a]
$\sigma_{{\rm host}-PL}/\sqrt{n}$	Mean of P–L values in SN hosts	1.5%	1.5%	0.6 %	0.6%
$\sigma_{\rm SN}/\sqrt{n}$	Mean of SN Ia calibrators	2.5%	2.5%	1.9%	1.9%
σ_{m-z}	SN Ia m–z relation	1%	0.5%	0.5%	0.5%
$R\sigma_{\lambda,1,2}$	Cepheid reddening, zeropoints, anchor-to-hosts	4.5%	0.3%	0.0%	1.4%
σ_Z	Cepheid metallicity, anchor-to-hosts	3%	1.1%	0.6 %	1.0%
$\sigma_{\rm PL}$	P–L slope, Δ log P, anchor-to-hosts	4%	0.5%	0.4%	0.6%
$\sigma_{\rm WFPC2}$	WFPC2 CTE, long-short	3%	0%	0%	0%
subtotal, σ_{H_0}		10%	4.7 %	4.0%	2.9%
Analysis Systematics		NA	1.3%	1.0%	1.0%
Total, σ_{H_0}		10%	4.8 %	4.1%	3.1%

*Derived from diagonal elements of the covariance matrix propagated via the error matrices associated with Equations 1, 3, 7, and 8.

[a]For Milky Way parallax, this term is already included with the term above.

single most powerful cosmological data set (the 7-year WMAP results from Komatsu et al. 2011), results in a predicted value of $H_0 = 71.0 \pm 2.5$ km s^{-1} Mpc^{-1}. This value agrees well with our determination of 73.8 ± 2.4 km s^{-1} Mpc^{-1}at better than the combined 1σ confidence level.

Alternatively, we can use the WMAP data together with the measured value of H_0 to constrain added complexity to the model. In Figure 10 we show the use of this data combination for constraining a redshift-independent dark energy equation-of-state parameter (w), the number of relativistic species (e.g., neutrino number), and the sum of neutrino masses. The result for dark energy is $w = -1.08 \pm 0.10$, about 20% more precise than the same result derived from the determination of H_0 in R09. If we had perfect knowledge of the CMB, our overall 30% increase in the precision of H_0 would yield the same-sized improvement in the determination of w. However, the fractional uncertainty in $\Omega_M h^2$ from the WMAP 7-year analysis is comparable to our measurement of H_0; thus, greater precision in w may still be wrung from future higher-precision measurements of the CMB by WMAP or *Planck*.

The enhanced precision in measuring H_0 also provides a strong rebuff to recent attempts to explain accelerated expansion without dark energy but rather by our presence in the center of a massive void of gigaparsec scale. Already such models are hard to fathom as they require an exotic location for the observer, at the center of the void to within a part in a million (Blomqvist & Mörtsell 2010) to avoid an excess dipole in the CMB. It is also not yet apparent if such a model is consistent with other observables of the CMB or the late-time integrated Sachs-Wolfe effect. However, using measurements of $H(z > 1)$ to constrain void models of the Lemaitre, Tolmon, and Bondi variety

already predicts slower-than-observed local expansion with values of H_0=60 (Nadathur & Sarkar 2010) or 62 (Wiltshire 2007) km s^{-1} Mpc^{-1}, more than 5 σ below our measurement.

Comparable improvements to cosmological constraints on relativistic species are also realized from R09, as shown in Figure 10. Most interesting may be the effective number of relativistic species, $N_{\rm eff} = 4.2 \pm 0.75$, which is nominally higher than the value of 3.046 expected from the three known neutrino species plus tau-neutrino heating from e^+e^- collisions (Mangano & Serpico 2005). While this nominal excess of relativistic species has been noted previously (Reid et al. 2010; Komatsu et al. 2011; Dunkley et al. 2010, e.g.,), and even interpreted as a possible indication of the presence of a sterile neutrino (Hamann et al. 2010), we caution that the cosmological model provides other avenues for reducing the significance of this result including additional degrees of freedom for curvature, dark energy, primordial helium abundance, and neutrino masses. The 30% improvement in the present constraint on H_0 combined with improved high resolution CMB data (e.g., Dunkley et al. (2010)) and ultimately with *Planck* satellite CMB data should reduce the present uncertainty in $N_{\rm eff}$ by a factor of ~ 3 which may provide a more definitive conclusion on the presence of excess radiation in the early Universe.

6. Discussion

Examination of the complete error budget for H_0 in the last two columns of Table 5 indicates additional approaches for improved precision in future measurements of H_0. Expanding the sample of well-measured parallaxes to Milky Way Cepheids (especially those at $\log P > 1$) with the GAIA satellite could drive the precision of the first rung of the distance ladder well under 1%. However, as we have found with the "baker's dozen" of present Milky Way parallaxes, much of this precision would be lost without better cross-calibration between the space and ground photometric systems used to measure Cepheids, near and far.

The largest remaining term comes from the quite limited sample of ideal SN Ia calibrators, just 8 objects. The occurrence of an ideal SN Ia in the small volume within which *HST* can measure Cepheids ($R \approx 30$ Mpc) is rare, on average only once every 2–3 yr. Given the recent proliferation of SN surveys and instances of multiple, independent discoveries, we are confident that all such SNe Ia within this volume are being found. Collecting more will require extending the range of Cepheid measurements — without introducing new systematics — and patience. The forthcoming *James Webb Space Telescope (JWST)* offers a promising route to extend Cepheid observations out to 50 Mpc and to redder wavelengths, where uncertainties due to possible variations in the extinction law and the dependence of Cepheid luminosities on metallicity are further reduced. This extension would increase the SN sample suitable for calibration by a factor of ~ 5, reaching ~ 40 ideal SNe Ia observed over the past 20 yr. Based on a 5% distance precision per ideal SN, such a sample would enable a determination of H_0 to better than 1%. However, discovering these Cepheids may require imaging at optical wavelengths where the amplitude of the variations is significant, a requirement which will challenge the short-wavelength capabilities of *JWST*.

7. Summary and Conclusions

We have improved upon the precision of the measurement of H_0 from Riess et al. (2009a) by (1) more than doubling the sample of Cepheids observed in the near-IR in SN Ia host galaxies, (2) expanding the SN Ia sample from 6 to 8 with the addition of SN 2007af and SN 2007sr, (3) increasing the sample of Cepheids observed in NGC 4258 by 20%, (4) reducing the difference in metallicity for the observed sample of Cepheids between the calibrator and the SN hosts, and (5) calibrating all optical Cepheid colors with WFC3 to remove cross-instrument zeropoint errors. Further improvements to the precision and reliability of the measurement of H_0 come from the use of additional sources of calibration for the first rung, foremost of these are the trigonometric parallaxex of 13 Cepheids in the Milky Way.

Our primary analysis gives $H_0 = 73.8 \pm 2.4$ km s^{-1} Mpc^{-1} including systematic errors determined from varying assumptions and priors used in the analysis. The combination of this result alone with the WMAP 7-year constraints yields $w = -1.08 \pm 0.10$ and improves constraints on a possible but still uncertain excess in relativistic species above the number of known neutrino flavors. The measured H_0 is also highly inconsistent with the simplest inhomogeneous matter models invoked to explain the apparent acceleration of the Universe without dark energy. Given that statistical errors still dominate over systematic errors, future work is likely to further improve the precision of the determination of H_0.

We are grateful to William Januszewski for his help in executing this program on *HST*. We are indebted to Mike Hudson for assisting with the peculiar-velocity calculations from the PSCz survey, to David Larson for contributions to the WMAP MCMC analysis, to Daniel Scolnic for donating some useful routines, and to Mark Huber for an analysis of pre-discovery observations of SN 2007sr. We thank Chris Kochanek and Kris Stanek for their support of GO-11570. Financial support for this work was provided by NASA through programs GO-11570 and GO-10802 from the Space Telescope Science Institute, which is operated by AURA, Inc., under NASA contract NAS 5-26555. A.V.F.'s supernova group at U. C. Berkeley is also supported by NSF grant AST–0607485 and by the TABASGO Foundation. L.M.M. acknowledges support from a Texas A&M University faculty startup fund. The metallicity measurements for NGC 5584 and NGC 4038/9 presented herein were obtained with the W. M. Keck Observatory, which is operated as a scientific partnership among the California Institute of Technology, the University of California, and NASA; the observatory was made possible by the generous financial support of the W. M. Keck Foundation.

Figure Captions

Figure 1: *HST* observations of the host galaxies used to measure H_0. The data employed to observe Cepheids in 8 SN Ia hosts and NGC 4258 have been collected over 15 yr with 4 cameras over ~ 500 orbits of *HST* time. Two-month long campaigns in $F555W$ and $F814W$ were initially used to discover Cepheids from their light curves. Subsequent follow-up observations in $F555W$ enabled the discovery of Cepheids with $P > 60$ d. Near-IR follow-up data have been used to reduce the effects of host-galaxy extinction and sensitivity to metallicity.

Figure 2: *HST* images of NGC 5584. The positions of Cepheids with periods in the range $P > 60$ d, $30 < P < 60$ d, and $10 < P < 30$ d are indicated by red, blue, and green circles, respectively. A yellow circle indicates the position of the host galaxy's SN Ia. The orientation is indicated by the compass rose whose vectors have lengths of $15''$. The black and white regions of the images show the WFC3 optical data and the color includes the WFC3-IR data.

Figure 3. As in Figure 2, for NGC 4038/4039.

Figure 4: *HST* WFC3-$F160W$ image of NGC 3370. Upper panel: The positions of Cepheids with periods in the range $P > 60$ d, $30 < P < 60$ d, and $10 < P < 30$ d are indicated by red, blue, and green circles, respectively. A yellow circle indicates the position of the host galaxy's SN Ia. The orientation is indicated by the compass rose whose vectors have lengths of $15''$. The fields of view for the NIC2 follow-up fields from Riess et al. (2009a) are indicated. Lower Panel: close-up showing the field of NGC3370-blue as observed with WFC3-IR (left) and with 4.7 times more exposure time with NIC2 (right).

Figure 5: Example of scene modeling for the $\sim 1''$ surrounding typical short, medium, and long-period Cepheids in one WFC3 field, NGC 5584. For each Cepheid, the stamp on the left shows the region around the Cepheid, the middle stamp shows the model of the stellar sources, and the right stamp is the residual of the image minus the model. The position of the Cepheid as determined from the optical data is indicated by the circle.

Figure 6: WFC3-IR versus NIC2 $F160W$ Cepheid photometry. Some of the apparent dispersion results from the random phases of the Cepheids observed with WFC3.

Figure 7: Near-IR Cepheid period-luminosity relations. For the 8 SN Ia hosts and the distance-scale anchor, NGC 4258, the Cepheid magnitudes are from the same instrument and filter combination, WFC3 $F160W$. This uniformity allows for a significant reduction in systematic error when utilizing the difference in these relations along the distance ladder. The measured metallicity for all of the Cepheids is comparable to solar ($\log [\mathrm{O/H}] \approx 8.9$). A single slope has been fit to the relations and is shown as the solid line. 20% of the objects were outliers from the relations (open diamonds) and are flagged as such for the subsequent analysis. Filled points with asterisks indicate Cepheids whose periods are shorter than the incompleteness limit identified from their optical detection.

Figure 8: Relative distances from Cepheids and SNe Ia. The bottom abscissa shows the peak apparent visual magnitude of each SN Ia (red points) corrected for reddening and to the fiducial

brightness (using the luminosity vs. light-curve shape relations), m_V^0. The top abscissa includes the intercept of the m_V^0–$\log cz$ relation for SNe Ia, a_v to provide SN Ia distance measures, $m_V^0 + 5a_v$, quantities which are independent of the choice of a fiducial SN Ia. The right-hand ordinate shows the relative distances between the hosts determined from the Cepheid VIH Wesenheit relations. The left ordinate shows the same thing, with the addition of the independent geometric distance to NGC 4258 (blue point) based on its circumnuclear megamasers. The contribution of the nearby SN Ia and Cepheid data to H_0 can be expressed as a determination of $m_{V,4258}^0$, the theoretical mean of 8 fiducial SNe Ia in NGC 4258.

Figure 9: Uncertainties in the determination of the Hubble constant. Uncertainties are squared to show their contribution to the quadrature sum. These terms are given in Table 5.

Figure 10: Confidence regions in the plane of H_0 and the equation-of-state parameter of dark energy, w and neutrino properties. The localization of the third acoustic peak in the WMAP 7-year data (Komatsu et al. 2011) produces a confidence region which is narrow but highly degenerate with the dark energy equation of state (upper panel). The improved measurement of H_0, 73.8 ± 2.4 km s^{-1} Mpc^{-1}, from the SH0ES program is complementary to the WMAP constraint, resulting in a determination of $w = -1.08 \pm 0.10$ assuming a constant w. This result is comparable in precision to determinations of w from baryon acoustic oscillations and high-redshift SNe Ia, but is independent of both. The inner regions are 68% confidence and the outer regions are 95% confidence. The modest tilt of the SH0ES measurement of 0.2% in H_0 for a change in w of 0.1 shown as the dotted lines in the upper panel, results from the mild dependence of a_v on w, corresponding to the change in H for changes from $w = -1$ at the mean SN rdshift of $z = 0.04$. The measurement of H_0 is made at $j_0 = 1$ (i.e., $w = -1$). Constraints on the mass and number of relativisitic species (e.g., neutrinos) are shown in the middle and lower panels, respectively.

REFERENCES

Andrievsky, S. M., Kovtyukh, V. V., Luck, R. E., Lépine, J. R. D., Bersier, D., Maciel, W. J., Barbuy, B., Klochkova, V. G., Panchuk, V. E., & Karpischek, R. U. 2002, A&A, 381, 32

Argon, A. L., Greenhill, L. J., Reid, M. J., Moran, J. M., & Humphreys, E. M. L. 2007, ApJ, 659, 1040

Asplund, M., Grevesse, N., Sauval, A. J., & Scott, P. 2009, ARA&A, 47, 481

Benedict, G. F., McArthur, B. E., Feast, M. W., Barnes, T. G., Harrison, T. E., Patterson, R. J., Menzies, J. W., Bean, J. L., & Freedman, W. L. 2007, AJ, 133, 1810

Blomqvist, M. & Mörtsell, E. 2010, J. Cosmology Astropart. Phys., 5, 6

Branchini, E., Teodoro, L., Frenk, C. S., Schmoldt, I., Efstathiou, G., White, S. D. M., Saunders, W., Sutherland, W., Rowan-Robinson, M., Keeble, O., Tadros, H., Maddox, S., & Oliver, S. 1999, MNRAS, 308, 1

Bresolin, F. 2011, ApJ, in press

Cardelli, J. A., Clayton, G. C., & Mathis, J. S. 1989, ApJ, 345, 245

Dunkley, J., Hlozek, R., Sievers, J., Acquaviva, V., Ade, P. A. R., Aguirre, P., Amiri, M., Appel, J. W., Barrientos, L. F., Battistelli, E. S., Bond, J. R., Brown, B., Burger, B., Chervenak, J., Das, S., Devlin, M. J., Dicker, S. R., Bertrand Doriese, W., Dunner, R., Essinger-Hileman, T., Fisher, R. P., Fowler, J. W., Hajian, A., Halpern, M., Hasselfield, M., Hernandez-Monteagudo, C., Hilton, G. C., Hilton, M., Hincks, A. D., Huffenberger, K. M., Hughes, D. H., Hughes, J. P., Infante, L., Irwin, K. D., Juin, J. B., Kaul, M., Klein, J., Kosowsky, A., Lau, J. M., Limon, M., Lin, Y., Lupton, R. H., Marriage, T. A., Marsden, D., Mauskopf, P., Menanteau, F., Moodley, K., Moseley, H., Netterfield, C. B., Niemack, M. D., Nolta, M. R., Page, L. A., Parker, L., Partridge, B., Reid, B., Sehgal, N., Sherwin, B., Spergel, D. N., Staggs, S. T., Swetz, D. S., Switzer, E. R., Thornton, R., Trac, H., Tucker, C., Warne, R., Wollack, E., & Zhao, Y. 2010, ArXiv e-prints

Fitzpatrick, E. L., Ribas, I., Guinan, E. F., DeWarf, L. E., Maloney, F. P., & Massa, D. 2002, ApJ, 564, 260

Fitzpatrick, E. L., Ribas, I., Guinan, E. F., Maloney, F. P., & Claret, A. 2003, ApJ, 587, 685

Fouqué, P., Arriagada, P., Storm, J., Barnes, T. G., Nardetto, N., Mérand, A., Kervella, P., Gieren, W., Bersier, D., Benedict, G. F., & McArthur, B. E. 2007, A&A, 476, 73

Freedman, W. L. & Madore, B. F. 2010, ARA&A, 48, 673

Freedman, W. L., Madore, B. F., Gibson, B. K., Ferrarese, L., Kelson, D. D., Sakai, S., Mould, J. R., Kennicutt, Jr., R. C., Ford, H. C., Graham, J. A., Huchra, J. P., Hughes, S. M. G., Illingworth, G. D., Macri, L. M., & Stetson, P. B. 2001, ApJ, 553, 47

Ganeshalingam, M., Li, W., Filippenko, A. V., Anderson, C., Foster, G., Gates, E. L., Griffith, C. V., Grigsby, B. J., Joubert, N., Leja, J., Lowe, T. B., Macomber, B., Pritchard, T., Thrasher, P., & Winslow, D. 2010, ApJS, 190, 418

Gibson, B. K. 2000, Mem. Soc. Astron. Italiana, 71, 693

Gibson, B. K., Stetson, P. B., Freedman, W. L., Mould, J. R., Kennicutt, Jr., R. C., Huchra, J. P., Sakai, S., Graham, J. A., Fassett, C. I., Kelson, D. D., Ferrarese, L., Hughes, S. M. G., Illingworth, G. D., Macri, L. M., Madore, B. F., Sebo, K. M., & Silbermann, N. A. 2000, ApJ, 529, 723

Greenhill, L. 2009, in ArXiv Astrophysics e-prints, Vol. 2010, astro2010: The Astronomy and Astrophysics Decadal Survey, 103

Groenewegen, M. A. T. 1999, A&AS, 139, 245

Guinan, E. F., Fitzpatrick, E. L., Dewarf, L. E., Maloney, F. P., Maurone, P. A., Ribas, I., Pritchard, J. D., Bradstreet, D. H., & Giménez, A. 1998, ApJ, 509, L21

Guy, J., Astier, P., Nobili, S., Regnault, N., & Pain, R. 2005, A&A, 443, 781

Hamann, J., Hannestad, S., Raffelt, G. G., Tamborra, I., & Wong, Y. Y. Y. 2010, Physical Review Letters, 105, 181301

Herrnstein, J. R., Moran, J. M., Greenhill, L. J., Diamond, P. J., Inoue, M., Nakai, N., Miyoshi, M., Henkel, C., & Riess, A. 1999, Nature, 400, 539

Hicken, M., Challis, P., Jha, S., Kirshner, R. P., Matheson, T., Modjaz, M., Rest, A., Wood-Vasey, W. M., Bakos, G., Barton, E. J., Berlind, P., Bragg, A., Briceño, C., Brown, W. R., Caldwell, N., Calkins, M., Cho, R., Ciupik, L., Contreras, M., Dendy, K., Dosaj, A., Durham, N., Eriksen, K., Esquerdo, G., Everett, M., Falco, E., Fernandez, J., Gaba, A., Garnavich, P., Graves, G., Green, P., Groner, T., Hergenrother, C., Holman, M. J., Hradecky, V., Huchra, J., Hutchison, B., Jerius, D., Jordan, A., Kilgard, R., Krauss, M., Luhman, K., Macri, L., Marrone, D., McDowell, J., McIntosh, D., McNamara, B., Megeath, T., Mochejska, B., Munoz, D., Muzerolle, J., Naranjo, O., Narayan, G., Pahre, M., Peters, W., Peterson, D., Rines, K., Ripman, B., Roussanova, A., Schild, R., Sicilia-Aguilar, A., Sokoloski, J., Smalley, K., Smith, A., Spahr, T., Stanek, K. Z., Barmby, P., Blondin, S., Stubbs, C. W., Szentgyorgyi, A., Torres, M. A. P., Vaz, A., Vikhlinin, A., Wang, Z., Westover, M., Woods, D., & Zhao, P. 2009a, ApJ, 700, 331

Hicken, M., Wood-Vasey, W. M., Blondin, S., Challis, P., Jha, S., Kelly, P. L., Rest, A., & Kirshner, R. P. 2009b, ApJ, 700, 1097

Hui, L. & Greene, P. B. 2006, Phys. Rev. D, 73, 123526

Humphreys, E. M. L., Argon, A. L., Greenhill, L. J., Moran, J. M., & Reid, M. J. 2005, in Astronomical Society of the Pacific Conference Series, Vol. 340, Future Directions in High Resolution Astronomy, ed. J. Romney & M. Reid, 466

Humphreys, E. M. L., Reid, M. J., Greenhill, L. J., Moran, J. M., & Argon, A. L. 2008, ApJ, 672, 800

Jha, S., Riess, A. G., & Kirshner, R. P. 2007, ApJ, 659, 122

Kalirai, J. S., Deustua, S., Baggett, S., Bohlin, R., Brown, T., MacKenty, J., McCullough, P., Rajan, A., Riess, A., Sabbi, E., & Sirianni, M. 2009, The Photometric Calibration of WFC3: SMOV and Cycle 17 Observing Plan, Tech. rep., Space Telescope Science Institute

Kelly, P. L., Hicken, M., Burke, D. L., Mandel, K. S., & Kirshner, R. P. 2010, ApJ, 715, 743

Kennicutt, Jr., R. C., Stetson, P. B., Saha, A., Kelson, D., Rawson, D. M., Sakai, S., Madore, B. F., Mould, J. R., Freedman, W. L., Bresolin, F., Ferrarese, L., Ford, H., Gibson, B. K., Graham, J. A., Han, M., Harding, P., Hoessel, J. G., Huchra, J. P., Hughes, S. M. G., Illingworth, G. D., Macri, L. M., Phelps, R. L., Silbermann, N. A., Turner, A. M., & Wood, P. R. 1998, ApJ, 498, 181

Kessler, R., Becker, A. C., Cinabro, D., Vanderplas, J., Frieman, J. A., Marriner, J., Davis, T. M., Dilday, B., Holtzman, J., Jha, S. W., Lampeitl, H., Sako, M., Smith, M., Zheng, C., Nichol, R. C., Bassett, B., Bender, R., Depoy, D. L., Doi, M., Elson, E., Filippenko, A. V., Foley, R. J., Garnavich, P. M., Hopp, U., Ihara, Y., Ketzeback, W., Kollatschny, W., Konishi, K., Marshall, J. L., McMillan, R. J., Miknaitis, G., Morokuma, T., Mörtsell, E., Pan, K., Prieto, J. L., Richmond, M. W., Riess, A. G., Romani, R., Schneider, D. P., Sollerman, J., Takanashi, N., Tokita, K., van der Heyden, K., Wheeler, J. C., Yasuda, N., & York, D. 2009, ApJS, 185, 32

Komatsu, E., Smith, K. M., Dunkley, J., Bennett, C. L., Gold, B., Hinshaw, G., Jarosik, N., Larson, D., Nolta, M. R., Page, L., Spergel, D. N., Halpern, M., Hill, R. S., Kogut, A., Limon, M., Meyer, S. S., Odegard, N., Tucker, G. S., Weiland, J. L., Wollack, E., & Wright, E. L. 2011, ApJS, "in press"

Kunz, M., Bassett, B. A., & Hlozek, R. A. 2007, Phys. Rev. D, 75, 103508

Lampeitl, H., Smith, M., Nichol, R. C., Bassett, B., Cinabro, D., Dilday, B., Foley, R. J., Frieman, J. A., Garnavich, P. M., Goobar, A., Im, M., Jha, S. W., Marriner, J., Miquel, R., Nordin, J., Östman, L., Riess, A. G., Sako, M., Schneider, D. P., Sollerman, J., & Stritzinger, M. 2010, ApJ, 722, 566

Macri, L. M., Riess, A. G., Casertano, S., Lampeitl, H., Ferguson, H. C., Filippenko, A. V., Jha, S. W., Li, W., & Chornock, R. 2011a, ApJS, in prep.

Macri, L. M., Riess, A. G., Casertano, S., Lampeitl, H., Ferguson, H. C., Filippenko, A. V., Jha, S. W., Li, W., Chornock, R., & Welch, D. L. 2011b, ApJ, in prep.

Macri, L. M., Riess, A. G., Casertano, S., Lampeitl, H., Ferguson, H. C., Filippenko, A. V., Jha, S. W., Li, W., Chornock, R., Welch, D. L., & Withmore, B. C. 2011c, ApJ, in prep.

Macri, L. M., Stanek, K. Z., Bersier, D., Greenhill, L. J., & Reid, M. J. 2006, ApJ, 652, 1133

Madore, B. F. 1982, ApJ, 253, 575

Madore, B. F. & Freedman, W. L. 1991, PASP, 103, 933

Mangano, G. & Serpico, P. D. 2005, Nuclear Physics B Proceedings Supplements, 145, 351

Marconi, M., Musella, I., & Fiorentino, G. 2005, ApJ, 632, 590

McGaugh, S. S. 1991, ApJ, 380, 140

Nadathur, S. & Sarkar, S. 2010, ArXiv e-prints

Neill, J. D., Hudson, M. J., & Conley, A. 2007, ApJ, 661, L123

Neill, J. D., Sullivan, M., Howell, D. A., Conley, A., Seibert, M., Martin, D. C., Barlow, T. A., Foster, K., Friedman, P. G., Morrissey, P., Neff, S. G., Schiminovich, D., Wyder, T. K., Bianchi, L., Donas, J., Heckman, T. M., Lee, Y., Madore, B. F., Milliard, B., Rich, R. M., & Szalay, A. S. 2009, ApJ, 707, 1449

Perlmutter, S., Aldering, G., Goldhaber, G., Knop, R. A., Nugent, P., Castro, P. G., Deustua, S., Fabbro, S., Goobar, A., Groom, D. E., Hook, I. M., Kim, A. G., Kim, M. Y., Lee, J. C., Nunes, N. J., Pain, R., Pennypacker, C. R., Quimby, R., Lidman, C., Ellis, R. S., Irwin, M., McMahon, R. G., Ruiz-Lapuente, P., Walton, N., Schaefer, B., Boyle, B. J., Filippenko, A. V., Matheson, T., Fruchter, A. S., Panagia, N., Newberg, H. J. M., Couch, W. J., & The Supernova Cosmology Project. 1999, ApJ, 517, 565

Persson, S. E., Madore, B. F., Krzemiński, W., Freedman, W. L., Roth, M., & Murphy, D. C. 2004, AJ, 128, 2239

Persson, S. E., Murphy, D. C., Krzeminski, W., Roth, M., & Rieke, M. J. 1998, AJ, 116, 2475

Pietrzyński, G., Thompson, I. B., Graczyk, D., Gieren, W., Udalski, A., Szewczyk, O., Minniti, D., Kołaczkowski, Z., Bresolin, F., & Kudritzki, R. 2009, ApJ, 697, 862

Pike, R. W. & Hudson, M. J. 2005, ApJ, 635, 11

Pilyugin, L. S. & Thuan, T. X. 2005, ApJ, 631, 231

Reid, B. A., Verde, L., Jimenez, R., & Mena, O. 2010, J. Cosmology Astropart. Phys., 1, 3

Ribas, I., Fitzpatrick, E. L., Maloney, F. P., Guinan, E. F., & Udalski, A. 2002, ApJ, 574, 771

Riess, A. G., Davis, M., Baker, J., & Kirshner, R. P. 1997, ApJ, 488, L1+

Riess, A. G., Filippenko, A. V., Challis, P., Clocchiatti, A., Diercks, A., Garnavich, P. M., Gilliland, R. L., Hogan, C. J., Jha, S., Kirshner, R. P., Leibundgut, B., Phillips, M. M., Reiss, D., Schmidt, B. P., Schommer, R. A., Smith, R. C., Spyromilio, J., Stubbs, C., Suntzeff, N. B., & Tonry, J. 1998, AJ, 116, 1009

Riess, A. G., Li, W., Stetson, P. B., Filippenko, A. V., Jha, S., Kirshner, R. P., Challis, P. M., Garnavich, P. M., & Chornock, R. 2005, ApJ, 627, 579

Riess, A. G., Macri, L., Casertano, S., Sosey, M., Lampeitl, H., Ferguson, H. C., Filippenko, A. V., Jha, S. W., Li, W., Chornock, R., & Sarkar, D. 2009a, ApJ, 699, 539

Riess, A. G., Macri, L., Li, W., Lampeitl, H., Casertano, S., Ferguson, H. C., Filippenko, A. V., Jha, S. W., Chornock, R., Greenhill, L., Mutchler, M., Ganeshalingham, M., & Hicken, M. 2009b, ApJS, 183, 109

Riess, A. G., Strolger, L., Casertano, S., Ferguson, H. C., Mobasher, B., Gold, B., Challis, P. J., Filippenko, A. V., Jha, S., Li, W., Tonry, J., Foley, R., Kirshner, R. P., Dickinson, M., MacDonald, E., Eisenstein, D., Livio, M., Younger, J., Xu, C., Dahlén, T., & Stern, D. 2007, ApJ, 659, 98

Romaniello, M., Primas, F., Mottini, M., Pedicelli, S., Lemasle, B., Bono, G., François, P., Groenewegen, M. A. T., & Laney, C. D. 2008, A&A, 488, 731

Saha, A., Sandage, A., Labhardt, L., Tammann, G. A., Macchetto, F. D., & Panagia, N. 1996, ApJ, 466, 55

—. 1997, ApJ, 486, 1

Saha, A., Sandage, A., Tammann, G. A., Dolphin, A. E., Christensen, J., Panagia, N., & Macchetto, F. D. 2001, ApJ, 562, 314

Sakai, S., Ferrarese, L., Kennicutt, Jr., R. C., & Saha, A. 2004, ApJ, 608, 42

Sandage, A., Tammann, G. A., Saha, A., Reindl, B., Macchetto, F. D., & Panagia, N. 2006, ApJ, 653, 843

Saviane, I., Momany, Y., da Costa, G. S., Rich, R. M., & Hibbard, J. E. 2008, ApJ, 678, 179

Schaefer, B. E. 2008, AJ, 135, 112

Schweizer, F., Burns, C. R., Madore, B. F., Mager, V. A., Phillips, M. M., Freedman, W. L., Boldt, L., Contreras, C., Folatelli, G., González, S., Hamuy, M., Krzeminski, W., Morrell, N. I., Persson, S. E., Roth, M. R., & Stritzinger, M. D. 2008, AJ, 136, 1482

Skrutskie, M. F., Cutri, R. M., Stiening, R., Weinberg, M. D., Schneider, S., Carpenter, J. M., Beichman, C., Capps, R., Chester, T., Elias, J., Huchra, J., Liebert, J., Lonsdale, C., Monet, D. G., Price, S., Seitzer, P., Jarrett, T., Kirkpatrick, J. D., Gizis, J. E., Howard, E., Evans, T., Fowler, J., Fullmer, L., Hurt, R., Light, R., Kopan, E. L., Marsh, K. A., McCallon, H. L., Tam, R., Van Dyk, S., & Wheelock, S. 2006, AJ, 131, 1163

Soszyński, I., Gieren, W., & Pietrzyński, G. 2005, PASP, 117, 823

Stetson, P. B. & Gibson, B. K. 2001, MNRAS, 328, L1

Sullivan, M., Conley, A., Howell, D. A., Neill, J. D., Astier, P., Balland, C., Basa, S., Carlberg, R. G., Fouchez, D., Guy, J., Hardin, D., Hook, I. M., Pain, R., Palanque-Delabrouille, N., Perrett, K. M., Pritchet, C. J., Regnault, N., Rich, J., Ruhlmann-Kleider, V., Baumont, S.,

Hsiao, E., Kronborg, T., Lidman, C., Perlmutter, S., & Walker, E. S. 2010, MNRAS, 406, 782

Tonry, J. L., Blakeslee, J. P., Ajhar, E. A., & Dressler, A. 2000, ApJ, 530, 625

Udalski, A., Soszynski, I., Szymanski, M., Kubiak, M., Pietrzynski, G., Wozniak, P., & Zebrun, K. 1999, Acta Astron., 49, 223

van Leeuwen, F., Feast, M. W., Whitelock, P. A., & Laney, C. D. 2007, MNRAS, 379, 723

Whitmore, B. C., Zhang, Q., Leitherer, C., Fall, S. M., Schweizer, F., & Miller, B. W. 1999, AJ, 118, 1551

Wiltshire, D. L. 2007, Physical Review Letters, 99, 251101

Zaritsky, D., Kennicutt, Jr., R. C., & Huchra, J. P. 1994, ApJ, 420, 87

Table 2. WFC3-IR Cepheids

Field	α (J2000)	δ (J2000)	Id	P (days)	$V-I$ (mag)	$F160W$ (mag)	σ (mag)	Offset (pix)	Bias (mag)	IM_{rms}	[O/H]	Flag
n4536	188.590	2.16830	27185	13.00	0.97	24.91	0.31	1.64	0.13	2.16	8.54	
n4536	188.604	2.18312	42353	13.07	0.73	26.29	0.74	3.32	0.37	4.30	8.97	rej
n4536	188.584	2.18070	50718	13.73	0.88	24.51	0.42	0.88	0.28	11.4	8.64	
n4536	188.583	2.19700	72331	13.91	0.89	24.84	0.44	0.07	0.22	1.40	8.81	
n4536	188.590	2.19545	65694	14.38	0.98	25.26	0.38	2.91	0.39	30.8	8.90	
n4536	188.587	2.18864	58805	14.44	1.13	23.41	0.35	3.94	0.26	47.9	8.78	rej
n4536	188.586	2.18406	53703	14.53	0.72	25.38	0.47	0.63	0.27	14.9	8.72	
n4536	188.592	2.20025	70938	14.62	0.64	25.81	0.58	2.39	0.30	17.4	8.94	rej
n4536	188.594	2.17693	40098	14.64	0.95	25.12	0.52	4.40	0.63	12.9	8.72	
n4536	188.597	2.18489	48539	15.03	0.90	23.53	0.31	0.46	0.29	7.28	8.89	rej
n4536	188.590	2.19521	65695	15.16	1.03	24.49	0.41	1.45	0.26	19.3	8.89	
n4536	188.584	2.19350	66974	15.65	1.13	23.43	0.44	0.85	0.56	71.9	8.79	rej
n4536	188.588	2.19589	67328	16.24	0.82	23.98	0.32	0.76	0.24	30.2	8.87	
n4536	188.593	2.20097	71258	17.02	0.82	24.01	0.27	0.70	0.22	23.5	8.95	
n4536	188.603	2.20339	68306	17.16	0.63	24.72	0.19	1.03	0.05	8.53	8.97	
n4536	188.590	2.17853	45164	17.31	0.93	24.72	0.56	1.80	0.43	7.22	8.69	
n4536	188.590	2.18273	50050	17.56	1.06	23.58	0.26	0.69	0.29	7.02	8.75	rej
n4536	188.592	2.19544	64661	17.65	0.94	24.29	0.30	4.48	0.19	15.0	8.92	
n4536	188.585	2.17323	40923	18.16	1.06	23.95	0.24	0.38	0.01	18.9	8.53	
n4536	188.578	2.19021	66029	18.39	0.67	24.72	0.24	1.40	0.13	8.38	8.67	
n4536	188.573	2.19417	75137	18.67	0.90	24.45	0.22	0.40	0.05	8.95	8.63	
n4536	188.589	2.17226	35584	18.89	0.60	25.24	0.36	1.13	0.16	0.90	8.58	rej
n4536	188.585	2.18952	60991	19.01	0.49	24.60	0.47	4.48	0.44	45.4	8.77	
n4536	188.589	2.20092	74017	19.31	0.85	25.22	0.50	0.34	0.37	19.2	8.91	rej
n4536	188.589	2.17081	33174	19.47	0.67	24.58	0.25	0.95	0.13	9.05	8.55	
n4536	188.587	2.17317	38963	19.60	1.04	24.38	0.26	0.69	0.11	2.62	8.57	
n4536	188.590	2.17361	37037	19.65	0.85	24.37	0.25	2.89	0.21	16.2	8.62	
n4536	188.576	2.18837	65214	19.69	0.75	24.13	0.23	0.18	0.11	14.9	8.61	
n4536	188.598	2.19878	65080	19.98	0.76	24.76	0.25	0.70	0.16	20.3	9.01	
n4536	188.576	2.19187	69821	20.41	0.92	24.43	0.21	0.69	0.06	20.9	8.65	
n4536	188.590	2.19151	60845	21.26	0.75	23.93	0.29	0.83	0.14	13.6	8.86	
n4536	188.596	2.17595	36586	21.29	0.95	25.16	0.61	3.13	0.48	8.65	8.74	rej
n4536	188.597	2.18182	45000	21.58	0.90	24.39	0.35	1.71	0.35	5.02	8.85	
n4536	188.588	2.18875	58232	21.94	0.89	24.34	0.25	3.15	0.24	11.1	8.80	
n4536	188.592	2.18304	49022	22.66	0.95	24.97	0.62	3.44	0.05	3.38	8.79	
n4536	188.586	2.18894	60060	22.68	1.11	24.80	0.47	3.15	0.36	22.5	8.77	
n4536	188.593	2.16838	25262	22.91	1.30	25.05	0.43	1.45	0.19	23.1	8.58	rej
n4536	188.583	2.18540	57215	23.21	0.91	24.48	0.34	1.05	0.12	16.9	8.68	
n4536	188.585	2.19171	64002	24.31	1.20	23.77	0.31	4.71	0.25	52.0	8.79	
n4536	188.599	2.20055	67162	24.43	0.96	24.02	0.18	0.50	0.07	13.2	9.00	
n4536	188.587	2.18386	52964	28.05	1.17	23.18	0.24	0.94	0.08	50.9	8.73	rej
n4536	188.591	2.18233	49080	28.74	0.97	23.89	0.32	0.83	0.15	5.33	8.76	
n4536	188.587	2.18716	56988	29.06	0.47	23.74	0.35	1.96	0.22	29.3	8.77	
n4536	188.598	2.17839	39040	29.98	1.12	23.48	0.36	0.72	0.28	21.8	8.81	
n4536	188.593	2.18398	49524	30.20	1.11	24.32	0.50	6.19	0.37	19.9	8.82	

Table 2—Continued

Field	α (J2000)	δ (J2000)	Id	P (days)	$V-I$ (mag)	$F160W$ (mag)	σ (mag)	Offset (pix)	Bias (mag)	IM_{rms}	[O/H]	Flag
n4536	188.592	2.16953	28024	30.22	1.13	24.14	0.26	1.55	0.10	35.7	8.58	
n4536	188.593	2.16817	24880	30.23	1.05	24.65	0.29	1.57	0.07	8.61	8.57	rej
n4536	188.598	2.18340	46407	31.32	1.00	23.55	0.21	1.05	0.12	9.07	8.89	
n4536	188.591	2.17663	41282	32.94	0.97	23.21	0.26	0.50	0.18	3.49	8.69	
n4536	188.583	2.19109	64465	35.16	0.90	22.90	0.24	0.56	0.16	4.45	8.75	rej
n4536	188.587	2.18693	56960	35.88	1.09	23.56	0.29	0.17	0.21	29.6	8.76	
n4536	188.588	2.18631	55447	37.27	0.92	23.91	0.32	0.41	0.23	18.7	8.77	
n4536	188.578	2.19303	70171	37.59	0.95	23.49	0.17	0.31	0.08	23.0	8.69	
n4536	188.605	2.19774	59779	39.62	0.75	24.23	0.16	0.31	0.05	8.52	9.05	rej
n4536	188.590	2.20194	74682	42.66	1.04	23.10	0.19	0.07	0.12	11.2	8.92	
n4536	188.587	2.17143	35530	42.93	1.06	24.10	0.19	1.15	0.06	9.11	8.54	rej
n4536	188.587	2.18828	58154	49.38	0.78	22.97	0.22	0.20	0.10	38.5	8.79	
n4536	188.599	2.19737	62963	50.04	1.09	23.47	0.14	0.27	0.02	1.93	9.02	
n4536	188.583	2.17335	42055	50.67	1.02	23.31	0.14	0.86	0.02	4.32	8.52	
n4536	188.584	2.19363	66973	52.41	0.75	22.79	0.21	0.14	0.19	0.88	8.79	
n4536	188.582	2.19568	71233	54.45	1.00	22.52	0.16	0.50	0.07	9.93	8.78	rej
n4536	188.583	2.17743	47585	54.53	0.97	22.68	0.12	0.34	0.03	13.8	8.57	rej
n4536	188.599	2.19942	65517	60.16	1.13	22.93	0.13	0.44	0.07	20.7	9.01	
n4536	188.589	2.20044	73471	64.74	1.04	21.34	0.16	0.27	0.06	37.9	8.90	rej
n4536	188.588	2.19976	72937	66.23	0.94	23.10	0.20	0.61	0.09	21.9	8.89	
n4536	188.600	2.18247	44078	111.9	0.90	22.61	0.13	0.56	0.04	9.95	8.90	rej
n4536	188.597	2.18476	48663	119.1	1.14	22.21	0.12	0.44	0.03	21.8	8.88	
n4536	188.587	2.18864	58929	158.1	1.09	21.79	0.12	0.02	0.02	22.6	8.78	
n4536	188.592	2.18447	51147	187.2	1.25	21.87	0.18	0.99	0.04	30.4	8.80	rej
n4639	190.731	13.2610	33734	21.69	0.86	24.58	0.30	0.30	0.15	0.26	8.88	
n4639	190.726	13.2570	42674	21.82	0.86	25.51	0.73	2.38	0.43	23.0	9.14	
n4639	190.725	13.2588	45895	21.89	0.95	24.51	0.43	5.73	0.42	8.56	9.13	
n4639	190.705	13.2507	102787	22.38	1.00	25.18	0.32	2.48	0.11	17.7	8.77	
n4639	190.715	13.2490	70860	24.25	1.05	24.68	0.59	5.88	0.44	19.3	8.97	
n4639	190.721	13.2473	46993	24.90	1.10	24.71	0.48	1.09	0.42	19.5	8.98	
n4639	190.724	13.2507	41122	25.80	0.92	23.87	0.35	5.19	0.69	49.5	9.10	rej
n4639	190.724	13.2492	39959	26.99	0.90	25.52	0.67	1.16	0.28	15.9	9.05	rej
n4639	190.721	13.2648	64316	27.14	0.93	23.82	0.60	0.37	0.41	1.85	9.03	rej
n4639	190.726	13.2481	34553	29.19	0.72	25.18	0.49	1.58	0.20	4.07	8.98	
n4639	190.709	13.2699	107795	30.02	0.87	24.81	0.28	0.17	0.19	15.0	8.87	
n4639	190.719	13.2680	78588	30.84	0.78	24.37	0.36	0.66	0.13	15.3	8.93	
n4639	190.716	13.2761	97020	30.90	1.13	25.24	0.14	0.69	0.01	0.56	8.63	rej
n4639	190.733	13.2565	27312	33.04	0.82	24.21	0.20	0.75	0.06	9.54	8.88	
n4639	190.710	13.2495	89925	33.44	0.75	24.93	0.26	0.41	0.14	2.61	8.87	
n4639	190.724	13.2547	45055	35.00	0.87	23.75	0.43	2.88	0.46	53.5	9.19	
n4639	190.723	13.2584	50944	35.16	0.97	24.17	0.61	1.86	0.43	20.9	9.20	
n4639	190.726	13.2430	32876	36.41	1.04	23.83	0.32	2.73	-0.10	16.4	8.81	
n4639	190.715	13.2566	81322	38.15	0.88	24.99	0.81	6.21	0.49	49.7	9.25	
n4639	190.711	13.2523	87883	40.90	0.88	23.52	0.32	1.02	0.23	10.6	9.01	
n4639	190.705	13.2679	114011	41.18	0.92	23.95	0.23	0.23	0.08	16.8	8.86	

Table 2—Continued

Field	α (J2000)	δ (J2000)	Id	P (days)	$V-I$ (mag)	$F160W$ (mag)	σ (mag)	Offset (pix)	Bias (mag)	IM_{rms}	[O/H]	Flag
n4639	190.717	13.2535	65236	41.36	0.78	25.04	0.80	4.98	0.67	62.6	9.20	rej
n4639	190.733	13.2561	26954	43.75	0.94	23.88	0.20	1.98	0.09	17.4	8.88	
n4639	190.715	13.2524	76749	45.67	1.06	24.23	0.67	3.35	0.45	26.6	9.10	
n4639	190.704	13.2685	115343	48.34	1.15	24.44	0.24	0.11	0.15	10.9	8.84	
n4639	190.718	13.2740	86917	48.91	1.03	23.98	0.11	0.18	-0.0	7.92	8.69	
n4639	190.711	13.2558	91692	49.61	1.18	23.35	0.39	2.04	0.33	33.4	9.11	
n4639	190.720	13.2466	47978	54.97	0.85	24.14	0.39	4.23	0.19	1.56	8.95	
n4639	190.715	13.2556	80923	58.32	1.12	24.21	0.40	2.05	0.42	16.2	9.21	
n4639	190.728	13.2564	36973	64.85	1.42	23.64	0.25	0.23	0.16	9.71	9.07	
n4639	190.714	13.2650	91486	86.69	0.93	24.90	0.71	4.73	0.50	7.54	9.09	rej
n4639	190.714	13.2631	89399	105.3	0.85	23.12	0.35	1.09	0.36	49.8	9.15	
n3370	161.759	17.2801	8807	23.72	1.05	25.78	0.45	3.95	0.58	7.55	8.92	
n3370	161.776	17.2596	47494	24.43	1.22	24.42	0.45	0.44	0.16	20.3	8.77	rej
n3370	161.761	17.2605	23575	24.45	0.94	25.74	0.23	0.34	0.13	5.02	8.58	
n3370	161.787	17.2600	53228	24.73	0.86	26.06	0.24	2.49	0.07	0.80	8.43	rej
n3370	161.768	17.2808	23818	26.33	1.04	25.20	0.53	1.01	0.66	7.35	8.94	
n3370	161.761	17.2623	22838	26.38	1.00	25.16	0.31	0.94	0.07	0.09	8.66	
n3370	161.770	17.2785	81239	26.42	0.67	24.69	0.59	1.69	0.93	60.9	8.95	
n3370	161.775	17.2754	39583	26.87	0.95	24.50	0.61	1.52	0.75	9.54	8.84	
n3370	161.782	17.2727	48470	27.35	1.07	25.61	0.27	0.38	0.17	7.90	8.55	
n3370	161.756	17.2805	5744	27.74	1.06	25.33	0.49	1.50	0.54	8.07	8.83	
n3370	161.780	17.2561	51334	28.79	0.98	26.88	0.62	0.56	0.26	0.44	8.61	rej
n3370	161.758	17.2889	4531	29.23	1.00	25.38	0.29	1.15	0.18	3.05	8.71	
n3370	161.758	17.2803	62219	29.43	1.11	25.16	0.58	2.50	0.39	21.2	8.89	
n3370	161.775	17.2574	46992	29.60	0.95	25.42	0.68	5.34	0.17	3.45	8.72	
n3370	161.781	17.2572	51430	30.43	1.04	24.55	0.23	4.61	0.11	13.8	8.62	
n3370	161.772	17.2840	27556	30.69	0.99	25.36	0.23	0.55	0.13	2.62	8.70	
n3370	161.762	17.2696	19943	30.80	0.73	24.19	0.81	0.60	0.85	6.91	8.97	rej
n3370	161.762	17.2787	13380	31.74	0.85	23.71	0.79	0.54	1.29	12.5	9.05	rej
n3370	161.766	17.2858	15081	32.56	1.22	25.12	0.26	0.37	0.12	0.65	8.80	
n3370	161.761	17.2686	18200	32.86	1.12	24.54	0.42	0.23	0.17	7.99	8.88	
n3370	161.765	17.2670	26416	33.40	1.19	24.68	0.50	0.86	0.34	24.4	8.98	
n3370	161.784	17.2609	52428	33.48	1.03	24.80	0.20	0.57	0.01	2.62	8.54	
n3370	161.773	17.2814	31439	33.49	1.00	25.28	0.34	2.52	0.24	3.33	8.76	
n3370	161.763	17.2752	17886	33.56	1.25	24.35	0.52	2.39	1.48	75.0	9.13	
n3370	161.780	17.2642	49211	33.57	0.96	24.57	0.37	0.43	0.20	12.6	8.72	
n3370	161.785	17.2658	52279	33.69	1.04	25.26	0.18	0.38	0.03	0.54	8.48	
n3370	161.756	17.2835	4345	34.07	1.21	24.82	0.38	5.57	0.28	17.9	8.79	
n3370	161.752	17.2858	1320	34.58	1.06	24.81	0.32	0.49	0.15	15.5	8.62	
n3370	161.761	17.2697	17969	34.71	1.17	24.43	0.60	6.27	0.53	19.9	8.93	
n3370	161.761	17.2807	10677	35.24	1.12	25.00	0.57	4.86	0.49	16.3	8.97	
n3370	161.763	17.2724	19618	35.66	1.20	24.81	0.57	5.94	1.16	38.1	9.10	
n3370	161.768	17.2810	22097	36.02	0.98	24.08	0.52	0.52	0.50	37.5	8.95	
n3370	161.781	17.2610	50582	36.69	1.07	24.74	0.26	0.25	0.08	2.83	8.67	
n3370	161.757	17.2839	59919	36.99	0.90	25.07	0.47	1.30	0.33	16.5	8.81	

Table 2—Continued

Field	α (J2000)	δ (J2000)	Id	P (days)	$V-I$ (mag)	$F160W$ (mag)	σ (mag)	Offset (pix)	Bias (mag)	IM$_{rms}$	[O/H]	Flag
n3370	161.775	17.2624	45614	37.02	0.82	24.45	0.34	2.97	0.25	2.64	8.86	
n3370	161.769	17.2864	21445	37.10	1.09	24.94	0.23	0.37	0.09	3.91	8.68	
n3370	161.759	17.2654	16214	37.21	1.18	23.10	0.39	7.88	0.06	57.2	8.67	rej
n3370	161.773	17.2820	30965	37.28	0.95	24.90	0.27	2.20	0.20	6.33	8.74	
n3370	161.763	17.2705	20306	37.28	0.76	24.52	0.68	5.55	1.02	36.9	9.02	
n3370	161.768	17.2841	21506	38.54	0.76	24.41	0.34	1.84	0.09	12.5	8.80	
n3370	161.773	17.2823	31251	39.29	0.92	24.80	0.26	0.14	0.13	3.78	8.72	
n3370	161.776	17.2584	47492	39.41	1.14	24.68	0.32	0.86	0.09	8.32	8.75	
n3370	161.769	17.2895	18990	40.01	0.80	24.66	0.12	0.33	0.00	1.33	8.56	
n3370	161.768	17.2832	20732	41.55	1.17	23.98	0.37	1.52	0.19	28.9	8.86	
n3370	161.761	17.2839	9431	43.10	0.84	24.52	0.36	2.43	0.40	24.9	8.89	
n3370	161.758	17.2821	6440	43.94	1.18	24.63	0.45	0.69	0.29	3.14	8.86	
n3370	161.772	17.2767	85483	44.57	1.14	23.90	0.59	4.94	0.39	42.2	8.93	
n3370	161.765	17.2649	28504	44.97	0.82	24.18	0.31	0.80	0.23	21.9	8.90	
n3370	161.760	17.2823	9014	45.10	1.12	25.24	0.34	4.86	0.22	11.8	8.91	
n3370	161.777	17.2792	40168	45.40	1.02	23.73	0.15	0.73	0.06	15.5	8.64	rej
n3370	161.757	17.2831	5439	45.82	0.97	24.10	0.25	0.20	0.43	19.6	8.83	
n3370	161.779	17.2685	46830	45.88	1.07	24.80	0.35	3.42	0.18	8.22	8.78	
n3370	161.780	17.2752	46035	50.13	1.09	24.39	0.19	2.93	0.03	7.59	8.59	
n3370	161.766	17.2683	28129	50.57	1.12	25.29	0.72	0.81	0.59	37.5	9.07	rej
n3370	161.757	17.2827	5361	50.60	0.89	24.42	0.33	0.41	0.33	9.09	8.82	
n3370	161.770	17.2797	28534	51.15	0.97	24.72	0.41	4.19	0.23	25.9	8.91	
n3370	161.778	17.2602	48903	51.68	1.07	24.40	0.25	0.28	0.11	7.61	8.74	
n3370	161.764	17.2808	15864	52.41	1.02	23.68	0.51	0.87	0.24	21.1	9.01	
n3370	161.755	17.2808	4367	52.72	1.23	25.34	0.39	0.60	0.17	1.26	8.78	rej
n3370	161.765	17.2873	13303	52.74	1.15	24.31	0.24	0.34	0.05	7.04	8.75	
n3370	161.752	17.2841	1528	60.68	0.82	24.03	0.17	0.22	0.08	6.74	8.63	
n3370	161.757	17.2819	5501	62.70	1.26	23.71	0.29	0.64	0.26	1.20	8.83	
n3370	161.759	17.2847	6706	64.79	0.96	24.11	0.28	1.38	0.12	10.8	8.84	
n3370	161.760	17.2868	7014	66.71	1.07	23.68	0.28	0.14	0.09	4.09	8.79	
n3370	161.768	17.2667	33669	67.23	1.38	23.99	0.35	0.70	0.37	33.7	9.06	
n3370	161.759	17.2789	9063	68.90	0.80	23.84	0.24	0.88	0.14	13.1	8.92	
n3370	161.769	17.2831	22612	69.35	1.03	23.68	0.19	0.17	0.14	5.44	8.83	
n3370	161.765	17.2642	29662	71.52	0.90	23.81	0.22	0.36	0.19	1.44	8.88	
n3370	161.768	17.2812	22718	73.36	0.90	23.59	0.32	0.18	0.14	12.9	8.93	
n3370	161.753	17.2861	1454	79.26	1.34	24.00	0.15	0.19	0.07	6.67	8.63	
n3370	161.769	17.2677	33346	80.84	0.89	24.04	0.60	4.44	0.17	10.6	9.10	
n3370	161.773	17.2814	33195	81.04	1.00	23.84	0.13	0.23	0.05	17.1	8.72	
n3370	161.757	17.2854	4471	83.28	1.43	23.83	0.18	0.18	0.04	8.78	8.78	
n3370	161.768	17.2812	22098	86.33	1.05	23.64	0.27	0.44	0.10	8.05	8.94	
n3370	161.753	17.2785	3205	88.25	1.02	23.62	0.13	0.49	0.00	7.03	8.66	
n3370	161.768	17.2697	31067	88.54	1.14	24.73	0.71	3.19	1.12	54.1	9.17	rej
n3370	161.778	17.2600	48741	96.48	0.97	23.75	0.13	0.03	0.05	7.22	8.75	
n3370	161.761	17.2879	8038	96.82	1.09	23.35	0.12	0.37	0.02	1.43	8.76	
n3370	161.762	17.2722	17501	98.72	1.07	23.79	0.41	3.27	0.17	39.4	9.02	

Table 2—Continued

Field	α (J2000)	δ (J2000)	Id	P (days)	$V-I$ (mag)	$F160W$ (mag)	σ (mag)	Offset (pix)	Bias (mag)	IM$_{rms}$	[O/H]	Flag
n3982	179.109	55.1304	48062	20.84	0.62	25.24	0.56	3.88	1.42	44.0	9.04	
n3982	179.117	55.1339	35102	21.38	0.90	24.67	0.46	0.63	0.80	7.47	8.98	
n3982	179.133	55.1149	16746	21.46	1.05	25.16	0.35	3.08	0.12	2.83	8.64	
n3982	179.126	55.1324	20027	22.73	1.00	25.58	0.52	3.25	0.92	11.6	8.97	
n3982	179.130	55.1205	85628	23.58	0.92	24.60	0.48	2.07	0.65	16.8	8.92	
n3982	179.113	55.1370	40688	23.69	0.86	25.24	0.51	2.80	0.29	5.17	8.78	
n3982	179.113	55.1055	51886	24.55	1.10	25.05	0.18	0.70	0.01	1.59	8.36	
n3982	179.097	55.1208	65962	24.58	0.86	26.43	0.59	0.82	0.19	6.04	8.70	rej
n3982	179.103	55.1296	57905	25.24	0.68	25.42	0.41	0.73	0.74	15.6	8.88	
n3982	179.121	55.1314	86821	25.36	0.75	25.35	0.65	3.65	1.44	39.4	9.10	
n3982	179.125	55.1333	21186	26.78	0.61	23.99	0.42	1.04	0.46	4.33	8.94	rej
n3982	179.109	55.1295	49777	27.33	0.79	25.66	0.89	4.69	1.25	51.2	9.05	rej
n3982	179.100	55.1102	65677	28.58	1.28	22.76	0.15	3.81	0.02	82.2	8.44	rej
n3982	179.121	55.1146	35316	29.03	1.20	24.77	0.45	4.48	0.62	16.4	8.84	
n3982	179.085	55.1225	72633	32.52	1.13	25.68	0.28	0.68	0.00	2.96	8.32	rej
n3982	179.119	55.1138	39405	33.84	0.75	23.21	0.36	0.87	0.20	51.1	8.81	rej
n3982	179.139	55.1187	10406	34.20	1.25	24.80	0.16	0.41	0.03	1.79	8.57	
n3982	179.129	55.1156	21055	37.34	1.22	24.48	0.24	1.12	0.11	13.2	8.76	
n3982	179.131	55.1228	16117	37.99	1.12	24.37	0.36	1.49	0.26	17.3	8.93	
n3982	179.137	55.1277	10837	38.47	1.10	24.19	0.26	0.47	0.07	20.9	8.77	
n3982	179.094	55.1095	69280	38.68	1.19	24.39	0.12	0.34	0.02	3.78	8.28	
n3982	179.128	55.1305	17690	39.19	1.09	25.51	0.58	2.32	0.56	37.2	8.98	rej
n3982	179.098	55.1200	82298	40.31	0.82	24.41	0.25	1.04	0.17	17.9	8.72	
n3982	179.096	55.1132	67799	40.44	1.01	24.54	0.12	0.10	0.00	2.51	8.46	
n3982	179.138	55.1253	10346	40.44	1.27	24.11	0.21	1.04	0.07	13.0	8.72	
n3982	179.122	55.1177	32060	40.72	1.26	25.03	0.58	2.49	0.54	7.58	8.99	
n3982	179.086	55.1217	72603	51.61	0.92	23.95	0.13	0.17	0.00	2.40	8.32	
n3982	179.106	55.1278	89486	62.44	0.88	23.28	0.40	4.86	0.44	34.2	9.02	
n3982	179.134	55.1305	12402	72.36	1.00	23.06	0.28	0.54	0.02	15.5	8.82	
n3021	147.725	33.5550	71145	16.12	0.67	24.88	0.36	0.11	0.26	4.11	8.73	rej
n3021	147.731	33.5582	64603	16.28	1.27	26.28	0.75	7.71	1.24	26.2	9.01	
n3021	147.749	33.5517	29320	18.68	0.73	25.66	0.69	3.30	1.29	27.9	8.90	
n3021	147.750	33.5472	26176	19.47	0.73	25.56	0.39	0.47	0.33	1.11	8.67	
n3021	147.737	33.5601	54363	20.45	1.13	26.89	0.76	4.88	0.61	6.35	8.80	rej
n3021	147.742	33.5490	42349	20.56	0.77	25.08	0.44	2.33	1.46	51.1	9.10	
n3021	147.747	33.5566	35001	20.99	0.96	25.48	0.60	6.21	0.73	17.2	8.77	
n3021	147.726	33.5558	70351	22.57	0.92	24.43	0.56	0.23	0.49	6.29	8.82	rej
n3021	147.721	33.5551	73805	22.90	0.77	25.61	0.20	0.47	-0.0	0.81	8.44	
n3021	147.727	33.5561	69513	23.98	0.97	24.70	0.44	0.86	0.41	7.44	8.88	
n3021	147.726	33.5600	70368	25.14	0.71	25.96	0.41	0.10	0.06	3.82	8.68	
n3021	147.732	33.5488	60391	28.67	0.86	24.89	0.31	0.61	0.11	10.4	8.76	
n3021	147.748	33.5503	31450	31.64	0.70	24.30	0.54	8.72	0.69	36.1	8.98	
n3021	147.737	33.5593	54600	32.59	0.86	24.80	0.47	1.07	0.27	20.1	8.92	
n3021	147.728	33.5475	66191	32.66	0.79	25.81	0.24	1.17	0.04	0.72	8.36	rej
n3021	147.734	33.5515	57991	35.43	0.67	24.93	0.62	2.19	0.49	1.85	9.18	

Table 2—Continued

Field	α (J2000)	δ (J2000)	Id	P (days)	$V-I$ (mag)	$F160W$ (mag)	σ (mag)	Offset (pix)	Bias (mag)	IM$_{rms}$	[O/H]	Flag
n3021	147.728	33.5589	68742	36.73	0.96	25.10	0.29	0.11	0.19	13.8	8.83	
n3021	147.746	33.5560	94290	37.11	1.11	25.10	0.73	4.34	0.86	16.0	8.93	
n3021	147.732	33.5489	59774	39.19	0.92	24.56	0.32	1.26	0.27	6.17	8.79	
n3021	147.748	33.5511	32262	44.79	1.26	24.24	0.55	3.30	0.57	19.2	9.02	
n3021	147.747	33.5550	34624	48.27	1.00	23.98	0.59	0.94	0.38	34.1	8.93	
n3021	147.739	33.5581	101986	56.24	1.20	24.70	0.53	5.76	0.70	21.8	9.03	
n3021	147.751	33.5541	26664	58.58	0.76	24.33	0.26	0.69	0.05	3.17	8.67	
n3021	147.745	33.5562	38746	74.77	0.81	23.18	0.52	2.32	0.27	31.4	8.96	
n3021	147.733	33.5579	61619	81.02	1.14	24.06	0.38	0.28	0.36	7.11	9.10	
n3021	147.747	33.5517	33806	108.3	0.87	23.76	0.49	2.64	0.39	49.6	9.08	
n1309	50.5352	-15.4110	7989	39.41	0.89	24.55	0.26	0.38	0.05	5.12	8.85	
n1309	50.5262	-15.4100	27980	39.92	1.07	25.06	0.60	3.55	0.52	17.2	8.93	
n1309	50.5131	-15.4122	52975	40.52	0.76	25.57	0.17	0.18	0.03	1.80	8.56	rej
n1309	50.5339	-15.3869	7994	40.68	0.89	25.35	0.61	4.59	0.45	3.05	8.81	
n1309	50.5416	-15.3965	1166	41.11	1.10	25.12	0.21	0.41	0.08	2.13	8.82	
n1309	50.5241	-15.4028	76534	41.86	0.62	25.55	0.77	2.05	1.45	36.5	9.09	
n1309	50.5282	-15.4087	22918	42.03	0.82	24.28	0.43	2.23	0.45	34.4	8.99	rej
n1309	50.5402	-15.3941	2032	42.53	0.72	24.45	0.24	0.22	0.05	5.20	8.85	
n1309	50.5161	-15.3861	48747	42.68	0.85	24.96	0.16	0.51	0.03	2.93	8.63	
n1309	50.5288	-15.3977	67393	42.74	0.85	25.01	0.67	1.40	1.08	42.6	9.23	
n1309	50.5351	-15.3855	58298	43.52	0.77	24.87	0.21	0.88	0.05	7.39	8.75	
n1309	50.5350	-15.4007	7331	44.58	0.52	24.73	0.81	4.11	0.98	59.2	9.08	
n1309	50.5406	-15.3946	1732	45.00	0.72	24.73	0.21	0.03	0.07	10.2	8.84	
n1309	50.5298	-15.4083	19368	45.25	0.79	26.25	0.67	2.51	0.38	0.21	9.00	rej
n1309	50.5162	-15.3983	49584	45.67	0.78	25.75	0.58	3.55	0.52	19.4	8.83	rej
n1309	50.5302	-15.3905	16143	46.74	1.00	25.05	0.37	0.70	0.37	14.6	8.97	
n1309	50.5315	-15.4069	15346	46.85	0.81	24.18	0.54	0.79	0.31	32.2	9.04	
n1309	50.5132	-15.4039	52566	47.41	0.53	24.70	0.38	5.01	0.16	1.76	8.70	
n1309	50.5135	-15.3988	52170	47.99	0.96	24.89	0.35	0.11	0.24	14.6	8.73	
n1309	50.5370	-15.4121	4882	48.91	0.75	25.24	0.19	0.31	0.00	6.58	8.78	
n1309	50.5283	-15.4053	68817	49.93	0.53	25.11	0.57	5.29	0.78	26.6	9.11	
n1309	50.5304	-15.3868	15318	51.45	0.76	24.71	0.18	0.41	0.05	1.49	8.84	
n1309	50.5266	-15.4058	71911	51.99	0.76	24.90	0.69	1.98	0.72	24.1	9.07	
n1309	50.5260	-15.4077	28132	52.24	1.02	25.43	0.65	8.51	0.50	1.50	9.00	
n1309	50.5360	-15.4115	6581	58.98	0.79	24.61	0.20	0.09	0.07	2.35	8.82	
n1309	50.5361	-15.4123	6542	59.12	0.90	24.49	0.21	0.22	0.04	9.43	8.79	
n1309	50.5120	-15.3991	53187	59.75	0.57	24.85	0.29	2.70	0.11	10.1	8.68	
n1309	50.5281	-15.4092	69494	60.17	0.92	24.34	0.33	2.48	0.26	19.7	8.97	
n1309	50.5296	-15.4089	19918	64.94	0.81	24.96	0.36	0.27	0.22	4.42	8.98	
n1309	50.5311	-15.4079	64757	65.02	1.09	24.02	0.37	0.18	0.18	8.58	9.01	
n1309	50.5315	-15.3895	13102	66.34	0.82	24.73	0.26	0.18	0.19	8.57	8.93	
n1309	50.5186	-15.3946	45088	71.40	0.78	24.44	0.56	5.02	0.32	30.0	8.88	
n1309	50.5379	-15.4064	3836	73.27	0.87	24.27	0.17	0.61	0.07	11.0	8.90	
n1309	50.5355	-15.4141	7702	73.76	0.86	24.12	0.22	0.11	0.02	6.18	8.74	
n1309	50.5284	-15.4175	23616	82.13	0.90	24.34	0.12	0.10	0.01	5.35	8.67	

Table 2—Continued

Field	α (J2000)	δ (J2000)	Id	P (days)	$V-I$ (mag)	$F160W$ (mag)	σ (mag)	Offset (pix)	Bias (mag)	IM$_{rms}$	[O/H]	Flag
n1309	50.5364	-15.4017	4908	97.89	0.96	23.99	0.27	0.25	0.08	14.9	9.02	
n5584	215.612	-0.393170	835998	97.75	1.38	23.67	0.14	0.57	0.02	17.0	8.81	rej
n5584	215.609	-0.384550	625643	93.91	1.17	24.11	0.23	0.56	0.08	8.95	8.85	rej
n5584	215.601	-0.377940	414458	91.51	1.52	23.37	0.21	0.11	0.05	4.01	8.88	
n5584	215.600	-0.374360	325718	88.51	1.14	23.18	0.18	1.13	0.06	40.0	8.80	
n5584	215.604	-0.378170	449432	84.69	1.03	23.39	0.23	0.38	0.06	22.3	8.83	
n5584	215.614	-0.387300	735368	81.35	1.09	23.15	0.16	0.20	0.05	0.75	8.74	
n5584	215.597	-0.379210	395114	81.19	1.28	23.91	0.23	0.47	0.12	1.19	8.95	
n5584	215.589	-0.372140	172880	79.48	1.23	23.18	0.16	0.13	0.07	0.33	8.73	
n5584	215.594	-0.378680	354807	75.26	1.17	23.83	0.20	0.73	0.07	2.32	8.92	
n5584	215.590	-0.373060	200686	74.80	1.34	23.62	0.20	1.11	0.08	29.2	8.76	
n5584	215.598	-0.398630	801059	71.46	1.04	23.45	0.17	0.57	0.09	12.3	8.86	
n5584	215.606	-0.393670	781327	68.17	0.97	24.62	0.38	1.10	0.20	2.26	8.96	rej
n5584	215.612	-0.402910	1	65.82	1.15	23.69	0.14	0.10	0.07	16.8	8.70	
n5584	215.589	-0.379540	325206	64.08	1.20	24.02	0.19	0.31	0.08	4.51	8.87	
n5584	215.595	-0.369590	185292	63.11	0.90	23.89	0.25	0.68	0.07	23.7	8.70	
n5584	215.600	-0.393670	715226	60.54	1.10	24.25	0.34	2.88	0.16	31.7	9.01	
n5584	215.608	-0.384140	607520	60.04	1.11	23.76	0.24	0.09	0.14	4.45	8.87	
n5584	215.607	-0.392060	758598	58.78	1.20	25.00	0.43	0.73	0.21	18.2	8.95	rej
n5584	215.608	-0.384910	628911	57.83	1.03	23.94	0.29	1.55	0.24	19.0	8.87	
n5584	215.616	-0.388220	770520	57.73	1.36	23.27	0.14	0.41	0.04	33.9	8.70	rej
n5584	215.587	-0.369790	111577	56.72	0.95	23.66	0.23	0.20	0.12	16.4	8.67	
n5584	215.608	-0.394910	823580	56.17	1.36	23.68	0.23	0.55	0.06	3.63	8.91	
n5584	215.606	-0.378690	473829	55.13	1.02	23.72	0.26	0.67	0.10	16.6	8.82	
n5584	215.592	-0.395400	673309	53.56	1.21	23.49	0.20	0.20	0.13	21.8	8.84	
n5584	215.596	-0.387210	549082	52.16	1.05	24.15	0.33	2.98	0.28	22.9	9.09	
n5584	215.601	-0.382500	502797	51.92	1.17	23.65	0.24	2.47	0.17	12.1	9.00	
n5584	215.603	-0.399250	858989	51.77	1.11	23.08	0.20	3.38	0.09	45.3	8.87	rej
n5584	215.616	-0.387860	766511	49.35	1.14	24.56	0.23	0.25	0.08	9.49	8.68	
n5584	215.613	-0.389650	775000	47.94	1.50	23.97	0.27	0.52	0.15	1.14	8.77	
n5584	215.606	-0.399040	891587	47.86	1.05	23.79	0.21	0.41	0.14	4.00	8.86	
n5584	215.613	-0.402950	1	47.05	1.09	24.17	0.17	0.28	0.10	14.3	8.70	
n5584	215.602	-0.380740	478350	46.75	1.36	24.41	0.29	0.94	0.16	4.59	8.94	
n5584	215.605	-0.394330	781586	46.66	0.65	24.38	0.36	0.83	0.36	26.7	8.97	
n5584	215.604	-0.378480	455911	46.10	1.15	25.36	0.54	5.50	0.27	8.08	8.84	rej
n5584	215.590	-0.377880	295981	45.66	0.93	24.23	0.21	0.02	0.11	7.26	8.85	
n5584	215.600	-0.375400	347072	44.98	0.89	23.05	0.35	0.11	0.27	11.7	8.83	rej
n5584	215.589	-0.368510	97566	43.49	1.42	23.84	0.26	3.50	0.14	10.4	8.65	
n5584	215.597	-0.379930	411135	43.46	1.01	24.20	0.38	0.56	0.25	19.5	8.97	
n5584	215.610	-0.388250	715986	42.45	1.46	24.46	0.32	0.25	0.14	1.60	8.85	
n5584	215.599	-0.377030	374736	41.52	1.07	24.12	0.44	1.19	0.36	30.4	8.88	
n5584	215.594	-0.373010	238461	39.16	1.35	24.65	0.46	0.91	0.13	18.7	8.79	
n5584	215.605	-0.383690	571414	39.16	1.07	24.04	0.31	0.50	0.28	6.99	8.93	
n5584	215.604	-0.406030	1	39.01	1.07	23.91	0.31	0.30	0.21	11.7	8.70	
n5584	215.603	-0.383460	545366	38.81	0.88	25.31	0.46	3.05	0.16	18.9	8.98	rej

Table 2—Continued

Field	α (J2000)	δ (J2000)	Id	P (days)	$V-I$ (mag)	$F160W$ (mag)	σ (mag)	Offset (pix)	Bias (mag)	IM$_{rms}$	[O/H]	Flag
n5584	215.614	-0.386790	727892	38.65	1.02	24.73	0.29	0.25	0.24	10.6	8.72	
n5584	215.593	-0.383720	449157	38.49	0.94	24.72	0.55	4.63	0.43	26.4	9.00	
n5584	215.597	-0.384860	513827	38.20	1.16	23.80	0.48	1.38	0.36	18.3	9.09	
n5584	215.593	-0.391580	605531	38.07	1.10	24.79	0.41	3.28	0.20	10.1	8.94	
n5584	215.612	-0.378940	550433	38.04	1.22	24.27	0.19	0.27	0.07	8.55	8.66	
n5584	215.611	-0.402760	1	37.17	1.00	24.15	0.26	4.17	0.11	11.8	8.72	
n5584	215.609	-0.383490	606041	36.88	0.86	23.84	0.32	5.17	0.24	14.1	8.83	
n5584	215.599	-0.394940	738261	36.54	1.29	24.60	0.48	1.15	0.36	29.2	8.98	
n5584	215.600	-0.377150	390652	36.48	0.86	24.25	0.49	7.21	0.22	34.2	8.86	
n5584	215.597	-0.380400	421192	36.29	1.09	23.90	0.38	1.50	0.11	29.5	8.98	
n5584	215.596	-0.372430	253461	36.27	1.36	24.54	0.60	3.98	0.54	10.8	8.77	
n5584	215.594	-0.370740	200467	35.85	1.40	24.93	0.35	0.28	0.28	3.16	8.73	
n5584	215.595	-0.370750	208725	35.13	0.98	24.76	0.44	3.60	0.31	24.5	8.73	
n5584	215.598	-0.383300	493790	34.44	1.01	24.94	0.60	2.71	0.53	0.50	9.05	
n5584	215.597	-0.372950	267902	33.47	0.84	25.99	0.65	5.00	0.62	8.74	8.78	rej
n5584	215.591	-0.394450	644384	33.11	0.89	25.58	0.69	1.96	0.23	12.7	8.83	rej
n5584	215.588	-0.375070	220248	31.36	1.05	24.49	0.28	0.13	0.09	2.92	8.77	
n5584	215.614	-0.391150	811974	31.06	1.04	24.33	0.37	1.02	0.14	15.5	8.76	
n5584	215.611	-0.398250	918325	30.50	0.95	24.61	0.31	1.04	0.14	11.6	8.81	
n5584	215.594	-0.386960	521128	30.46	1.07	24.45	0.40	2.11	0.44	26.5	9.02	
n5584	215.590	-0.386380	464626	30.31	1.21	24.64	0.36	0.68	0.28	14.9	8.90	
n5584	215.609	-0.372140	378235	30.17	1.15	24.69	0.19	0.20	0.09	10.8	8.59	
n5584	215.589	-0.384210	418643	30.10	1.09	23.99	0.30	0.43	0.32	23.1	8.90	
n5584	215.600	-0.383340	511109	30.00	1.07	24.72	0.44	3.01	0.55	23.8	9.04	
n5584	215.601	-0.380690	466137	29.60	1.19	24.53	0.55	1.11	0.26	9.32	8.96	
n5584	215.609	-0.406810	1	29.51	1.20	23.91	0.21	0.52	-0.10	16.9	8.66	rej
n5584	215.600	-0.378480	412396	28.87	0.79	24.66	0.66	5.53	0.46	25.3	8.91	
n5584	215.589	-0.374740	230093	28.36	1.36	24.49	0.37	5.96	0.29	21.7	8.79	
n5584	215.596	-0.384910	504490	28.31	0.76	24.40	0.51	6.73	0.56	4.91	9.08	
n5584	215.613	-0.397280	927325	27.86	1.34	24.68	0.29	0.03	0.23	7.12	8.76	
n5584	215.601	-0.372440	298430	27.53	0.93	25.12	0.30	1.26	0.26	13.2	8.73	
n5584	215.609	-0.383140	602554	26.71	1.06	24.19	0.46	0.80	0.34	19.4	8.82	
n5584	215.605	-0.383200	563696	26.66	1.10	24.94	0.34	6.03	0.32	21.9	8.92	
n5584	215.613	-0.386730	711358	26.64	0.98	25.59	0.39	0.43	0.02	8.44	8.77	
n5584	215.611	-0.394850	852752	26.36	1.20	23.96	0.27	0.33	0.22	12.6	8.84	rej
n5584	215.595	-0.386440	519642	25.75	1.02	23.63	0.43	0.27	0.47	38.1	9.05	rej
n5584	215.613	-0.378740	550434	25.59	1.09	24.99	0.28	1.72	0.07	6.68	8.64	
n5584	215.601	-0.394200	740028	25.57	0.97	24.66	0.63	1.80	0.38	12.4	9.00	
n5584	215.598	-0.400160	825506	25.30	1.01	26.32	0.49	4.23	0.16	10.2	8.81	rej
n5584	215.610	-0.398360	912240	25.06	0.92	25.21	0.41	3.17	0.27	19.3	8.82	
n5584	215.612	-0.396350	892554	25.02	1.32	24.48	0.38	0.49	0.20	3.84	8.81	
n5584	215.588	-0.400160	729270	24.71	1.00	25.06	0.27	0.72	0.23	4.88	8.64	
n5584	215.587	-0.368490	82928	24.28	0.85	25.13	0.43	1.00	0.09	8.70	8.64	
n5584	215.583	-0.393870	552392	23.44	0.92	25.91	0.33	0.09	0.14	4.35	8.64	rej
n5584	215.582	-0.393560	534937	23.33	1.03	25.03	0.13	0.38	0.33	17.5	8.61	

Table 2—Continued

Field	α (J2000)	δ (J2000)	Id	P (days)	$V-I$ (mag)	$F160W$ (mag)	σ (mag)	Offset (pix)	Bias (mag)	IM$_{rms}$	[O/H]	Flag
n5584	215.594	-0.388450	549585	22.92	0.89	24.82	0.47	2.86	0.65	30.6	9.01	
n5584	215.612	-0.393990	853244	22.52	1.00	26.65	0.69	2.85	0.28	12.1	8.80	rej
n5584	215.598	-0.375010	321323	21.51	1.09	24.77	0.76	2.71	0.92	34.0	8.83	
n5584	215.603	-0.395320	787283	21.07	0.97	24.90	0.50	2.39	0.54	17.9	8.97	
n5584	215.598	-0.402950	889136	20.77	1.15	24.54	0.35	2.16	0.20	5.19	8.75	
n5584	215.595	-0.373140	258671	20.28	1.00	25.50	0.43	4.15	0.81	24.6	8.79	
n4038	180.478	-18.8573	2899	28.29	1.31	24.23	0.39	1.57	0.33	18.1	8.98	
n4038	180.486	-18.8701	50618	30.05	1.09	25.62	0.61	5.42	1.02	41.0	9.00	rej
n4038	180.486	-18.8727	61212	30.06	1.18	23.69	0.55	0.81	0.61	33.5	8.97	rej
n4038	180.482	-18.8616	14127	32.61	0.94	24.77	0.50	4.32	0.74	33.9	9.05	
n4038	180.457	-18.8744	66568	35.15	1.11	24.87	0.57	0.41	0.17	17.5	9.00	
n4038	180.468	-18.8564	2098	36.06	1.10	24.64	0.45	3.47	0.32	31.4	8.95	
n4038	180.463	-18.8704	52139	36.53	1.13	24.13	0.42	4.38	1.01	99.4	9.12	
n4038	180.458	-18.8717	56965	37.87	1.01	23.26	0.57	2.09	0.58	103.	9.05	rej
n4038	180.466	-18.8612	12318	38.71	0.94	23.93	0.57	2.23	1.01	130.	9.06	
n4038	180.455	-18.8718	57613	39.82	1.10	23.70	0.51	0.81	0.36	58.8	9.01	
n4038	180.458	-18.8723	59401	40.07	1.40	24.34	0.43	1.42	0.67	9.46	9.04	
n4038	180.458	-18.8728	61493	40.84	0.93	24.56	0.54	4.28	0.39	69.6	9.04	
n4038	180.458	-18.8746	67110	41.07	0.92	24.66	0.48	1.23	0.37	9.32	9.01	
n4038	180.467	-18.8844	87068	42.41	1.20	24.85	0.54	3.80	0.28	14.4	8.82	
n4038	180.457	-18.8726	60844	42.91	1.04	23.83	0.54	6.32	0.47	49.5	9.03	
n4038	180.471	-18.8783	75207	42.99	1.27	24.19	0.37	5.52	0.12	17.0	8.97	
n4038	180.474	-18.8558	1757	43.98	1.26	23.81	0.27	0.81	0.21	26.7	8.95	
n4038	180.457	-18.8680	40839	45.85	1.13	24.25	0.35	3.97	0.55	40.5	9.05	
n4038	180.457	-18.8734	63839	46.16	1.12	24.09	0.39	1.30	0.34	33.4	9.02	
n4038	180.484	-18.8781	74894	46.31	0.93	22.97	0.50	0.89	0.69	112.	8.89	rej
n4038	180.473	-18.8812	80094	46.73	1.48	23.27	0.47	0.76	0.33	38.8	8.89	rej
n4038	180.485	-18.8699	49858	50.34	1.00	24.36	0.49	1.67	0.77	27.3	9.02	
n4038	180.475	-18.8849	88457	53.95	1.27	23.99	0.43	7.73	1.06	16.7	8.78	
n4038	180.473	-18.8612	12435	54.50	0.81	23.95	0.52	1.63	0.80	95.6	9.09	
n4038	180.458	-18.8728	61356	58.78	1.23	24.59	0.57	2.70	0.39	14.7	9.04	rej
n4038	180.481	-18.8825	82809	61.04	1.03	23.11	0.43	2.81	0.50	82.2	8.81	
n4038	180.476	-18.8796	77376	61.36	1.40	23.70	0.62	2.16	0.79	0.20	8.91	
n4038	180.485	-18.8731	62538	64.41	1.28	23.14	0.29	0.22	0.27	54.2	8.97	
n4038	180.469	-18.8606	10441	66.68	1.23	24.70	0.63	3.52	0.83	73.5	9.06	rej
n4038	180.469	-18.8748	67639	72.93	1.28	23.53	0.38	0.51	0.26	6.33	9.07	
n4038	180.487	-18.8749	67811	76.83	1.45	23.03	0.21	0.30	0.21	13.4	8.92	
n4038	180.470	-18.8585	5006	102.9	1.13	23.42	0.45	4.17	0.31	67.8	9.02	
n4038	180.475	-18.8622	16265	117.6	1.32	22.80	0.39	0.44	0.21	75.3	9.11	
n4038	180.475	-18.8644	24649	118.8	1.00	22.71	0.35	1.08	0.39	76.3	9.16	
n4038	180.477	-18.8599	8342	121.8	1.23	23.24	0.27	0.69	0.05	0.20	9.05	
n4038	180.468	-18.8588	5625	133.9	1.27	22.29	0.31	1.30	0.13	134.	9.02	
n4038	180.459	-18.8681	41146	162.1	0.84	22.60	0.21	0.20	0.15	54.4	9.07	
n4038	180.470	-18.8757	69575	197.1	1.07	22.09	0.16	0.54	0.05	26.2	9.04	
n4038	180.475	-18.8651	27608	203.3	0.89	22.30	0.30	0.75	0.10	8.49	9.17	

Table 2—Continued

Field	α (J2000)	δ (J2000)	Id	P (days)	$V-I$ (mag)	$F160W$ (mag)	σ (mag)	Offset (pix)	Bias (mag)	IM_{rms}	[O/H]	Flag
n4258	184.713	47.3122	50193	93.23	0.82	21.20	0.15	0.37	0.05	55.7	8.95	rej
n4258	184.715	47.3114	42837	95.92	0.93	20.74	0.18	0.18	0.05	219.	8.96	
n4258	184.728	47.3159	9633	69.46	1.18	20.60	0.23	0.10	0.10	259.	9.00	
n4258	184.719	47.3101	31107	58.21	1.21	21.59	0.24	6.69	0.07	26.3	8.97	
n4258	184.727	47.3178	15470	50.70	1.48	20.89	0.27	6.80	0.22	150.	8.99	rej
n4258	184.714	47.3127	47358	50.89	0.86	21.58	0.27	0.31	0.14	232.	8.96	
n4258	184.720	47.3110	29058	40.54	0.95	21.59	0.33	9.81	0.30	279.	8.97	
n4258	184.719	47.3121	34159	41.57	1.01	21.77	0.32	0.16	0.26	85.9	8.97	
n4258	184.723	47.3121	19435	39.53	0.82	20.92	0.35	0.14	0.25	453.	8.99	rej
n4258	184.731	47.3206	8480	37.63	0.75	21.27	0.43	0.27	0.11	125.	8.98	
n4258	184.712	47.3096	49279	36.12	0.94	21.70	0.27	1.66	0.16	216.	8.94	
n4258	184.730	47.3200	8723	35.57	0.96	22.73	0.46	5.21	0.52	121.	8.99	
n4258	184.724	47.3119	17423	34.57	1.27	22.24	0.40	1.63	0.38	29.3	8.99	
n4258	184.724	47.3106	15103	34.36	1.14	23.36	0.61	2.91	0.50	134.	8.99	rej
n4258	184.720	47.3141	33434	34.48	0.78	20.86	0.32	0.38	0.41	196.	8.97	rej
n4258	184.722	47.3069	17369	34.93	1.00	21.59	0.37	5.77	0.10	95.5	8.97	
n4258	184.715	47.3083	189390	34.41	0.95	22.09	0.29	1.26	0.22	62.6	8.95	
n4258	184.722	47.3120	22927	33.99	1.04	21.58	0.29	0.72	0.47	214.	8.98	
n4258	184.732	47.3184	3147	33.39	1.01	22.50	0.41	1.99	0.37	232.	8.99	
n4258	184.719	47.3150	36217	31.10	1.25	23.29	0.53	6.28	0.34	12.3	8.97	rej
n4258	184.717	47.3114	36357	29.48	0.86	22.50	0.41	0.56	0.49	8.14	8.96	
n4258	184.720	47.3056	21518	30.95	0.46	21.53	0.34	4.57	0.30	99.9	8.96	
n4258	184.725	47.3111	14316	29.63	1.14	22.45	0.44	4.71	0.62	37.4	8.99	
n4258	184.715	47.3113	44839	24.95	1.10	22.42	0.47	2.88	0.64	56.5	8.95	
n4258	184.720	47.3132	30136	26.07	1.21	22.47	0.47	3.19	0.64	178.	8.98	
n4258	184.714	47.3117	46945	25.12	0.90	22.09	0.49	4.13	0.37	122.	8.95	
n4258	184.724	47.3169	24960	25.49	1.06	22.19	0.38	2.44	0.56	100.	8.99	
n4258	184.711	47.3124	56661	23.83	0.68	23.31	0.42	2.64	0.34	10.8	8.94	
n4258	184.731	47.3212	9241	27.25	0.72	22.26	0.50	3.18	0.53	280.	8.98	
n4258	184.720	47.3132	31615	23.98	1.32	22.20	0.50	0.34	0.71	95.0	8.97	
n4258	184.715	47.3111	43119	23.81	0.85	21.87	0.38	1.92	0.40	63.7	8.96	rej
n4258	184.729	47.3175	8361	23.79	1.22	22.32	0.44	0.67	0.69	172.	8.99	
n4258	184.728	47.3197	17151	22.35	1.65	22.23	0.35	0.50	0.57	137.	8.99	
n4258	184.724	47.3162	23741	22.68	1.43	22.98	0.56	2.51	0.51	152.	8.99	
n4258	184.726	47.3146	14643	22.04	1.92	23.66	0.44	2.01	0.92	19.8	8.99	rej
n4258	184.727	47.3176	17357	22.45	1.21	22.11	0.36	1.62	0.60	177.	8.99	
n4258	184.719	47.3141	34408	22.42	0.85	22.11	0.55	2.65	0.68	273.	8.97	
n4258	184.728	47.3164	12898	22.82	0.94	23.19	0.56	8.13	0.78	270.	8.99	
n4258	184.726	47.3134	14775	21.61	0.72	22.44	0.39	0.69	1.11	113.	8.99	
n4258	184.731	47.3164	1824	20.10	0.94	22.96	0.45	0.81	0.77	59.1	9.00	
n4258	184.729	47.3169	8052	20.76	0.90	22.05	0.53	2.71	0.81	178.	9.00	rej
n4258	184.728	47.3133	6616	16.99	0.93	23.16	0.49	3.34	1.17	239.	9.00	
n4258	184.719	47.3189	40434	16.43	1.22	22.66	0.48	1.17	0.82	85.4	8.98	
n4258	184.716	47.3109	38988	17.53	0.85	23.34	0.67	3.80	1.00	270.	8.96	
n4258	184.728	47.3173	158057	16.68	1.22	23.95	0.62	1.11	0.98	80.0	8.99	rej

Table 2—Continued

Field	α (J2000)	δ (J2000)	Id	P (days)	$V-I$ (mag)	$F160W$ (mag)	σ (mag)	Offset (pix)	Bias (mag)	IM_{rms}	[O/H]	Flag
n4258	184.728	47.3223	19414	16.38	0.90	23.27	0.44	2.88	0.68	145.	8.98	
n4258	184.714	47.3134	49332	16.00	0.71	23.33	0.49	2.24	0.80	104.	8.96	
n4258	184.728	47.3161	11066	15.91	1.21	23.70	0.55	6.82	1.15	113.	9.00	
n4258	184.711	47.3149	60978	15.21	1.17	24.55	0.67	1.67	0.80	146.	8.95	rej
n4258	184.723	47.3192	29222	14.58	0.96	22.86	0.60	7.09	0.75	320.	8.98	
n4258	184.727	47.3176	16299	12.28	1.28	24.49	0.72	3.35	1.30	183.	8.99	rej
n4258	184.712	47.3097	51416	11.09	0.77	23.45	0.56	2.45	1.07	122.	8.94	
n4258	184.711	47.3118	57246	10.90	0.89	23.47	0.45	0.13	1.09	80.5	8.94	
n4258	184.728	47.3228	20566	10.36	1.04	22.52	0.56	0.88	1.10	9.65	8.98	rej
n4258	184.725	47.3206	25811	10.30	0.89	23.62	0.61	2.54	1.25	167.	8.98	
n4258	184.726	47.3218	25760	9.979	0.92	24.38	0.54	1.95	1.46	122.	8.98	
n4258	184.709	47.3142	64217	10.06	0.99	23.40	0.51	3.27	0.95	120.	8.94	
n4258	184.703	47.3262	89807	98.42	1.26	21.11	0.11	0.20	0.03	114.	8.93	rej
n4258	184.705	47.3209	80885	65.23	1.13	20.75	0.15	5.40	0.04	251.	8.93	rej
n4258	184.737	47.3354	10849	51.51	1.34	21.63	0.29	0.28	0.20	98.1	8.92	
n4258	184.719	47.3489	77289	46.39	1.53	21.69	0.18	0.63	0.11	14.7	8.90	
n4258	184.739	47.3340	1625	45.43	1.03	21.19	0.29	0.49	0.16	95.5	8.92	
n4258	184.743	47.3424	2686	44.05	1.06	21.78	0.31	0.22	0.10	85.2	8.88	
n4258	184.706	47.3209	77610	42.82	1.00	21.58	0.23	0.22	0.16	211.	8.94	
n4258	184.731	47.3383	32759	42.31	0.94	21.78	0.23	0.68	0.31	188.	8.92	
n4258	184.739	47.3324	475	41.88	0.97	21.80	0.34	0.87	0.17	75.1	8.93	
n4258	184.713	47.3226	62769	33.02	0.77	21.80	0.25	0.67	0.18	192.	8.96	
n4258	184.708	47.3456	97135	31.78	1.20	22.85	0.28	1.22	0.10	27.5	8.92	
n4258	184.709	47.3512	99756	29.05	1.04	22.82	0.27	0.64	0.21	147.	8.90	
n4258	184.696	47.3331	106960	28.26	0.97	22.81	0.27	0.72	0.13	27.6	8.92	
n4258	184.703	47.3195	83857	28.13	0.76	21.51	0.30	1.48	0.19	141.	8.93	rej
n4258	184.724	47.3262	37683	26.18	1.41	22.82	0.31	0.56	0.48	119.	8.97	
n4258	184.701	47.3380	103070	24.86	1.12	22.91	0.45	4.15	0.21	53.7	8.92	
n4258	184.733	47.3425	33002	22.48	0.75	23.72	0.56	4.53	0.44	182.	8.90	rej
n4258	184.698	47.3334	104131	22.89	0.87	22.34	0.25	2.90	0.20	41.5	8.92	
n4258	184.699	47.3369	105183	23.00	1.11	22.50	0.26	0.81	0.22	36.2	8.92	
n4258	184.734	47.3390	24365	22.38	0.92	22.83	0.59	3.91	0.52	165.	8.91	
n4258	184.712	47.3515	95003	20.57	1.20	23.15	0.29	4.42	0.36	74.8	8.90	
n4258	184.703	47.3314	93585	18.19	0.97	22.98	0.41	1.94	0.42	14.2	8.93	
n4258	184.706	47.3457	99411	17.02	0.98	24.05	0.50	2.02	0.35	9.51	8.92	rej
n4258	184.709	47.3242	75254	16.52	0.98	22.85	0.39	2.94	0.38	15.6	8.95	
n4258	184.710	47.3475	94632	16.03	1.14	22.22	0.44	0.89	0.39	141.	8.91	rej
n4258	184.727	47.3452	54398	15.73	1.06	22.74	0.53	0.50	0.81	109.	8.91	
n4258	184.691	47.3461	122858	14.28	0.78	23.08	0.33	1.10	0.25	40.1	8.90	
n4258	184.701	47.3507	111064	14.59	0.98	22.51	0.33	0.92	0.35	42.7	8.90	rej
n4258	184.736	47.3575	43585	14.80	0.94	23.36	0.31	0.60	0.09	72.1	8.84	
n4258	184.703	47.3257	90355	14.50	0.92	23.57	0.49	3.05	0.24	44.1	8.93	
n4258	184.710	47.3538	99783	14.31	0.80	23.19	0.67	1.77	0.65	110.	8.89	
n4258	184.725	47.3447	58469	13.08	1.03	24.42	0.84	2.55	0.88	256.	8.91	rej
n4258	184.714	47.3221	59576	12.65	1.10	23.91	0.61	3.81	0.72	55.4	8.96	

Table 2—Continued

Field	α (J2000)	δ (J2000)	Id	P (days)	$V-I$ (mag)	$F160W$ (mag)	σ (mag)	Offset (pix)	Bias (mag)	IM_{rms}	[O/H]	Flag
n4258	184.700	47.3341	102255	12.25	1.04	24.59	99.0	0.44	0.52	33.9	8.92	rej
n4258	184.705	47.3291	89618	12.47	1.01	23.37	0.38	0.41	0.55	77.1	8.94	
n4258	184.709	47.3244	74725	11.99	0.80	23.19	0.43	5.67	0.67	71.2	8.95	
n4258	184.687	47.3467	126765	11.64	1.02	24.97	0.56	4.73	0.28	11.2	8.89	rej
n4258	184.708	47.3500	100093	12.02	0.72	22.65	0.58	6.25	0.46	232.	8.91	rej
n4258	184.738	47.3365	7952	11.92	0.90	23.46	0.53	3.27	1.04	142.	8.91	
n4258	184.701	47.3493	110213	11.60	1.19	23.15	0.46	0.47	0.53	98.1	8.90	
n4258	184.709	47.3329	84547	11.30	0.81	23.52	0.36	1.47	0.79	86.2	8.94	
n4258	184.698	47.3422	109630	10.93	0.82	23.91	0.49	1.97	0.66	83.9	8.91	
n4258	184.711	47.3499	95403	11.58	1.03	24.27	0.62	4.36	0.61	47.7	8.91	
n4258	184.703	47.3279	91129	11.16	1.00	23.50	0.35	0.41	0.55	25.8	8.93	
n4258	184.705	47.3318	91209	10.80	0.88	23.60	0.48	0.76	0.67	2.96	8.94	
n4258	184.709	47.3423	91907	10.51	1.20	22.71	0.42	0.55	0.73	46.0	8.93	rej
n4258	184.710	47.3483	94562	10.20	1.03	23.90	0.41	3.58	0.91	74.4	8.91	
n4258	184.706	47.3414	97498	9.987	0.98	24.22	0.62	3.80	0.73	64.6	8.93	
n4258	184.706	47.3497	104039	9.770	1.17	23.20	0.56	2.20	0.63	37.5	8.91	
n4258	184.858	47.2018	10401	5.297	0.75	24.97	0.67	2.73	1.45	18.7	8.70	
n4258	184.871	47.2067	5387	6.487	0.71	22.65	0.56	0.28	1.15	245.	8.68	rej
n4258	184.853	47.1854	9483	6.803	0.75	25.14	0.72	4.32	1.10	62.8	8.69	rej
n4258	184.850	47.1925	11990	8.024	0.65	23.83	0.65	5.28	0.83	87.0	8.71	
n4258	184.872	47.1820	2134	8.137	0.72	24.73	0.60	4.98	1.25	27.2	8.66	
n4258	184.852	47.2056	13262	8.288	0.92	24.61	0.64	2.60	0.75	95.3	8.72	
n4258	184.859	47.2006	9786	8.920	0.72	24.23	0.59	2.09	0.87	91.6	8.70	
n4258	184.703	47.3161	81614	20.31	1.01	21.94	0.30	0.18	0.29	118.	8.92	rej
n4258	184.705	47.3086	67208	18.29	1.09	22.49	0.37	1.34	0.28	106.	8.92	
n4258	184.690	47.3326	116159	21.87	0.89	22.79	0.30	1.40	0.12	42.4	8.90	
n4258	184.649	47.3196	143829	18.28	1.25	23.13	0.13	0.10	0.03	17.5	8.73	
n4258	184.687	47.3347	121078	18.42	0.97	22.94	0.31	0.69	0.19	106.	8.89	
n4258	184.668	47.3360	138294	15.81	0.93	22.95	0.20	0.18	0.12	5.28	8.83	
n4258	184.692	47.3224	106997	15.29	0.84	23.29	0.39	0.88	0.25	59.7	8.89	
n4258	184.653	47.3302	144134	15.61	0.89	23.34	0.16	0.05	0.05	43.4	8.77	
n4258	184.691	47.3215	107947	14.67	1.03	23.60	0.30	0.41	0.32	2.21	8.89	
n4258	184.689	47.3355	118961	12.82	1.26	22.30	0.26	0.31	0.31	34.2	8.89	rej
n4258	184.695	47.3162	95987	11.26	1.28	24.91	0.73	4.07	0.34	39.3	8.89	rej
n4258	184.655	47.3223	141685	10.99	0.83	23.72	0.21	2.46	0.11	12.7	8.76	
n4258	184.651	47.3319	145186	10.69	0.88	23.36	0.23	0.27	0.10	3.72	8.77	
n4258	184.827	47.1922	26262	5.007	0.77	23.86	0.28	3.54	0.46	88.0	8.73	rej
n4258	184.807	47.1879	40543	5.372	0.80	25.43	0.73	2.02	0.39	21.4	8.72	rej
n4258	184.812	47.1725	31191	5.834	0.70	22.71	0.34	0.10	0.17	73.3	8.67	rej
n4258	184.823	47.1940	29843	5.864	0.72	24.13	0.40	5.54	0.48	53.3	8.73	
n4258	184.837	47.1950	20639	6.735	1.03	24.57	0.53	0.69	0.63	1.61	8.73	
n4258	184.830	47.1966	25502	7.538	0.92	23.72	0.54	1.52	0.45	76.9	8.73	
n4258	184.833	47.1973	24134	8.937	0.87	24.87	0.52	2.54	0.33	19.7	8.73	rej
n4258	184.839	47.1708	12705	9.942	0.84	24.37	0.59	5.65	0.38	25.4	8.67	
n4258	184.836	47.1743	14709	10.97	0.84	22.58	0.26	0.44	0.17	44.1	8.68	rej

Table 2—Continued

Field	α (J2000)	δ (J2000)	Id	P (days)	$V-I$ (mag)	$F160W$ (mag)	σ (mag)	Offset (pix)	Bias (mag)	IM$_{rms}$	[O/H]	Flag
n4258	184.839	47.1948	19312	13.55	0.82	23.98	0.47	5.13	0.20	88.2	8.72	
n4258	184.835	47.1738	15276	16.43	0.87	22.34	0.20	3.56	0.17	61.6	8.68	rej
n4258	184.699	47.3561	118782	25.56	0.89	22.43	0.22	0.63	0.17	42.2	8.89	
n4258	184.698	47.3593	121312	17.85	1.02	24.78	0.32	0.47	0.16	3.48	8.88	rej
n4258	184.699	47.3550	117710	14.30	0.83	24.32	0.49	1.46	0.30	48.9	8.89	rej
n4258	184.714	47.3568	95711	10.94	1.12	23.80	0.61	1.20	0.40	33.5	8.88	
n4258	184.849	47.2111	17005	5.739	0.92	24.97	0.57	5.57	0.94	41.4	8.73	
n4258	184.842	47.2190	23710	5.920	0.77	25.75	0.31	2.81	1.21	33.1	8.75	rej
n4258	184.856	47.2120	12774	6.189	0.68	22.91	0.51	0.16	0.79	68.0	8.71	rej
n4258	184.728	47.3634	999999	92.00	1.00	20.50	0.10	0.38	0.02	256.	8.84	rej
n4258	184.811	47.2035	42010	8.961	0.95	24.41	0.32	1.28	0.17	20.0	8.76	
n4258	184.795	47.2022	28881	86.15	1.80	19.94	0.10	0.34	0.00	50.4	8.75	rej
n4258	184.800	47.2073	28076	31.17	1.06	22.51	0.11	0.31	0.00	27.3	8.77	
n4258	184.800	47.2062	27963	21.26	1.27	22.76	0.15	0.00	0.06	18.4	8.77	
n4258	184.800	47.2073	220887	31.29	1.26	22.52	0.12	0.31	0.01	27.3	8.77	
n4258	184.800	47.2062	220789	21.29	1.04	22.73	0.14	0.00	0.03	18.4	8.77	
n4258	184.842	47.2107	21853	6.063	0.96	25.86	0.35	2.93	0.17	15.7	8.74	rej
n4258	184.852	47.2138	15227	7.140	0.95	23.78	0.32	1.41	0.13	42.3	8.72	
n4258	184.840	47.2134	24025	9.253	0.84	22.82	0.25	1.03	0.05	15.9	8.75	rej
n4258	184.836	47.2201	28606	53.88	1.03	23.34	0.10	0.09	0.01	7.13	8.76	rej
n4258	184.836	47.2201	19756	48.79	1.22	21.85	0.10	0.00	0.00	9.52	8.76	
n4258	184.845	47.2127	16719	109.3	1.25	21.02	0.10	0.00	0.00	51.8	8.74	rej
n4258	184.858	47.2297	8073	32.29	1.30	22.20	0.10	0.00	0.00	5.61	8.71	
n4258	184.857	47.2298	307758	32.40	1.02	22.20	0.10	0.00	-0.0	5.61	8.71	
n4258	184.658	47.3445	144755	12.05	1.16	23.06	0.20	0.46	0.13	45.5	8.81	
n4258	184.827	47.2018	29163	6.739	0.80	24.48	0.57	2.86	0.38	42.1	8.75	
n4258	184.819	47.1987	34729	14.92	1.12	23.12	0.50	6.29	0.00	108.	8.75	
n4258	184.696	47.3103	89375	12.38	0.92	22.79	0.45	1.66	0.42	78.8	8.89	
n4258	184.697	47.3108	246695	11.20	0.91	22.97	0.40	1.17	0.49	152.	8.89	
n4258	184.833	47.2491	312665	39.09	0.80	23.10	0.11	0.47	0.01	15.1	8.78	rej

Table 4. Fits for H_0

χ^2_{dof}	#	H_0	<P	a_v	M^0_V	[O/H]	$\delta M/\delta$[O/H]	b	z_{min}	Fit	Scale	PLW	C R_V	SNe	SN R_V
0.65	448	**74.80(3.02)**	Y	0.697	-19.12	zkh	-0.25(0.10)	-3.02(0.06)	0.023	37	4258	$H_{V,I}$	3.1	UBVRI	2.5
0.65	448	75.62(3.05)	Y	0.702	-19.12	zkh	-0.25(0.10)	-3.02(0.06)	0.010	37	4258	$H_{V,I}$	3.1	UBVRI	2.5
0.64	497	76.03(3.02)	N	0.697	-19.09	zkh	-0.25(0.09)	-2.99(0.06)	0.023	37	4258	$H_{V,I}$	3.1	UBVRI	2.5
0.61	448	76.52(3.05)	Y	0.697	-19.07	zkh	-0.29(0.10)	-2.91(0.06)	0.023	37	4258	H	3.1	UBVRI	2.5
0.66	448	73.85(2.96)	Y	0.697	-19.15	zkh	——	-3.06(0.06)	0.023	37	4258	$H_{V,I}$	3.1	UBVRI	2.5
0.65	448	74.45(3.05)	Y	0.700	-19.15	zkh	-0.27(0.10)	-3.02(0.06)	0.023	61	4258	$H_{V,I}$	3.1	BVRI	2.5
1.87	570	76.16(3.83)	Y	0.697	-19.08	zkh	-0.27(0.15)	-2.89(0.09)	0.023	37	4258	$H_{V,I}$	3.1	UBVRI	2.5
0.65	448	74.52(3.04)	Y	0.701	-19.15	zkh	-0.24(0.10)	-3.02(0.06)	0.023	20	4258	$H_{V,I}$	3.1	UBVRI	3.1
0.64	448	75.12(3.02)	Y	0.697	-19.11	zkh	-0.26(0.10)	-3.00(0.06)	0.023	37	4258	$H_{V,I}$	2.5	UBVRI	2.5
0.65	448	74.83(3.00)	Y	0.690	-19.09	zkh	-0.26(0.10)	-3.02(0.06)	0.023	28	4258	$H_{V,I}$	3.1	UBVRI	2.0
0.66	448	75.00(2.99)	Y	0.684	-19.06	zkh	-0.27(0.10)	-3.02(0.06)	0.023	29	4258	$H_{V,I}$	3.1	UBVRI	1.5
0.64	448	73.42(3.04)	Y	0.691	-19.13	zkh	-0.22(0.10)	-3.03(0.06)	0.023	26	4258	$H_{V,I}$	3.1	UBVRI	2.5
0.64	448	74.71(3.11)	Y	0.699	-19.14	zkh	-0.25(0.10)	-3.02(0.06)	0.023	27	4258	$H_{V,I}$	3.1	UBVRI	3.1
0.65	497	75.92(2.99)	N	—-	—-	zkh	-0.25(0.09)	-3.00(0.06)	0.023	42	4258	$H_{V,I}$	3.1	UBVRI	—-
0.64	497	76.25(2.99)	N	—-	—-	zkh	-0.25(0.09)	-2.97(0.06)	0.023	42	4258	$H_{V,I}$	2.5	UBVRI	—-
0.65	448	74.80(3.02)	Y	0.697	-19.12	T_e	-0.37(0.15)	-3.02(0.06)	0.023	37	4258	$H_{V,I}$	3.1	UBVRI	2.5
0.76	514	**75.66(2.61)**	Y	0.697	-19.10	zkh	-0.20(0.11)	-3.19(0.03)	0.023	37	MW	$H_{V,I}$	3.1	UBVRI	2.5
0.76	514	76.49(2.63)	Y	0.702	-19.10	zkh	-0.20(0.11)	-3.19(0.03)	0.010	37	MW	$H_{V,I}$	3.1	UBVRI	2.5
0.75	563	76.70(2.58)	N	0.697	-19.07	zkh	-0.17(0.10)	-3.18(0.03)	0.023	37	MW	$H_{V,I}$	3.1	UBVRI	2.5
0.88	553	75.98(2.73)	Y	0.697	-19.09	zkh	-0.24(0.12)	-3.08(0.02)	0.023	37	MW	H	3.1	UBVRI	2.5
0.77	514	74.92(2.55)	Y	0.697	-19.12	zkh	——	-3.20(0.03)	0.023	37	MW	$H_{V,I}$	3.1	UBVRI	2.5
0.76	514	75.29(2.65)	Y	0.700	-19.13	zkh	-0.21(0.11)	-3.19(0.03)	0.023	61	MW	$H_{V,I}$	3.1	BVRI	2.5
1.86	636	77.58(4.07)	Y	0.697	-19.04	zkh	-0.19(0.15)	-3.14(0.04)	0.023	37	MW	$H_{V,I}$	3.1	UBVRI	2.5
0.76	514	75.38(2.64)	Y	0.701	-19.13	zkh	-0.19(0.11)	-3.19(0.03)	0.023	20	MW	$H_{V,I}$	3.1	UBVRI	3.1
0.75	514	76.10(2.60)	Y	0.697	-19.09	zkh	-0.20(0.11)	-3.17(0.03)	0.023	37	MW	$H_{V,I}$	2.5	UBVRI	2.5
0.77	514	75.70(2.58)	Y	0.690	-19.06	zkh	-0.20(0.11)	-3.19(0.03)	0.023	28	MW	$H_{V,I}$	3.1	UBVRI	2.0
0.77	514	75.88(2.56)	Y	0.684	-19.03	zkh	-0.21(0.11)	-3.19(0.03)	0.023	29	MW	$H_{V,I}$	3.1	UBVRI	1.5
0.76	514	74.29(2.66)	Y	0.691	-19.11	zkh	-0.16(0.11)	-3.19(0.03)	0.023	26	MW	$H_{V,I}$	3.1	UBVRI	2.5
0.76	514	75.56(2.72)	Y	0.699	-19.11	zkh	-0.20(0.11)	-3.19(0.03)	0.023	27	MW	$H_{V,I}$	3.1	UBVRI	3.1
0.76	563	76.62(2.53)	N	—-	—-	zkh	-0.17(0.10)	-3.18(0.03)	0.023	42	MW	$H_{V,I}$	3.1	UBVRI	—-
0.75	563	77.05(2.52)	N	—-	—-	zkh	-0.18(0.10)	-3.16(0.03)	0.023	42	MW	$H_{V,I}$	2.5	UBVRI	—-
0.76	514	77.72(3.15)	Y	0.697	-19.04	T_e	-0.29(0.16)	-3.19(0.03)	0.023	37	MW	$H_{V,I}$	3.1	UBVRI	2.5
0.75	514	**71.31(3.84)**	Y	0.697	-19.23	zkh	-0.20(0.11)	-3.19(0.03)	0.023	37	LMC	$H_{V,I}$	3.1	UBVRI	2.5
0.75	514	72.09(3.88)	Y	0.702	-19.23	zkh	-0.20(0.11)	-3.19(0.03)	0.010	37	LMC	$H_{V,I}$	3.1	UBVRI	2.5
0.73	563	72.46(3.82)	N	0.697	-19.19	zkh	-0.18(0.10)	-3.18(0.03)	0.023	37	LMC	$H_{V,I}$	3.1	UBVRI	2.5

Table 4—Continued

χ^2_{dof}	#	H_0	<P	a_v	M^0_V	[O/H]	$\delta M/\delta$[O/H]	b	z_{min}	Fit	Scale	PLW	C R_V	SNe	SN R_V
0.86	553	69.68(3.91)	Y	0.697	-19.28	zkh	-0.24(0.11)	-3.08(0.02)	0.023	37	LMC	H	3.1	UBVRI	2.5
0.75	514	73.34(3.76)	Y	0.697	-19.17	zkh	——	-3.19(0.03)	0.023	37	LMC	$H_{V,I}$	3.1	UBVRI	2.5
0.75	514	70.76(3.85)	Y	0.700	-19.26	zkh	-0.21(0.11)	-3.19(0.03)	0.023	61	LMC	$H_{V,I}$	3.1	BVRI	2.5
1.84	636	72.70(5.31)	Y	0.697	-19.18	zkh	-0.19(0.15)	-3.14(0.04)	0.023	37	LMC	$H_{V,I}$	3.1	UBVRI	2.5
0.75	514	71.13(3.85)	Y	0.701	-19.25	zkh	-0.19(0.11)	-3.19(0.03)	0.023	20	LMC	$H_{V,I}$	3.1	UBVRI	3.1
0.74	514	71.37(3.83)	Y	0.697	-19.22	zkh	-0.21(0.11)	-3.17(0.03)	0.023	37	LMC	$H_{V,I}$	2.5	UBVRI	2.5
0.75	514	71.24(3.82)	Y	0.690	-19.20	zkh	-0.21(0.11)	-3.19(0.03)	0.023	28	LMC	$H_{V,I}$	3.1	UBVRI	2.0
0.76	514	71.26(3.82)	Y	0.684	-19.17	zkh	-0.22(0.11)	-3.19(0.03)	0.023	29	LMC	$H_{V,I}$	3.1	UBVRI	1.5
0.74	514	70.48(3.86)	Y	0.691	-19.22	zkh	-0.16(0.11)	-3.19(0.03)	0.023	26	LMC	$H_{V,I}$	3.1	UBVRI	2.5
0.74	514	71.23(3.90)	Y	0.699	-19.24	zkh	-0.20(0.11)	-3.19(0.03)	0.023	27	LMC	$H_{V,I}$	3.1	UBVRI	3.1
0.74	563	72.44(3.80)	N	—-	—-	zkh	-0.17(0.10)	-3.18(0.03)	0.023	42	LMC	$H_{V,I}$	3.1	UBVRI	—-
0.73	563	72.51(3.79)	N	—-	—-	zkh	-0.18(0.10)	-3.16(0.03)	0.023	42	LMC	$H_{V,I}$	2.5	UBVRI	—-
0.75	514	73.22(3.75)	Y	0.697	-19.17	T_e	-0.29(0.16)	-3.19(0.03)	0.023	37	LMC	$H_{V,I}$	3.1	UBVRI	2.5
0.76	514	**74.53(2.25)**	Y	0.697	-19.13	zkh	-0.19(0.11)	-3.20(0.03)	0.023	37	4258+MW	$H_{V,I}$	3.1	UBVRI	2.5
0.76	514	75.34(2.26)	Y	0.702	-19.13	zkh	-0.19(0.11)	-3.20(0.03)	0.010	37	4258+MW	$H_{V,I}$	3.1	UBVRI	2.5
0.75	563	75.61(2.23)	N	0.697	-19.10	zkh	-0.17(0.10)	-3.19(0.02)	0.023	37	4258+MW	$H_{V,I}$	3.1	UBVRI	2.5
0.88	553	75.48(2.39)	Y	0.697	-19.10	zkh	-0.24(0.12)	-3.08(0.02)	0.023	37	4258+MW	H	3.1	UBVRI	2.5
0.77	514	73.90(2.20)	Y	0.697	-19.15	zkh	——	-3.20(0.03)	0.023	37	4258+MW	$H_{V,I}$	3.1	UBVRI	2.5
0.76	514	74.15(2.30)	Y	0.700	-19.16	zkh	-0.21(0.11)	-3.20(0.03)	0.023	61	4258+MW	$H_{V,I}$	3.1	BVRI	2.5
1.86	636	75.90(3.44)	Y	0.697	-19.09	zkh	-0.18(0.15)	-3.15(0.04)	0.023	37	4258+MW	$H_{V,I}$	3.1	UBVRI	2.5
0.76	514	74.25(2.28)	Y	0.701	-19.16	zkh	-0.19(0.11)	-3.20(0.03)	0.023	20	4258+MW	$H_{V,I}$	3.1	UBVRI	3.1
0.75	514	74.92(2.24)	Y	0.697	-19.12	zkh	-0.20(0.11)	-3.18(0.03)	0.023	37	4258+MW	$H_{V,I}$	2.5	UBVRI	2.5
0.77	514	74.56(2.21)	Y	0.690	-19.10	zkh	-0.20(0.11)	-3.20(0.03)	0.023	28	4258+MW	$H_{V,I}$	3.1	UBVRI	2.0
0.77	514	74.72(2.19)	Y	0.684	-19.06	zkh	-0.21(0.11)	-3.20(0.03)	0.023	29	4258+MW	$H_{V,I}$	3.1	UBVRI	1.5
0.76	514	73.19(2.32)	Y	0.691	-19.14	zkh	-0.16(0.11)	-3.20(0.03)	0.023	26	4258+MW	$H_{V,I}$	3.1	UBVRI	2.5
0.76	514	74.43(2.38)	Y	0.699	-19.15	zkh	-0.19(0.11)	-3.20(0.03)	0.023	27	4258+MW	$H_{V,I}$	3.1	UBVRI	3.1
0.76	563	75.55(2.16)	N	—-	—-	zkh	-0.17(0.10)	-3.19(0.02)	0.023	42	4258+MW	$H_{V,I}$	3.1	UBVRI	—-
0.75	563	75.93(2.15)	N	—-	—-	zkh	-0.17(0.10)	-3.17(0.02)	0.023	42	4258+MW	$H_{V,I}$	2.5	UBVRI	—-
0.77	514	75.06(2.45)	Y	0.697	-19.12	T_e	-0.18(0.14)	-3.20(0.03)	0.023	37	4258+MW	$H_{V,I}$	3.1	UBVRI	2.5
0.75	514	**72.34(2.28)**	Y	0.697	-19.20	zkh	-0.17(0.10)	-3.19(0.03)	0.023	37	4258+LMC	$H_{V,I}$	3.1	UBVRI	2.5
0.75	514	73.13(2.30)	Y	0.702	-19.20	zkh	-0.17(0.10)	-3.19(0.03)	0.010	37	4258+LMC	$H_{V,I}$	3.1	UBVRI	2.5
0.73	563	73.45(2.26)	N	0.697	-19.16	zkh	-0.16(0.09)	-3.18(0.03)	0.023	37	4258+LMC	$H_{V,I}$	3.1	UBVRI	2.5
0.87	553	72.64(2.44)	Y	0.697	-19.19	zkh	-0.17(0.10)	-3.08(0.02)	0.023	37	4258+LMC	H	3.1	UBVRI	2.5
0.75	514	72.90(2.28)	Y	0.697	-19.18	zkh	——	-3.19(0.03)	0.023	37	4258+LMC	$H_{V,I}$	3.1	UBVRI	2.5
0.75	514	71.89(2.33)	Y	0.700	-19.23	zkh	-0.19(0.10)	-3.19(0.03)	0.023	61	4258+LMC	$H_{V,I}$	3.1	BVRI	2.5

Table 4—Continued

χ^2_{dof}	#	H_0	<P	a_v	M^0_V	[O/H]	$\delta M/\delta$[O/H]	b	z_{min}	Fit	Scale	PLW	C R_V	SNe	SN R_V
1.84	636	73.41(3.50)	Y	0.697	-19.16	zkh	-0.18(0.14)	-3.14(0.04)	0.023	37	4258+LMC	$H_{V,I}$	3.1	UBVRI	2.5
0.75	514	72.10(2.31)	Y	0.701	-19.22	zkh	-0.17(0.10)	-3.19(0.03)	0.023	20	4258+LMC	$H_{V,I}$	3.1	UBVRI	3.1
0.74	514	72.56(2.28)	Y	0.697	-19.19	zkh	-0.18(0.10)	-3.17(0.03)	0.023	37	4258+LMC	$H_{V,I}$	2.5	UBVRI	2.5
0.75	514	72.32(2.25)	Y	0.690	-19.16	zkh	-0.18(0.10)	-3.19(0.03)	0.023	28	4258+LMC	$H_{V,I}$	3.1	UBVRI	2.0
0.76	514	72.42(2.24)	Y	0.684	-19.13	zkh	-0.19(0.10)	-3.19(0.03)	0.023	29	4258+LMC	$H_{V,I}$	3.1	UBVRI	1.5
0.74	514	71.24(2.36)	Y	0.691	-19.20	zkh	-0.14(0.10)	-3.19(0.03)	0.023	26	4258+LMC	$H_{V,I}$	3.1	UBVRI	2.5
0.74	514	72.25(2.40)	Y	0.699	-19.21	zkh	-0.17(0.10)	-3.19(0.03)	0.023	27	4258+LMC	$H_{V,I}$	3.1	UBVRI	3.1
0.74	563	73.42(2.22)	N	—-	—-	zkh	-0.15(0.09)	-3.18(0.03)	0.023	42	4258+LMC	$H_{V,I}$	3.1	UBVRI	—-
0.73	563	73.64(2.21)	N	—-	—-	zkh	-0.16(0.09)	-3.16(0.03)	0.023	42	4258+LMC	$H_{V,I}$	2.5	UBVRI	—-
0.75	514	73.13(2.29)	Y	0.697	-19.17	T_e	-0.29(0.16)	-3.19(0.03)	0.023	37	4258+LMC	$H_{V,I}$	3.1	UBVRI	2.5
0.77	514	**74.41(2.43)**	Y	0.697	-19.13	zkh	-0.09(0.09)	-3.20(0.03)	0.023	37	MW+LMC	$H_{V,I}$	3.1	UBVRI	2.5
0.77	514	75.23(2.45)	Y	0.702	-19.13	zkh	-0.09(0.09)	-3.20(0.03)	0.010	37	MW+LMC	$H_{V,I}$	3.1	UBVRI	2.5
0.75	563	75.43(2.40)	N	0.697	-19.10	zkh	-0.08(0.08)	-3.19(0.02)	0.023	37	MW+LMC	$H_{V,I}$	3.1	UBVRI	2.5
0.88	553	74.24(2.54)	Y	0.697	-19.14	zkh	-0.09(0.09)	-3.09(0.02)	0.023	37	MW+LMC	H	3.1	UBVRI	2.5
0.77	514	74.45(2.43)	Y	0.697	-19.13	zkh	——	-3.20(0.03)	0.023	37	MW+LMC	$H_{V,I}$	3.1	UBVRI	2.5
0.77	514	74.00(2.48)	Y	0.700	-19.16	zkh	-0.10(0.09)	-3.20(0.03)	0.023	61	MW+LMC	$H_{V,I}$	3.1	BVRI	2.5
1.86	636	76.14(3.78)	Y	0.697	-19.08	zkh	-0.09(0.13)	-3.15(0.04)	0.023	37	MW+LMC	$H_{V,I}$	3.1	UBVRI	2.5
0.76	514	74.15(2.46)	Y	0.701	-19.16	zkh	-0.09(0.09)	-3.20(0.03)	0.023	20	MW+LMC	$H_{V,I}$	3.1	UBVRI	3.1
0.76	514	74.74(2.43)	Y	0.697	-19.12	zkh	-0.09(0.09)	-3.18(0.03)	0.023	37	MW+LMC	$H_{V,I}$	2.5	UBVRI	2.5
0.77	514	74.42(2.40)	Y	0.690	-19.10	zkh	-0.10(0.09)	-3.20(0.03)	0.023	28	MW+LMC	$H_{V,I}$	3.1	UBVRI	2.0
0.78	514	74.56(2.38)	Y	0.684	-19.07	zkh	-0.11(0.09)	-3.20(0.03)	0.023	29	MW+LMC	$H_{V,I}$	3.1	UBVRI	1.5
0.76	514	73.21(2.50)	Y	0.691	-19.14	zkh	-0.07(0.09)	-3.20(0.03)	0.023	26	MW+LMC	$H_{V,I}$	3.1	UBVRI	2.5
0.76	514	74.30(2.55)	Y	0.699	-19.15	zkh	-0.09(0.09)	-3.20(0.03)	0.023	27	MW+LMC	$H_{V,I}$	3.1	UBVRI	3.1
0.76	563	75.41(2.35)	N	—-	—-	zkh	-0.08(0.08)	-3.19(0.02)	0.023	42	MW+LMC	$H_{V,I}$	3.1	UBVRI	—-
0.75	563	75.73(2.34)	N	—-	—-	zkh	-0.08(0.08)	-3.17(0.02)	0.023	42	MW+LMC	$H_{V,I}$	2.5	UBVRI	—-
0.77	514	75.37(2.64)	Y	0.697	-19.11	T_e	-0.13(0.13)	-3.20(0.03)	0.023	37	MW+LMC	$H_{V,I}$	3.1	UBVRI	2.5
0.77	514	**73.75(2.15)**	Y	0.697	-19.15	zkh	-0.10(0.09)	-3.21(0.03)	0.023	37	4258+MW+LMC	$H_{V,I}$	3.1	UBVRI	2.5
0.77	514	74.56(2.16)	Y	0.702	-19.15	zkh	-0.10(0.09)	-3.21(0.03)	0.010	37	4258+MW+LMC	$H_{V,I}$	3.1	UBVRI	2.5
0.75	563	74.82(2.12)	N	0.697	-19.12	zkh	-0.09(0.08)	-3.19(0.02)	0.023	37	4258+MW+LMC	$H_{V,I}$	3.1	UBVRI	2.5
0.88	553	74.26(2.28)	Y	0.697	-19.14	zkh	-0.09(0.09)	-3.09(0.02)	0.023	37	4258+MW+LMC	H	3.1	UBVRI	2.5
0.77	514	73.68(2.15)	Y	0.697	-19.16	zkh	——	-3.21(0.03)	0.023	37	4258+MW+LMC	$H_{V,I}$	3.1	UBVRI	2.5
0.77	514	73.34(2.21)	Y	0.700	-19.18	zkh	-0.11(0.09)	-3.21(0.03)	0.023	61	4258+MW+LMC	$H_{V,I}$	3.1	BVRI	2.5
1.86	636	75.08(3.29)	Y	0.697	-19.11	zkh	-0.10(0.13)	-3.16(0.04)	0.023	37	4258+MW+LMC	$H_{V,I}$	3.1	UBVRI	2.5
0.76	514	73.48(2.18)	Y	0.701	-19.18	zkh	-0.09(0.09)	-3.21(0.03)	0.023	20	4258+MW+LMC	$H_{V,I}$	3.1	UBVRI	3.1
0.76	514	74.07(2.14)	Y	0.697	-19.14	zkh	-0.10(0.09)	-3.18(0.02)	0.023	37	4258+MW+LMC	$H_{V,I}$	2.5	UBVRI	2.5

Table 4—Continued

χ^2_{dof}	#	H_0	<P	a_v	M^0_V	[O/H]	$\delta M/\delta$[O/H]	b	z_{min}	Fit	Scale	PLW	C R_V	SNe	SN R_V
0.77	514	73.76(2.11)	Y	0.690	-19.12	zkh	-0.10(0.09)	-3.20(0.03)	0.023	28	4258+MW+LMC	$H_{V,I}$	3.1	UBVRI	2.0
0.78	514	73.90(2.09)	Y	0.684	-19.09	zkh	-0.11(0.09)	-3.20(0.03)	0.023	29	4258+MW+LMC	$H_{V,I}$	3.1	UBVRI	1.5
0.76	514	72.53(2.23)	Y	0.691	-19.16	zkh	-0.07(0.09)	-3.21(0.02)	0.023	26	4258+MW+LMC	$H_{V,I}$	3.1	UBVRI	2.5
0.76	514	73.64(2.28)	Y	0.699	-19.17	zkh	-0.10(0.09)	-3.21(0.02)	0.023	27	4258+MW+LMC	$H_{V,I}$	3.1	UBVRI	3.1
0.76	563	74.80(2.06)	N	—-	—-	zkh	-0.09(0.08)	-3.20(0.02)	0.023	42	4258+MW+LMC	$H_{V,I}$	3.1	UBVRI	—-
0.75	563	75.12(2.06)	N	—-	—-	zkh	-0.09(0.08)	-3.17(0.02)	0.023	42	4258+MW+LMC	$H_{V,I}$	2.5	UBVRI	—-
0.77	514	74.18(2.26)	Y	0.697	-19.14	T_e	-0.10(0.13)	-3.21(0.03)	0.023	37	4258+MW+LMC	$H_{V,I}$	3.1	UBVRI	2.5

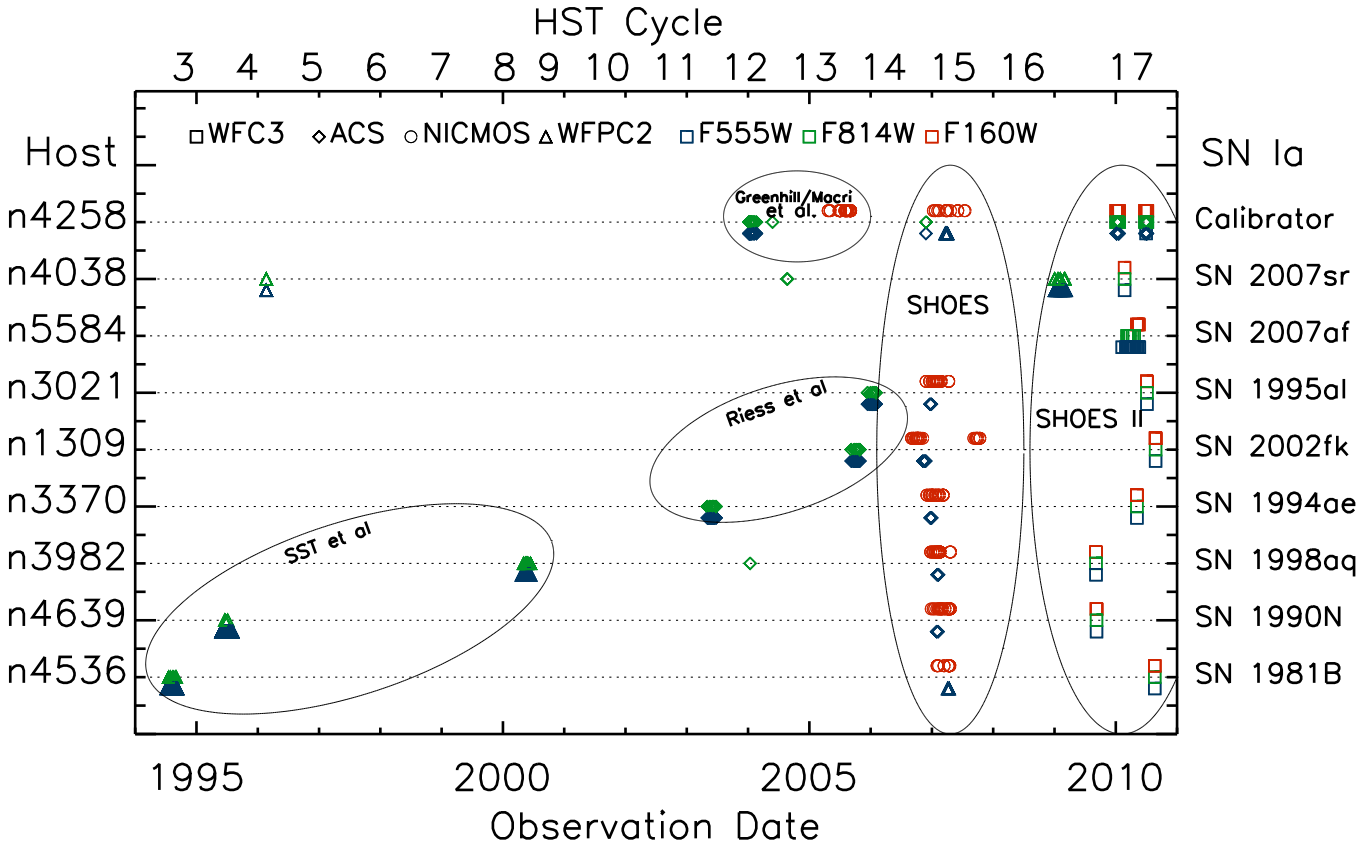
HST Cycle
3 4 5 6 7 8 9 10 11 12 13 14 15 16 17
WFC3 ACS NICMOS WFPC2 F555W F814W F160W
Host
SN Ia
n4258
n4038
n5584
n3021
n1309
n3370
n3982
n4639
n4536
Calibrator
SN 2007sr
SN 2007af
SN 1995al
SN 2002fk
SN 1994ae
SN 1998aq
SN 1990N
SN 1981B
Greenhill/Macri et al.
SHOES
Riess et al
SHOES II
SST et al
1995
2000
2005
2010
Observation Date

Fig. 1.—

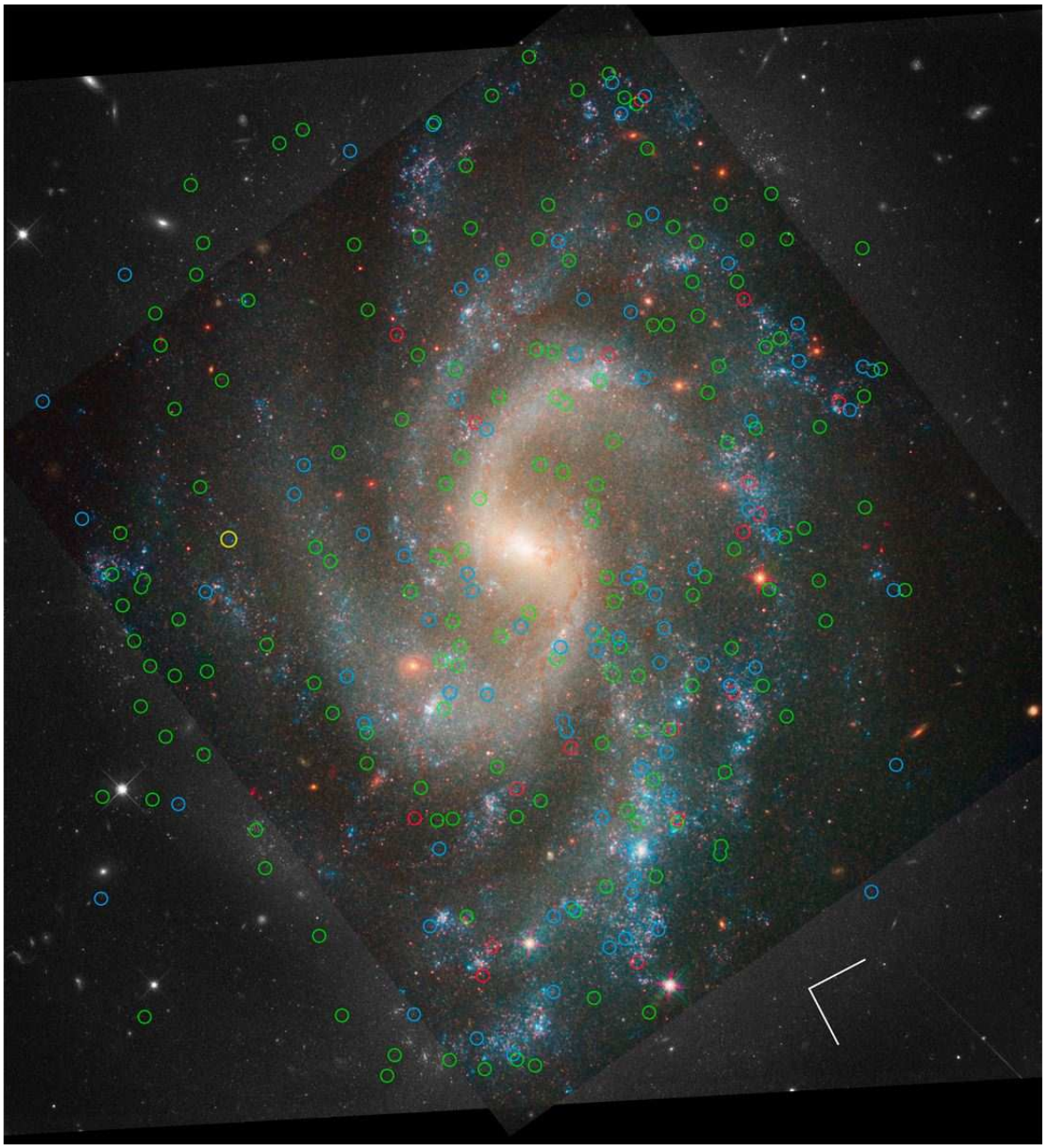

Fig. 2.—

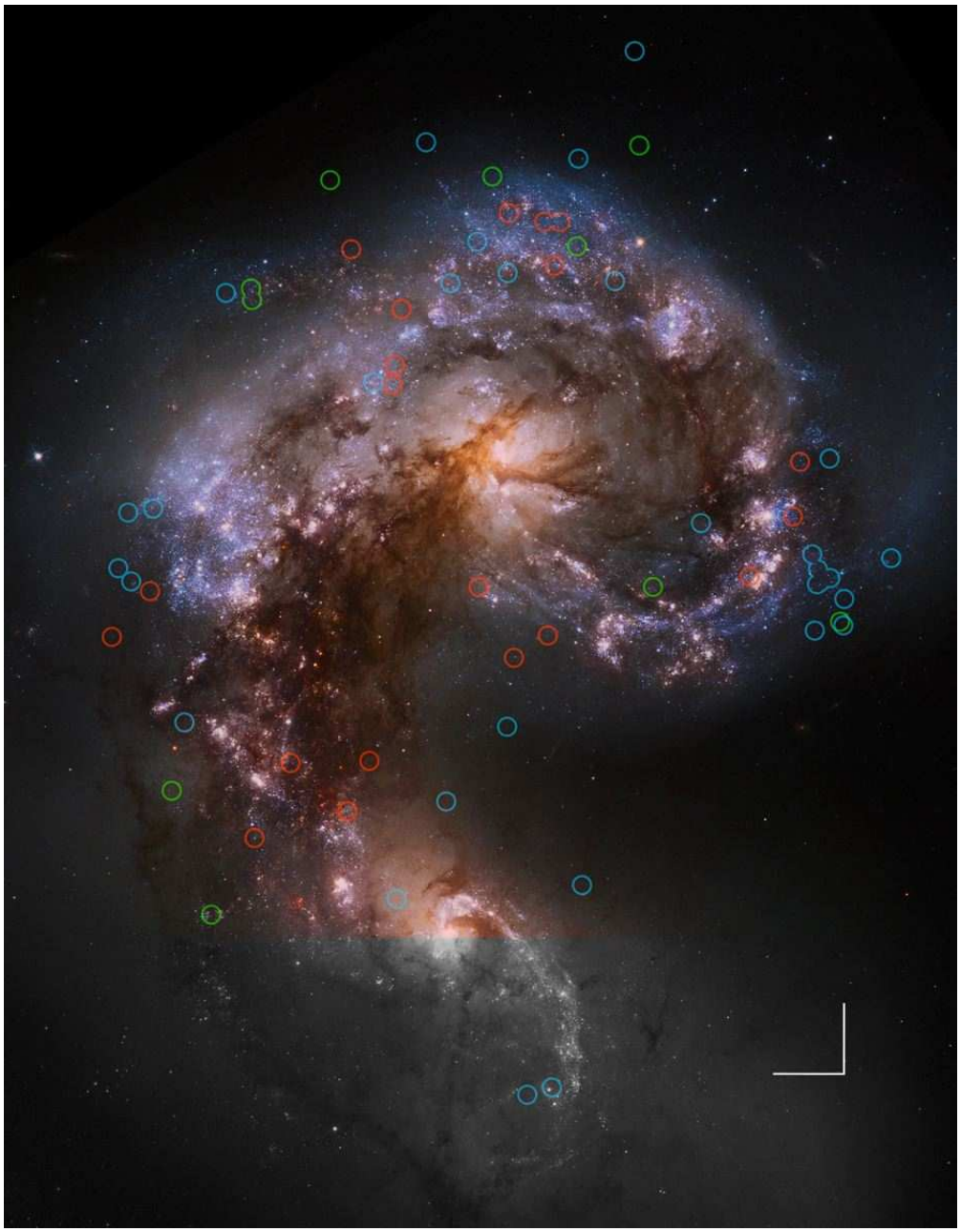

Fig. 3.—

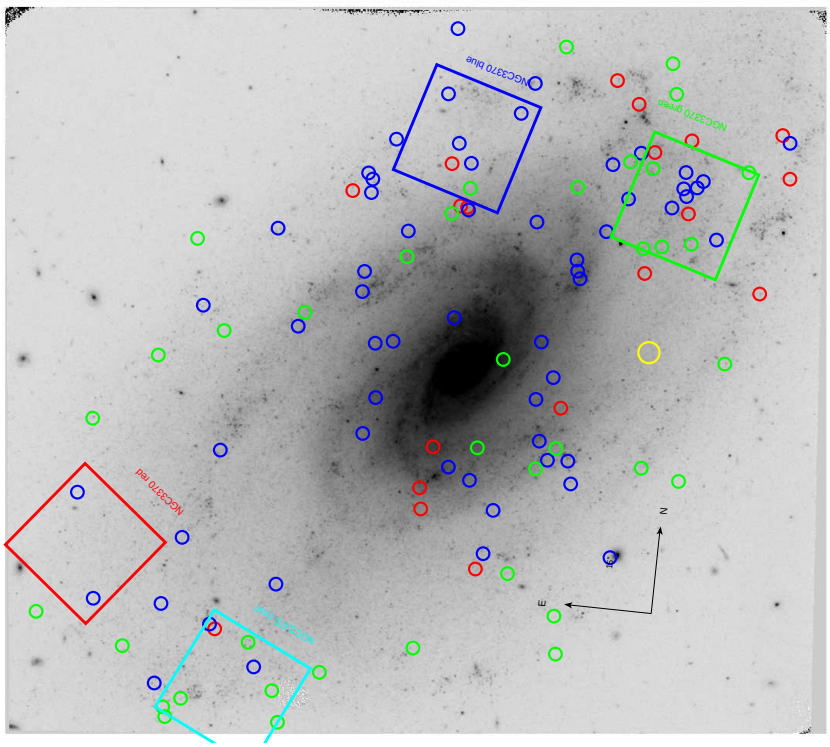

Fig. 4a.—

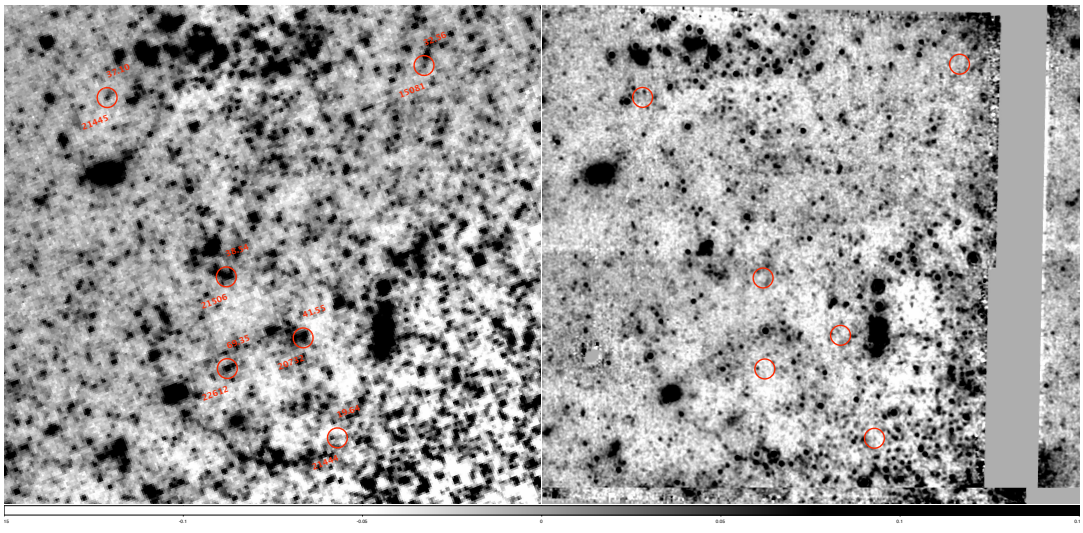

Fig. 4b.—

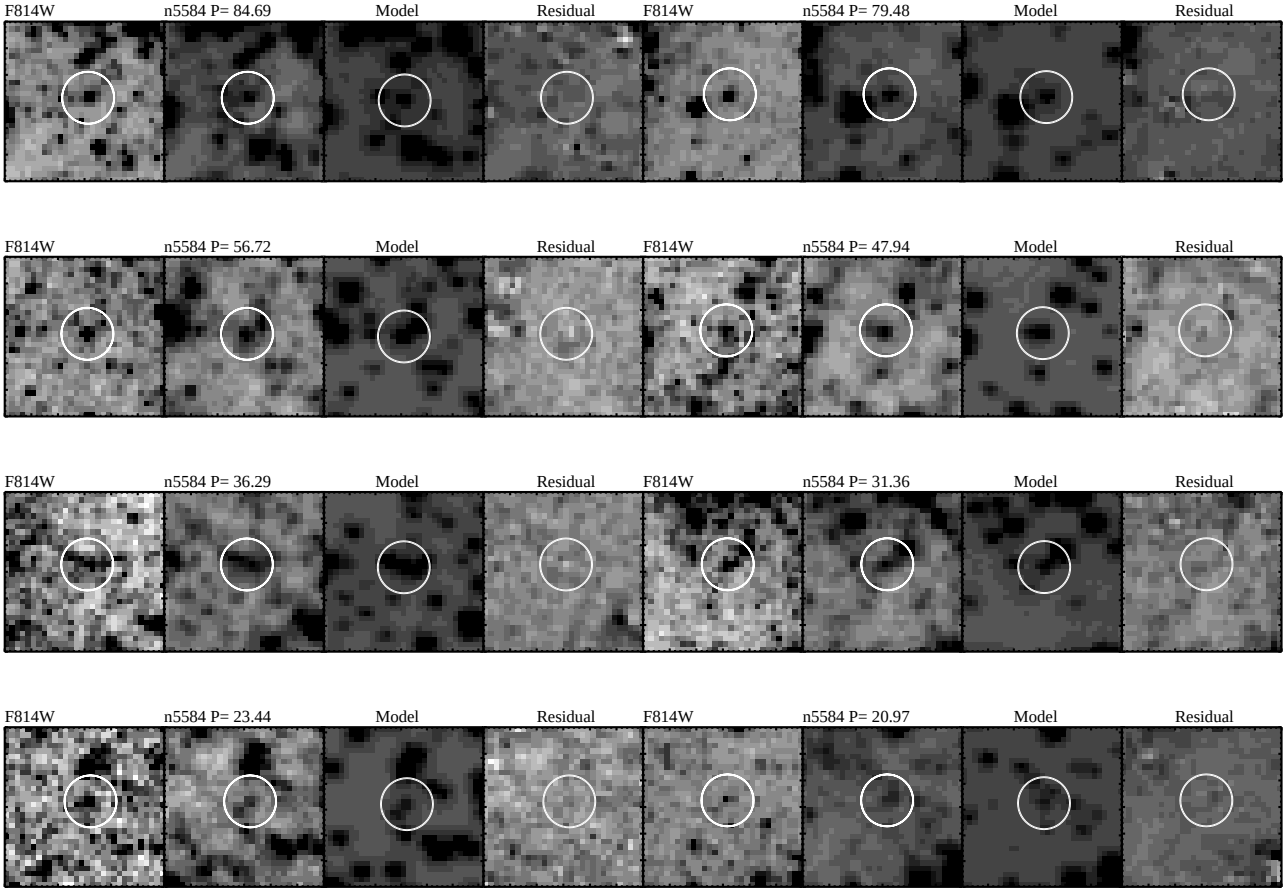
F814W
n5584 P= 84.69
Model
Residual
F814W
n5584 P= 79.48
Model
Residual
F814W
n5584 P= 56.72
Model
Residual
F814W
n5584 P= 47.94
Model
Residual
F814W
n5584 P= 36.29
Model
Residual
F814W
n5584 P= 31.36
Model
Residual
F814W
n5584 P= 23.44
Model
Residual
F814W
n5584 P= 20.97
Model
Residual

Fig. 5.—

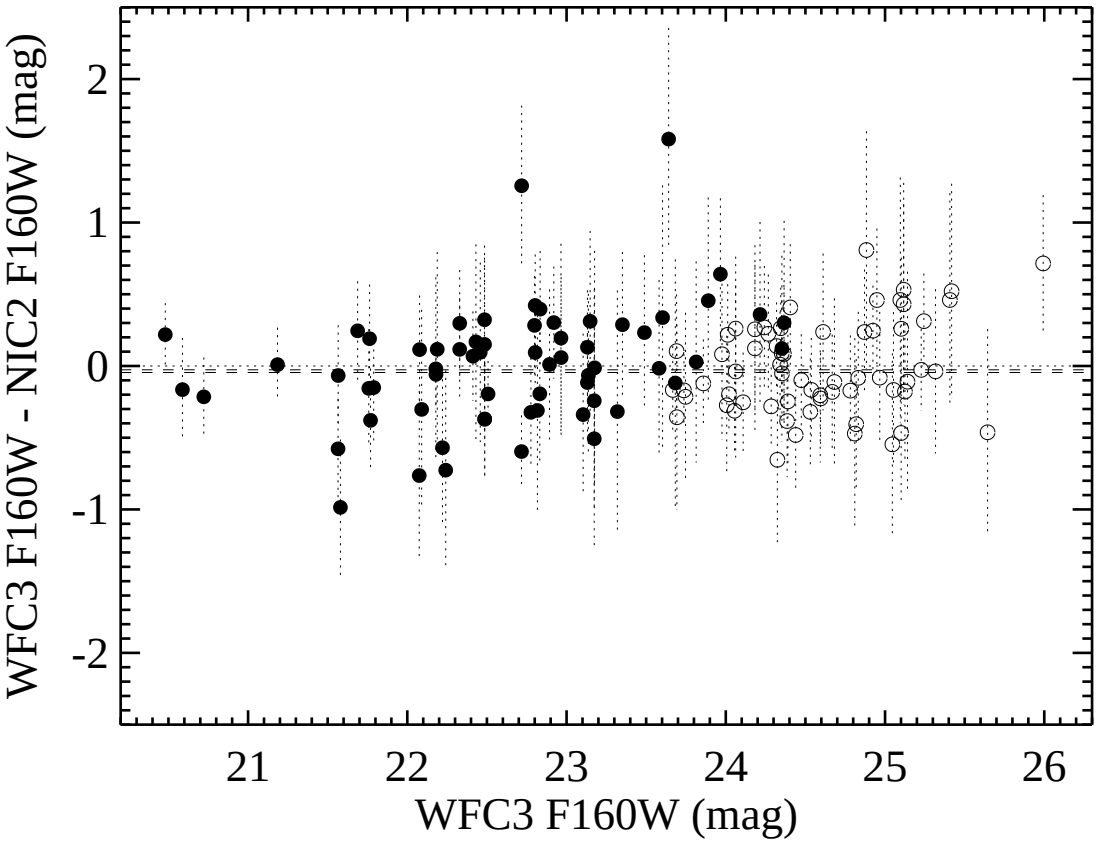
WFC3 F160W - NIC2 F160W (mag)
2
1
0
-1
-2
21
22
23
24
25
26
WFC3 F160W (mag)

Fig. 6.—

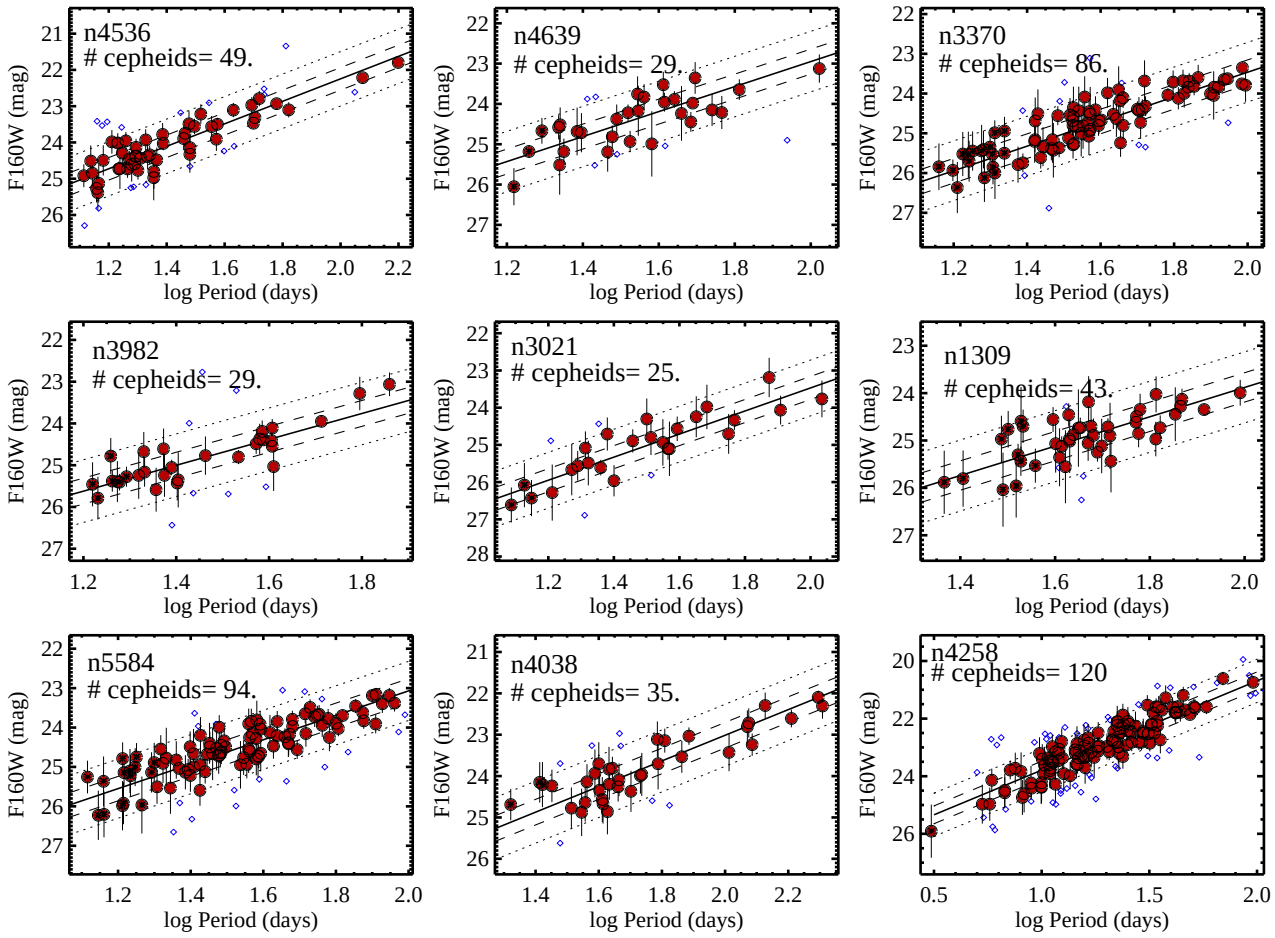
n4536
cepheids= 49.
n4639
cepheids= 29.
n3370
cepheids= 86.
n3982
cepheids= 29.
n3021
cepheids= 25.
n1309
cepheids= 43.
n5584
cepheids= 94.
n4038
cepheids= 35.
n4258
cepheids= 120
F160W (mag)
log Period (days)

Fig. 7.—

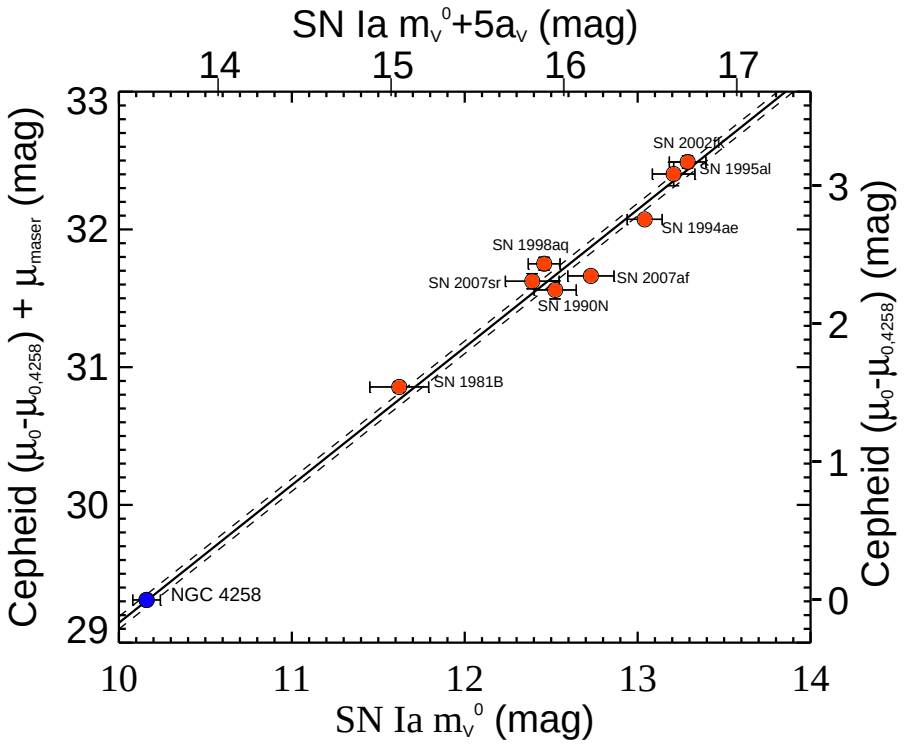
SN Ia $m_V^0+5a_V$ (mag)
14
15
16
17
33
32
31
30
29
Cepheid (μ_0-$\mu_{0,4258}$) + μ_{maser} (mag)
SN 2002fk
SN 1995al
SN 1994ae
SN 1998aq
SN 2007sr
SN 2007af
SN 1990N
SN 1981B
NGC 4258
10
11
12
13
14
SN Ia m_V^0 (mag)
3
2
1
0
Cepheid (μ_0-$\mu_{0,4258}$) (mag)

Fig. 8.—

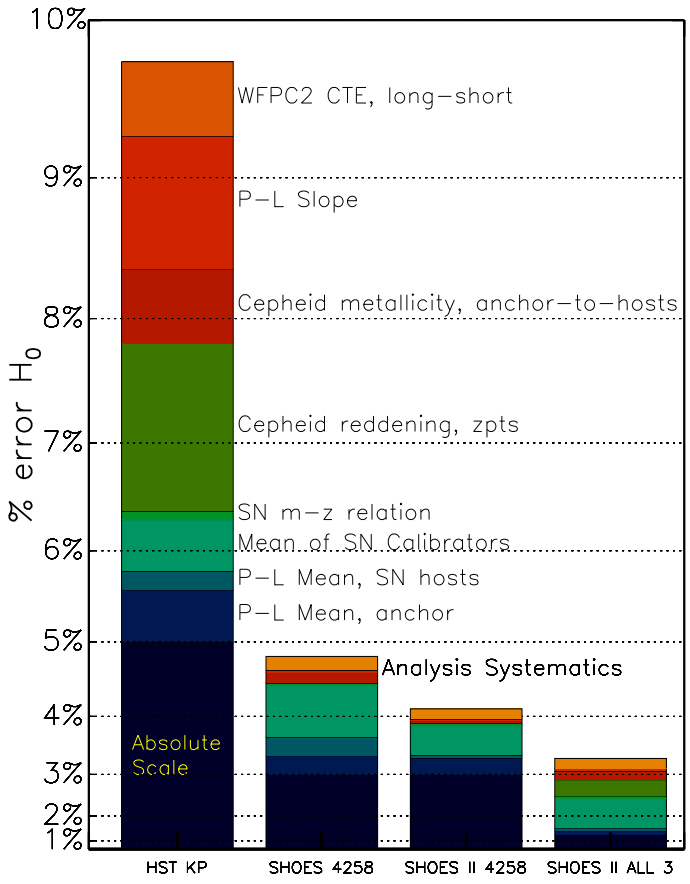
10%
9%
8%
7%
6%
5%
4%
3%
2%
1%
% error H_0
WFPC2 CTE, long−short
P−L Slope
Cepheid metallicity, anchor−to−hosts
Cepheid reddening, zpts
SN m−z relation
Mean of SN Calibrators
P−L Mean, SN hosts
P−L Mean, anchor
Analysis Systematics
Absolute Scale
HST KP
SHOES 4258
SHOES II 4258
SHOES II ALL 3

Fig. 9.—

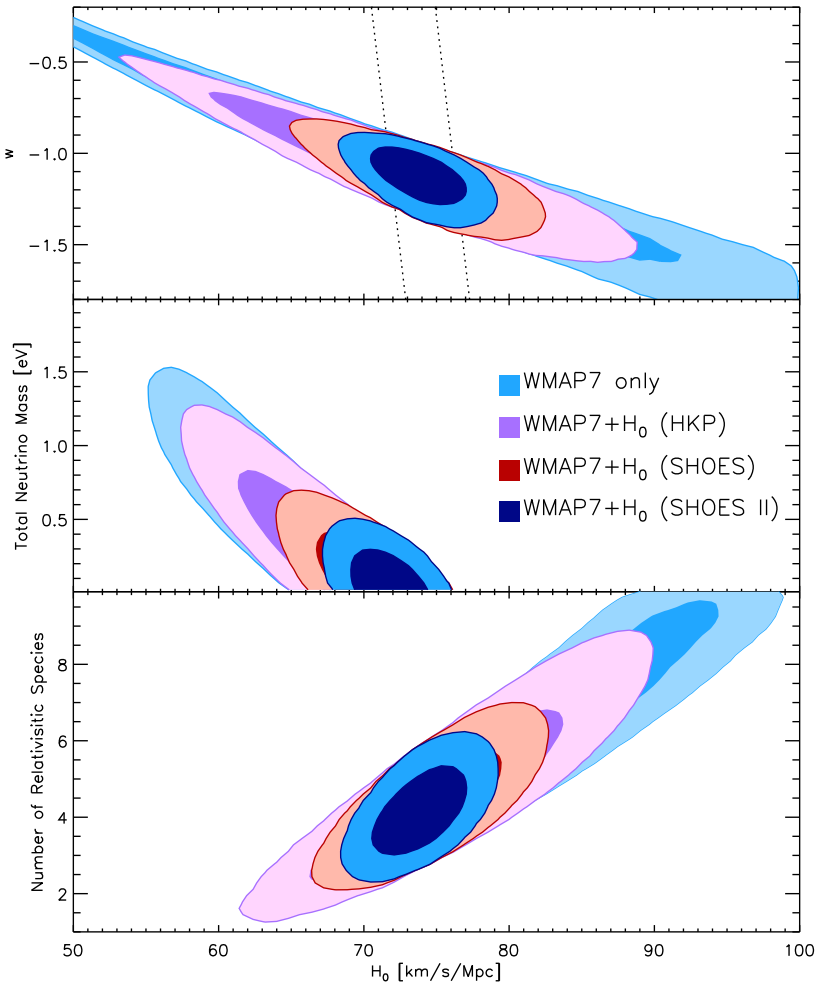
w
−0.5
−1.0
−1.5
Total Neutrino Mass [eV]
1.5
1.0
0.5
WMAP7 only
WMAP7+H0 (HKP)
WMAP7+H0 (SHOES)
WMAP7+H0 (SHOES II)
Number of Relativisitic Species
8
6
4
2
50
60
70
80
90
100
H0 [km/s/Mpc]

Fig. 10.—